## Authors‘ response to referee comments

Always given as: Referee comment – Authors‘ response – Changes to manuscript

### General Remark:

First of all, we wish to thank the reviewers for their detailed reading of the manuscript, their constructive comments and their advice to modify and improve our manuscript!

There have been several comments asking us to provide quantitative description of selected processes in the main manuscript, while our intention was to keep it away from there and put it into the online supplement, for clarity and readability reasons. This decision was made after thorough consideration of potential advantages and disadvantages.

Showing some equations and model constants in the main text and hiding others, that is, giving an incomplete quantitative description, would lead to a somewhat unbalanced choice of which processes we think are important. On the other hand, giving a complete quantitative description would certainly expand the manuscript length towards an unreadable volume. This can be easily estimated by looking at the complete description of the model equations given in the supplement. Even if the quite technical description might deflate a bit when being translated into mathematical formulae, about 20-30 pages might remain. We decided not to present the whole set of equations because they are quite common and appear in a number of other models on the biogeochemistry of diagenesis in a very similar way. Presenting them would be essentially a repetition.

We agree with all three reviewers that a more thorough description of the non-common processes we added to the ancestor models is required. Therefore, we modified this part of our concept and now include a quantitative mathematical description of these ones. We hope that this compromise – qualitative description only of ‘established’ processes and thorough mathematical description of “un-common” processes, complemented by the precise technical description of the complete model in the supplement – is acceptable for the scientific community. Non-modelers might appreciate the possibility to get a quick qualitative overview of which processes are considered in the model and which are not. Modelers who wish to include the “non-common” processes into their own models will find a thorough description. Readers interested in applying our model will need to dig into the details anyway and will have to familiarize with our naming of the state variables etc., so the (rather technical) complete model description serves their potential needs.

Therefore, we appreciate and follow the reviewers’ suggestions and include a thorough quantitative description of processes in the main text, but only for those processes that are not common in previous models.

### Reviewer 1 – specific comments

The model description section needs much more explanations; authors should provide more equations and possibly schemes. Sometimes I had a feeling that authors did not want to be understood.

While we agree that more detailed descriptions are sometimes needed, we strongly reject the last speculation. The limited clarity rather arises from the attempt to avoid that the paper gets too long which might distract interested readers.

We readjust the balance between clarity and conciseness and add more explanations, making the paper longer than before. We especially add detail on (a) fluff layer representation and (b) added biogeochemical processes. At the same time, we keep the quantitative description of the "old" processes taken from the ancestor models in the online supplement.

Authors do not validate their model against benthic fluxes which are usually used as the major constraint. Modeled benthic fluxes should be reported and comparison of modelled benthic fluxes to their measured values should be provided.

We invited two additional co-authors who added flux measurements by benthic chamber landers at the selected stations for additional model validation.

Authors do not provide any result related to water column. For example depth dependent mean reactivity of sinking organic carbon can be reported.

The reason for this is that the measurements taken during the sampling campaign focused on the sediment, so we have limited data to compare to.

We add graphs of mean reactivity of sinking organic carbon to the online supplement.

Having 115 parameters to optimize, authors need to provide a reasonable explanation of how certain local optimum was chosen.

The automatic method was started after manual calibration of the model. Since the optimisation method is deterministic, the local optimum is defined by this initial condition.

We clarify this in section 4.3.

**Reviewer 1 – minor comments**

P.5, L.26: 22 layers with 1mm at the surface is not enough. The grid should be much finer.

The resolution represents a compromise between accuracy and the need for a limited numerical effort. The latter is essential for the later application in a three-dimensional context.

For sensitivity analysis to the vertical resolution, we add a comparison to a model with doubled vertical resolution in every layer to the online supplement.

P.9, L.21-23: 3% per day, please explain how this number was estimated?

We add: "This number was estimated from calibration of a 3-dimensional Baltic Sea ecosystem model (Neumann et al. …) where the process showed to be critical for transporting organic matter to the deep basins below a depth of approx. … m. In these depths, a resuspension due to wave-induced shear stress is no longer possible."

P.10, L.16-18: Please, provide the equation for DB(z).

We give the requested equation.

Eq. 1,2 and 3: Replace $\phi$ with $\phi(z)$, c with $c(t,z)$, DB with $DB(z)$

We did the requested replacements.

Eq. 3: Move ϕ(z) out of differential as it is time independent

We agree that this simplifies the equation, even if the presented formulation is still correct.

We did this in eq. 2 and 3

P.12, L.10-11: This is probably not true. Lateral migration assumes removal of organic particles of all kind but the same time it can be considered as a source of detritus from the other parts of the sea.

I guess this is a misunderstanding: Fluff material above sandy sediments partly decomposes there before being advected to deeper areas. Therefore, as an approximation, we assume that the quickest degradable parts will not arrive at the mud stations because they were already mineralized at the shallow sandy locations.

We changed the sentence to: "We assume that the quickest-degradable part of the detritus is already mineralised in the shallow coastal areas, before its lateral migration to the mud stations, and therefore exclude the first two classes from this artificial input."

P.12, L.19-27: Please provide some general equation for plankton growth here.

We decided after thorough consideration of advantages and disadvantages to provide the quantitative description of the "old" parts of the BGC model only in the online supplement. Giving some equations like this one and hiding others would be inconsistent. Giving all equations would massively increase the length of the manuscript and is therefore not an option for us.

No changes to manuscript

Section 2.4.2: Please provide some general equation for phytoplankton respiration and mortality. Also, how do you account for day/night phytoplankton metabolism?

See comment above. / We do not account for day/night metabolism, but represent phytoplankton as a Redfield-ratio state variable which will only grow when light is present. This is a simplification used in many ecosystem models.

We added the sentence: "This simplifying description of phytoplankton growth does not describe day/night metabolism."

Section 2.4.3: Please provide some general equation for zooplankton growth here.

See comments above

No changes to manuscript

P.17, L.17: This simplification should be quantified. For example, you can run the model with constant and depth-dependent porosity and show that the results (benthic fluxes, porewater profiles) are similar.

This simplification has been made due to limited spatial availability of data for the 3-dimensional approach. While detailed spatial maps of surface porosity exist, vertical profiles are rare.

We added a new appendix section showing a comparison between a constant-porosity profile and another one with vertically varying porosity.

Section 2.7.1: Very hard to understand, more detailed explanation is needed. Some equations/schemes would help.

We did not go into too much detail here since we expect that only few readers are actually interested in the numerical details.

We added a new appendix section describing the application of the Al-Hassan method.

P.22, L.25: Sedimentation rate is 0.00001 per day. Is this correct? I would say it should be 10 times higher. / P.23, L.15-16: With ω = 0.00001d-1 100y is not enough to fill the column with solid species, nor does it work with ω = 0.0001d-1. It basically means that sedimentation is neglected in the model.

Yes, you are right. This is an artificially small value, but different from zero for numerical purposes. It basically reflects the fact that the decay time scale of chlorophyll is much lower than the time scale for sediment accumulation.

We changed the sentence: “Experimentally derived chlorophyll decay constants of 0.01 d-1 for mud and 0.02 d-1 for sand (Morys, 2016) and an artificially small sedimentation rate ω of 0.00001 cm d-1 were used, the latter just reflecting the fact that chlorophyll decay is much faster than sedimentation.”

Section 4.2: In this section authors need to specify the boundary conditions for each functional level (water column, fluffy layer and sediments). Mathematical formulation of boundaries (fixed concentration or gradient) is needed.

We added a mathematical description of the boundary conditions.

P.24, L.20-21: How the weighting function was applied?

This is already described in Equation 9.

No changes to manuscript.

P.25, L.4: AHR-ES abbreviation is given without explanation. / P.25, L.16: “We used 200 ”individuals” ”. Please, bring the formula to calculate the number of individuals required by AHR-ES. / P.25, L.4-18: What is the rational to put this in the paper? I think it is not needed as long as you do not compare all major evolutionary strategies.

Our intention to put it in here was to serve as a justification for using the simple strategy, illustrating that we have not used it because of its simplicity but because of its better performance compared to this more complicated method which had been suggested to us by colleagues. But probably this is not needed. Also, we thought it is useful information for others that we did not succeed applying this method.

We skip the description of the AHR-ES method (which we spell out as Adaptative Hierarchical Recombination – Evolutionary Strategies) and just mention that it was our first attempt but we did not succeed.

P.25, L.27-28: “The optimisation converged after 30 iteration steps and reduced the error function from 6363 (the value obtained by previous manual tuning) to 4797”. In other words, this optimization provides the result which is just 25% better then original guess. Necessity of this optimization is questioned.

We don’t know whether 25% is a little or a lot, because we would not expect anyway that a perfect optimization method arrives at an error of zero. There are (a) structural errors induced in the model by using a simplified set of processes and (b) errors due to a suboptimal choice of the parameters, and only the latter ones can be reduced by the optimisation. By “necessity is questioned” you probably mean a cost-benefit analysis? Traditionally, modelers just use a manual optimisation of parameters, we also did that and ended at the starting point for the additional automatic calibration, from where we could gain another 25%.

No changes to manuscript.

P.25, L.29-31: How many optima have been found? What can you say about sensitivity of the model to the different parameter groups?

Since the method is deterministic, only one optimum has been found.

We mention this fact here. Also, we add an additional appendix section giving the sensitivities of the penalty function to changes in individual model parameters.

P.26, L.18-20: This should be mentioned right after P.23, L.15-16.

We add the following sentence there: “While this period of 100 years is not sufficient to fill the considered 22 cm of sediment by accumulation, it is sufficient to almost reach a steady state in the pore water concentrations. While the sixth class of detritus, which is considered non-biodegradable, continues accumulating in the sediments after 100 years, those classes which affect the pore water concentrations decay on smaller time scales.”

P.26, L.31: 23km away? I would consider it as a different station. You should at least clearly mark the point representing this site on the plots.

We use different symbols for the different locations in the plot now.

P.27, L.11-12: Please provide modeled fluxes of dissolved species through sediment water interface and compare them to measured values or the values typical for each region.

We invited two additional co-authors who added flux measurements by benthic chamber landers at the selected stations for additional model validation.

**Reviewer 2 – general comments**

1. Introduction and text structure: The introduction needs to be improved/restructured, better putting the model/work into context. Referring to another paper (i.e. Yakushev et al., 2017) for an overview of existing coupled models (pg. 2 ln. 13-14) is not sufficient. This part of the manuscript is critical for putting your work into context and for the motivation of your work!

We spell out an overview of existing models now, mostly repeating what Yakushev et al. compiled in addition to referring to it.

Why did you decide to use a new model? How does your model differ from those? Why is it better suited to your study site? I think, especially the explicit fluff layer (which is also know as the bottom boundary layer, I suppose – or are they different things?) deserves some more detail.

Thank you for this suggestion! The basic idea was to extend our existing ecosystem model ERGOM into the sediment, and the fluff layer transport was already implemented there. But you may be right in stating that emphasizing this difference to other early diagenetic models might be critical.

We add a paragraph after the description of existing bentho-pelagic models which answers this question.

Also the introduction should be restructured, e.g. starting with a better introduction of the importance of coupled benthic-pelagic processes and linking this to your site of interest (i.e. the German part of the Baltic Sea). This should motivate why the modelling exercise is needed (especially why using a coupled model and not just running a stand-alone sediment model if you are mainly interested in “the type of ecosystem services that coastal sediments can perform”). How can your new model help to improve our understanding of this environment (e.g. what are the most important processes here)?

Very good point that spelling out the importance of bentho-pelagic coupling in nature puts the work into context!

We start the introduction now with a paragraph on the importance of bentho-pelagic coupling for coastal ecosystems. Also we add an “outlook of an outlook” by explaining which type of questions might be answered one day with the 3-d version of the model, motivating this new modelling approach.

Also the results/conclusion section does not address these kind of questions. In general, the results section is rather short and a “story” behind your experiments or what you learn from them is missing.

It’s a model description paper, not a presentation of scientific results. As such, it does not focus on a detailed story.

No changes to manuscript.

As this model is mainly developed to investigate benthic-pelagic interactions a discussion of simulated sediment-water interface fluxes and its comparison with observations would improve the validation of the model. Especially, as the conclusion states "... where the efflux of nutrients from the sediment strongly influences water column biogeochemistry, like in our study area."

We invited two additional co-authors who added flux measurements by benthic chamber landers at the selected stations for additional model validation.

It was not clear to me what questions you would like to answer with the model eventually? This could be included in a section on “Scope of applicability and model limitations” which is expected for a model development paper anyway and is currently missing.

We add this section explicitly as part of the “conclusions” section.

2. The technical details of the implementation are incomplete: Just describing the processes/state variables qualitatively is not appropriate for a GMD paper which is supposed to be "detailed and complete". Include the most important equations and tables of parameters for e.g. (but not exclusively) the biogeochemical processes (2.4 +2.5) in the main manuscript (e.g. compare ERSEM: Butenschön et al., 2016; PISCES: Aumont et al., 2015).

Please see our general reply to this at the first page.

We follow the suggestion and add a detailed mathematical description, but only for those processes which are new in the model.

Give values of parameters and references to justify your decision making. I know they are in the supplementary document but it is 189 pages long, therefore it is not easy to find what one is looking for …

Including everything in the main text would cause the same problem as in the supplementary document.

No changes to manuscript

… and the very technical parameter names do not help either. I suggest not to use the code-names for the parameters in the text and equations. Give them more recognizable names and add Tables in the appendix which relates them to the code-names - if you wish (compare e.g. Aumont et al., 2015).

I agree that the names for the process rates (shaped p_precursor_process_product) are very technical. For the parameters, this seems to be a matter of taste. I particularly dislike parameters called $\alpha_3$ or similar whose names give no indication of what they are, and I also very much dislike if they are called differently in the manuscript and in the code.

No changes to manuscript.

For the diagenetic model: Add the 1-D mass conservation (general reaction-transport) equation and add table of reaction network for primary and secondary redox reactions and for precipitation/dissolution reactions (compare e.g. Reed et al., 2011; Jourabchi et al., 2005; Hülse et al., 2018).

We add the general reaction-transport equation in the beginning of the model description section. Also, we add a reaction network table as suggested.

The diffusivity (Section 2.3.1) and the initial and boundary conditions (Section 4.2) are from an unpublished MOM5 and ERGOM runs. More information on the model setups is needed as it is not possible to reproduce your results like this. This could go into the supplementary information together with the results needed to recreate your ERGOM SED results.

The model output for the different stations is already included in the online supplement, and the ERGOM-SED results can be reproduced with the information given there. We agree that adding more details on the 3-d model run is required, but reproducing the exact 3-d model results just from a description in a paper is impossible anyway.

We add more information on the 3-d model run which produced the data.

3. Model development: Make it more clear in the body of the manuscript what your model improvements are and describe them in more detail. Apart from abstract and conclusion this is not clearly mentioned and the explanation of the new developments are generally very short.

We add detailed information on the new processes.

The coupling of the different modules (i.e. water column, fluff-layer, sediment) is obviously a new development as well but it is not clear to me how it is done. E.g. how do you calculate the bidirectional fluxes of dissolved species (give equations). Or the coupling of the fluff layer with sediment-column: You assume zero porosity? How are solute species transported from the fluff to the sediments?

We give mathematical equations on these exchange processes.

4. Text structure and referencing: The manuscript could benefit from another round of editing, looking at the structure and referencing (technique and missing citations). Examples of wrong referencing can be found: pg. 1 ln.7 ; pg. 2 ln. 5 + 15; pg. 10 ln. 15; pg. 22 ln. 5; pg. 27 ln. 1-2; etc.

Thank you for the suggestion, we change these.

The breakdown of the text into paragraphs and linebreaks should be revisited. Linebreaks after just 1 or 2 sentences are often used (e.g. 2.3.7, 2.3.8, 2.3.9, 2.4.5, 2.5.2, 2.5.5 etc.) which does not help with the flow of the paper.

I prefer if paragraphs indicate when a line of thought has ended, but I agree that most others might prefer longer paragraphs.

We combine short paragraphs throughout the manuscript to improve the flow of reading.

Also some of the crosslinks given to other sections of the text are not correct (see specific comments).

Thank you for pointing this out!

We change the mistakes given and check all references again.

**Reviewer 2 – specific comments**

Abstract: Abstract should include some information about the main findings/how the model performs.

We add a description of model performance to the abstract.

ln. 11: what does SECOS stand for?

We spell it out as “The Service of Sediments in German Coastal Seas”.

pg. 2 ln.8-9: Why are there so few coupled benthic-pelagic model studies?

Answering this would be pure speculation, so we will not do it in the paper. We guess it is because (a) the communities of early diagenetic modellers and pelagic ecosystem modellers are traditionally separate, (b) the spatial focus is different (single site versus whole ocean basin) and (c) for studies of pelagic processes, it is perfectly accepted to just state that the coarse representation of benthic processes is a weakness of the model, and that’s much easier than trying to improve it.

No changes to manuscript.

pg. 3 ln. 16 – 20. You introduce here the seven study sites you are modelling and categorize them by their granulometric properties. Some information on how these three categories differ and what these differences mean for modelling the sites would be good.

We add a short summary of main biological differences between sand, silt and mud sediments.

pg. 5 2.1 Ancestor models + 2.2 Model compartments and state variables: A better short summary of the main, specific features of the ancestor models is needed for the reader to understand the model setup. Both sections could be combined. Then make it more clear would are the improvements done here to the sediment model.

We improve the description of these models. The improvements are pointed out better in the description of the physical and biogeochemical processes.

pg. 5 footnote: Mention that these input files can be found in the specific stations folder. It took me a while to find it.

We add this to the first footnote of its kind.

pg. 6 ln. 1-3: Does that mean, porosity is always constant in the sediment column? Does the model also work with varying porosity?

This simplification has been made due to limited spatial availability of data for the 3-dimensional approach. While detailed spatial maps of surface porosity exist, vertical profiles are rare.

We added a new appendix section showing a comparison between a constant-porosity profile and another one with vertically varying porosity.

pg. 6 ln. 10 – 15: The alkalinity description is unmotivated and too technical. It would be more clear if you describe in a sentence or two how alkalinity is calculated and add the change in parameters in parenthesis. Also, I can't find a clear explanation for the reasoning of the approach in Section 2.6 as promised here (pg. 6, ln. 15).

We add here: "Alkalinity is a quantity describing the buffering capacity of a solution against adding acids, it describes the amount of a strong acid that needs to be added to titrate it to a pH of 4.3." In Section 2.6, we add: "Total alkalinity changes if acidic or alkaline substances are added or removed. The substances occurring in our model equations which change alkalinity are OH-, H3O+ and PO43- ions." Also, we move the quantitative description of alkalinity change to Section 2.6.

pg. 6 Section 2.3 Transport processes: There are a lot of often very short subsections. I would propose to have just 2 subsections: 2.3.1 Ocean 2.3.2 Fluff layer/Sediment. Then using different paragraphs for different processes to increase readability.

We prefer to keep the short subsections since the length of the text now increases due to the description of the fluff layer processes.

No changes to manuscript.

pg. 6 ln. 25: "... lateral transport processes have a major impact." please give reference

We add three references, Schneider et al. 2010 and Emeis et al. and Christiansen et al. 2002.

pg. 6 ln. 29-30 relax wintertime nutrients in the surface layer: Is this approach adopted from somewhere (Ref)? Does this lead to realistic results?

No, this approach is not adopted. It by definition leads to realistic results for the wintertime nutrient concentrations, which mostly determine the export production of the surface layer.

pg. 7 ln. 2: The parameterisation of lateral tranport is transport is discussed in this section (see 2.3.9 Parameterisation of lateral transport)

We change the reference from 2.4 to 2.3.9

pg. 7 ln. 6-9: more information needed fo unpublished model run. KPP used without explanation

We add more information on the 3-d model run which produced the data. KPP is spelled out as K profile parametrisation.

pg. 9 Particle sinking: Is there a reference for the different sinking speeds?

They are taken from the previous ERGOM version, where they were just obtained by model calibration as described.

No changes to manuscript.

pg. 9 ln. 14: replace "from" with "as"

We do the suggested replacement.

pg. 9ln. 23: where does the rate of bioerosion come from? Ref?

They are taken from a previous ERGOM version (Neumann and Schernewski, 2008), where they were just obtained by model calibration.

We add "This value was obtained by calibration of a previous 3-d version of ERGOM (Neumann and Schernewski, 2008)." We also add a reference for the bioresuspension process (Graf and Rosenberg, 1996).

pg. 10 ln. 10-15: coupling of fluff and sediments unclear Also why 3mm? What is a typical thickness, what influences it?

We agree that a more mathematical formulation is required to clearly describe the coupling of fluff and sediments. For the 3mm, they are estimated from observed SPM concentrations during times when fluff was suspended due to exceedance of the critical bottom shear stress.

We add a mathematical formulation of the coupling between fluff and sediment. Also, we add the following:

"We, however, assume it to be perfectly compacted (phi = 0) to be able to apply the above equation to describe the exchange process, and therefore assume a thickness of 3 mm. This describes a volume estimate of SPM taken from this region: Typical SPM concentrations in the lowermost 40 cm of the water column are about 8 mg/l higher compared to the value 5 m above the sea floor (Christiansen et al. 2002). As the density of these particles is just slightly higher than that of the surrounding water, we can estimate their volume at approximately 3 l/m² which gives 3 mm of height if perfectly compacted. Assuming this perfect compaction is not a physical assumption but rather a numerical trick which we use to transport the fluff material into the sediments. In reality, the fluff layer may be up to a few centimetres thick, and the incorporation of organic matter into the sediment is done by macrofaunal activities, e.g. (van de Bund et al., 2001)."

pg. 10 ln. 16-20: reference for the approach? Also, the oxygenation of the sediment column effects the depth/rate of bioturbation! Is this not represented in the model? I.e. is bioturbation possible even in the sulfidic zone? If you just fit your model to a specific site you probably change this manually but what are you doing when coupled to a 3D ocean model?

There is no reference for the approach, it is just based on the assumptions that (a) bioturbation decreases with depth and (b) there is no bioturbation below a certain maximum depth. In the present model we have no "switching-off" of bioturbation in the sulfidic zone. This partly reflects the fact that certain bioturbators may generate local oxic zones inside a sulphidic environment, e.g. by ventilating their burrows, and we do not account for this spatial heterogeneity, but partly it is just an unrealistic simplification. An extension of the model where the vertical transport of solids is influenced by biogeochemistry would certainly be a desirable extension of the model.

We add: "The present formulation of the model has no explicit dependence of bioturbation depth on the availability of oxidants, i.e. bioturbation will take place in oxic as well as in sulphidic environments; adding this dependence should be essential if the model shall be applied to sulphidic areas."

pg. 11 ln. 6-9: Give equation for the exchange flux. Again the 3mm here...

We give this equation. We add: “In reality, the diffusive boundary layer thickness is on the order of 1 mm at low bottom shear situations and becomes even shallower if the bottom shear increases (e.g. Jorgensen and Des Marais, 1990). We choose a larger value because we need to account for the transport through the fluff layer as well. A future model version might include a dependence of this parameter on the bottom shear stress.”

pg. 11 ln. 22: replace “sediments” with settles or is deposited. I assume the sediment accumulation is taken as advective transport in the diagenetic model!? Clarify in the text.

We do the replacement by “is deposited”. We replace “as a downward movement” by “as a downward advection” in the following sentence to clarify.

pg.12 ln. 6-11: why transport away/towards different sites? explain/justify

We replace “movement” in the explanation above by “advection of fluff layer material” to clarify the explanation.

pg. 12 Biogeochemical processes in the water column: add references for previously published ERGOM version you mean (ln. 16) and the equations for the processes described in the following subsections (2.4.1 – 2.4.5) with tables of parameters and their values as used in the model equations (see general comments).

As described on top of this author’s response document, it is by purpose that we do not include all equations and constants in the main text of the manuscript. We did not change anything in the water column BGC processes compared to the previous model version, so we do not give their quantitative description in our main text. We insist on keeping the details separate in the supplementary material.

We give references for previous ERGOM versions and make clear to which one we refer (Neumann et al. 2017) as our “ancestor model version”.

pg. 13 ln. 18: rewrite to “from previous ERGOM versions”. I find the use of the term detritus here confusing as you use organic carbon/material in the rest of your manuscript - Particulate organic carbon (POC) might be a better choice

The term “detritus” is used as this in all previous ERGOM model descriptions, so we use it here as well. “Particulate organic carbon” neglects the fact that our “detritus” contains N and P as well. “Particulate organic material” is also inaccurate as this would include living organisms, while detritus is the dead component only. This is why we use the footnote to exactly describe what we mean.

No changes to manuscript.

pg. 13 ln. 19-23 / 24-26: The decay rate constants and the partitioning into reactivity-classes are probably the most important steps for the model output (e.g. Arndt et al., 2013, Hülse et al., 2018). Therefore, this deserves some more words and justification.

The choice of classes is just designed to match the Middelburg model.

We give a justification of the chosen values in a new appendix section, where we compare the Middelburg decay rate over time with ours.

pg. 13 decay rate constants: where do the 0-degree values come from? - are they representative for your study area? - how do you know? - and how is it temperature dependent? Give equation!

The Middelburg equation does not include a temperature dependence, and the geographic locations at which their measurements were made include a large temperature range. Since we know that microbial decomposition is temperature dependent, we have to choose a baseline temperature, and the 0°C choice is indeed somewhat arbitrary. Luckily the model is not very sensitive to this choice, as a higher baseline temperature, meaning a lower decomposition rate of each class, would be compensated for by a shift in the class composition, leaving higher concentrations of quickly-degradable detritus classes which means an overall very similar total decomposition rate.

We give references (Thamdrup et al. 1998, Sawicka et al. 2012) for the temperature dependence and include these sentences: “The 0°C choice is somewhat arbitrary. Luckily the model is not very sensitive to this choice, as a higher baseline temperature, meaning a lower decomposition rate of each class, would be compensated for by a shift in the class composition, leaving higher concentrations of quickly-degradable detritus classes which means an overall very similar total decomposition rate.”

pg. 13 Partitioning: Is the Middelburg approach not for OM at the sediment-water interface? Could you please clarify and give the equation used to calculate the fractions. Also what is the fraction of the non-decaying detrital?

Middelburg 1989 actually includes a graph showing the dependency of sulphate reduction rates with depth up to 1 m to support the exponential model.

We give details on the calculation in the new appendix section. We add a table giving decay rates and the corresponding mass fractions, including that of the non-decaying one of 18%.

pg.15 ln. 25-26: Give equation for conversion from SO4 to H2S depending on the diffusive CH4 flux from below the model domain

We give this stoichiometric equation together with all others in a table.

pg. 16 ln. 1: you DO favour the latter theory because your rate constants are independent of the TEA. Or am I wrong? / pg. 16 ln. 1-2: You say:”...we chose to adopt the decay rates proposed by Middelburg (1989), which may implicitly take the effect of the oxidant into account.” I do not understand this statement. If I remember it right, the Middelburg (1989) rate model is the same for oxic and anoxic conditions.

Middelburg states that material which is decomposed later will be decomposed slower. This may be because the material itself is different, or because the oxidant is different. The Middelburg model includes both effects. Now in a mechanistic model we might want to separate the effects, but that’s tricky because there is this controversial discussion. So what we do assume if we just apply the Middelburg model is that the time which a particle spends in the oxic zone, in the anoxic zone, in the sulphidic zone is similar in our setting and in Middelburg’s experiments. In this case, the Middelburg model will include the correct slowing-down of degradation caused by the less efficient oxidant. If, in contrast, our particle enters the sulphidic zone very quickly, the Middelburg model might predict a faster degradation since it anticipates the particle might still be in an oxic environment.

We add a footnote after “implicitly takes the effect of the oxidant into account”: “Middelburg states that material which is decomposed later will be decomposed slower. This may be because the material itself is different, or because the oxidant is different. The Middelburg model includes both effects, and splitting them in a mechanistic model would mean preferring one theory or the other. So what we do assume if we just apply the Middelburg model is that the time which a particle spends in the oxic zone, in the anoxic zone, in the sulphidic zone is similar in our setting and in Middelburg’s experiments. In this case, the Middelburg model will include the correct slowing-down of degradation caused by the less efficient oxidant.”

Also what are the values of your degradation rate constants? They are the most important parameters in the diagenetic model. List them e.g. in a table, together with the rate constants for the water column and the fractions for the OM partitioning.

We add the requested table.

pg. 16 ln. 3: change “their study”. It is just one author.

We change it.

pg. 16 ln. 4-7 preferential release of P: under which conditions is P preferentially released? Is this important for your study area? As you say on page 13 ln. 16: "anoxic conditions which, however, do not occur in our study area."

The study of Jilbert et al. 2011 states that this is the case in anoxic conditions, so the corresponding factor is applied in the absence of oxygen only in Reed et al. and in our model. Our model description is wrong here in stating that the factor is constant, in fact it is redox dependent, thank you for noticing this! Anoxic conditions occur inside the sediments in our region of interest, not at the sediment surface.

We change the sub-sentence to “as well as a constant factor_pref_remin_p which describes a redox-dependent ratio between the mineralisation speeds of OP and organic carbon and nitrogen. This factor is set equal to 1 under oxic conditions and greater than 1 under anoxic conditions.”

pg. 16 t_detp_n :refer to table A1. How do you get the t_detp_n and t_det_n numbers for H? I understand that detritus is 50% enriched in C and P and how the values for C, N, O, P are calculated. But H does not add up. Should H for t_det_n & t_sed_n not be 22.875?; pref_remin_p: what’s the value and where does it come from?

You are right, the value given here for H is wrong, in fact it is 22.875, as t_det_? is $(CH_2O)_{1.5*106/16}(NH_3)_1$ and t_detp_n is $(H_3PO_4)_{1.5*1/16}$. factor_pref_remin_p equals to 10, which is the geometric average of the values used in Reed et al. 2011, but we do not give values in the main text.

We change the value for H in Table A1 and add a reference to it.

pg. 16 2.5.2 Specific mineralisation processes: Add table for reaction network as mentioned in general comments

We add the desired table.

pg. 16 ln. 17-20: The description is very vage - list the station specific content e.g. in table 2 and what is the “small amount of reducible iron”? Quantify!

We add the station-specific content to Table 2 and add the number of 0.1 mass-% to the text.

pg. 16 ln. 24-25: reference for statement

We add the following reference: e.g. Sunagawa, Ichiro. 1994. „Nucleation, Growth And Dissolution Of Crystals During Sedimentogenesis and Diagenesis“. In: Developments in Sedimentology, K. H. Wolf and G. V. Chilingarian, 51:19–47. Diagenesis, IV. Elsevier. https://doi.org/10.1016/S0070-4571(08)70435-7.

pg. 17 2.5.4 Pyrite formation: you did some model development here: add equations to make in more clear

We describe our additions in detail here, giving a quantitative mathematical description.

pg. 18 ln. 8-9: state the formula

We give the formula.

pg. 18 2.5.6 Reoxidation of reduced substances: There is a lot of information about the reaction network here. A summary of all that in a table would be very helpful! Also just use either iron-II/III or Fe-II/III, don’t mix them up

We add a table of the reaction network. We replace iron-II and iron-III by Fe-II and Fe-III throughout the manuscript.

pg. 19 2.6 Carbon cycle: this is also a new model development – at least include the equations you use to calculate pH and pCO2.

We give the formulas we use for the iterative calculation process.

pg. 20 ln. 4 mode splitting method: give some quick background what this is and a reference

We combine the two sentences: “The equations which determine the temporal evolution of the state variables are solved by a mode splitting method, i.e. concentration changes due to physical and biogeochemical processes are applied alternately in separate sub-timesteps. For a discussion of this method and alternatives we refer to Butenschön et al. (2012)”

pg. 21 ln. 7: style. Change to: ... in the Southern Baltic Sea (see Fig. 1, we always present the stations from west to east).

We change this following your suggestion.

pg. 21 ln. 9: units of salinity of 20 is missing

We add g/kg as unit.

pg. 21 ln. 21: replace “interface” with interfaces / pg. 22 ln. 14: replace “So” with thus / pg. 22 ln. 22: replace “sampled” with samples

We do the requested replacements.

pg. 23 4.2 Initial and boundary conditions: ERGOM model: more information needed for the unpublished model run as stated in general comments Is the relaxation approach of DIN and DIP adopted from somewhere? Does this lead to realistic results?

No, this approach is not adopted. It by definition leads to realistic results for the wintertime nutrient concentrations, which mostly determine the export production of the surface layer.

We add more information on the 3-d model run which produced the data.

pg. 24+25 4.3.2 Optimisation strategies: Why do you talk about the application of the AHR-ES algorithm which is in the end not used at all? Delete this part.

We delete it and just mention that we used it and were not successful, since we believe this may be an important piece of information for others.

pg. 25 ln. 19 - end: What parameters are changed? What is the range they are varied in (add table to appendix)? Why don’t you show any results of the optimisation? Are the final parameter values realistic, e.g. compared with other models or data? What are the most important parameters?

We add a table of original and changed parameters to a new appendix section which also includes a discussion of model sensitivity to the different parameter choices.

pg. 26 4.4 Manual correction of sand and silt station: How exactly did you modify the parameters? This is needed for reproducibility of your results!

We add: “This modification meant raising bioturbation and bioirrigation intensity by a factor of 10 at each station. Afterwards we reduced the parameter r_fluffy_moveaway which describes the rate at which fluff layer material is transported to the deeper areas until realistic concentrations in the pore water profiles were reached.”

pg. 26 ln. 6: which detritus is meant here (just POC or POC with mineral particles)? - rephrase “out of the sediments”

We rephrase “by keeping detritus out of the sediments” to “by an unrealistically low incorporation of reactive particulate material into the sediments”.

pg. 26 - 5.1.1 Pore water profiles at mud stations: It should be easy to check with the data if the variability at site AB is because they are 23km apart.

We use different symbols for the different locations in the plot now.

pg. 30 ln. 1 phosphate is in the right panel

We correct this to “the profiles of ammonium and phosphate (middle and right panel in Fig. 6)”

pg. 31. ln. 3-4: reference for this statement

We add the following reference: Meysman, Filip J.R., Volodymyr S. Malyuga, Bernard P. Boudreau, and Jack J. Middelburg. 2008. „A Generalized Stochastic Approach to Particle Dispersal in Soils and Sediments“. Geochimica et Cosmochimica Acta 72 (14): 3460–78. https://doi.org/10.1016/j.gca.2008.04.023.

pg. 31 ln. 6: rephrase

Rephrased to “In Figure 8a, we compare measured bioturbation diffusivities DB to those used in the model.”

pg. 33 Conclusion: ignoring the N-cycle because it’s not part of the SECOS project: This is a rather poor justification, especially as you say later: "... where the efflux of nutrients from the sediment strongly influences water column biogeochemistry, like in our study area." and "... denitrification [...] may strongly influence marine ecosystems".

Within the SECOS project, no measurements of e.g. nitrification or denitrification rates have been performed. This prevents us from a comparison of the model performance regarding the N cycle with direct measurements.

We rephrase the sentence to “For example, the nitrogen cycle was not compared to observations, which is due to the fact that the project SECOS in which this work was done did not focus on it and so the required observations of nitrification or denitrification rates were missing.”

pg. 37 Table A1: stoichiometry of t_h2s is wrong: it should have 2*H and 1*S

We correct this error in the manuscript, thank you for noticing!

**Reviewer 3 – general comments**

* In the introduction and conclusion, the emphasis while presenting the ERGOMSED model is put on the online coupling between the Benthic and Pelagic part. However this online coupling is not valorised in the results and discussion section. This should be enhanced. Neither the pelagic part nor the solutes exchanges between the benthic and pelagic part are mentioned in the results, although the conclusion states that “In the long term, biogeochemical ocean models should aim at a process-resolving description of surface sediments. This is especially true for shallow ocean areas where the efflux of nutrients from the sediment strongly influences water column biogeochemistry, like in our study area.” In the case that benthic fluxes, for any reason, are not available within SECOS (which would be surprising), ranges from the litterature could be used for comparison, and it would also be relevant to compare benthic fluxes to the lateral fluxes (inferred from the nudging procedure for the pelagic nutrients) to stress the relevance of such coupled framework.

We do include a comparison to measured exemplified bentho-pelagic fluxes now as an additional model validation.

* The fluff layer approach is an interesting feature of the coupling set-up, and a practical solution to handle solids lateral transport and exchanges between benthic and pelagic part. To my knowledge, the use of a fluff layer is not systematic in B-P coupled models and I would have found relevant to enforce introduction and discussion on this aspect.

We put more emphasis on this coupling approach now by mentioning its novelty and adding a more detailed mathematical description of the coupling.

* Appendix B supposedly justifies the inclusion of enhanced dynamics in the benthic model. This should be more developed. In particular: 1) Has the same calibration procedure been applied "from scratch" after having switched off those processes;

No, it has not, since the calibration procedure was very time consuming. So the comparison is somewhat unfair in this context.

We mention this in Appendix B now.

2) Some of the “reduced” experiments actually seems to behave better than the reference simulation. Can the authors justify their modification in this context ?

Both the model without correction for the diffusion of alkalinity and the model without adsorption to clay minerals gives higher concentrations of Fe-II in the pore water, which is in this case closer to observations. However, for both processes we know they exist, so leaving them out would mean a contradiction to our approach of a mechanistic representation. This approach is now pointed out stronger in the introduction.

**Reviewer 3 – specific comments**

* P3L13 : I suggest to add a references on ecosystem services ( for instance : https://cices.eu/content/uploads/sites/8/2012/07/CICES-V43_Revised-Final_Report_29012013.pdf)

We add the suggested reference.

* From P9L17-19 and P10L10-15 I had understood that solid compounds were only transferred from the distinct fluff and upper sediment layers through bioturbation (which includes here also other mixing effects). However, at P11L29 we learn that accumulation (advection) also induces a transfer from the fluff to the sediments. This may be introduced earlier (eg. end of Sect. 2.3.3) and explained in more details.

We give a more thorough mathematical description of the vertical transport processes now, which includes the representation of sediment growth as a downward advection.

* Tab 1. : Benthic tracers (both solids and dissolved) are defined in mol/m2 which doesn't correspond with the definitions given in P10L6 and P10L25. Is there a general transfomation applied to get those in units of mol/volume of liquids/solids ?

Yes there is, and the conversion is absolutely straightforward.

We give this transformation in the framework of the mathematical description of the vertical transport processes now.

* P10L10-20 : Bioturbation rate are defined for the sediment compartment. Is the uppermost value used for diffusion between the fluff layer and the uppormost sediment cell ? please precise.

Yes it is.

In our new formulation we are more precise and explicitly describe the flux between the compartments.

* Sect 2.4: Interactions between phosphate and iron aren't described for the water column. Are t_ipw, t_ihw and t_mow only included to enable a lateral transport of resuspended solids, or is there possible biogeochemical transformation in the water column ?

Indeed oxidation of Fe-II and Mn-II, reduction of Fe-III and Mn-IV, and adsorption of phosphate to iron oxyhydroxides may also happen in the water column.

We added the corresponding sections to the description of water column processes.

*P24L3 : In general, it might be relevant to comment which parameters were considered for the calibration and which were adapted, which were considered as equals for all stations and which were considered to differ between stations.

We add a table stating this to a new appendix section which also describes the sensitivity of the model to a variation in the parameters.

* P24L15: It is not clear whether $\Delta_i$ is defined specific only to each variables, or specific also to each station, or also to each sampling depth. This is relevant as refferred to when discussing model performances.

It is neither individual to a station nor to a sampling depth.

We add a footnote stating this.

* P26L3 : Should the first “bioirrigation” be replaced by “bioturbation” ?

Yes indeed. Thank you for noticing!

We replace „estimated bioirrigation rates“ by “bioturbation rates”

* Sect 5.12 : As is true for numerous model of this type, application in sandy sediments might be limited to the the lack of consideration of processes specific to permeable sediments. “Whashout” is mentioned in Sect 2.3.3, but this isn’t the only aspect of it. This should be discussed. For instance in this section. You might refer to the review from Huettel et al, 2013.

Thank you for this suggestion!

We add some discussion on the specifics of permeable sediments and refer to the suggested review article.

* P30L2-3 : Switch “higher” and “lower”.

Corrected, thanks!

* P30L19 : I don’t see a TOC maximum at the top of sediments for station DS.

That’s because the measurements we show in the background of the DS graph are mistakenly duplicated from the ST station.

We correct this in the figure.

Concerning this last paragraph, you could maybe consider the fact that the inability of the model to provide a TOC profile increasing with depth is related to the absence of dynamics specific to permeable sediments , washout in particular ? I insist on this point since it represents a major challenge for BP coupling intended to be implemented on shelves with mixed sand/mud conditions. I don’t ask that this be solved in this study, but the issue should be commented.

Very good point, we add some discussion on this. But this need not necessarily be washout, also nonlocal transport of fluff material into higher depths by bioturbating organisms might explain TOC profiles increasing with depth.

* Table A1 : t_h2s has one H and 2 S ? Is that an error in table or in the model ?

Corrected, thank you for noticing!

# Ecological ReGional Ocean Model with vertically resolved sediments (ERGOM SED 1.0): Coupling benthic and pelagic biogeochemistry of the south-western Baltic Sea

Hagen Radtke[1], Marko Lipka[2], Dennis Bunke[3,4], Claudia Morys[5,6], Jana Woelfel[7], Bronwyn Cahill[1,8], Michael E. Böttcher[2], Stefan Forster[5], Thomas Leipe[9], Gregor Rehder[7], and Thomas Neumann[1]

[1]Leibniz Institute for Baltic Sea Research Warnemuende (IOW), Department of Physical Oceanography and Instrumentation, Seestr. 15, 18119 Warnemünde, Germany
[2]Leibniz Institute for Baltic Sea Research Warnemuende (IOW), Department of Marine Geology, Geochemistry and Isotope Biogeochemistry Group, Seestr. 15, 18119 Warnemünde, Germany
[3]Leibniz Institute for Baltic Sea Research Warnemuende (IOW), Department of Marine Geology, Paleooceanography and Sedimentology Group, Seestr. 15, 18119 Warnemünde, Germany
[4]Current address: Leipzig University, Institute of Geophysics and Geology, Talstr. 15, 04013 Leipzig, Germany
[5]University of Rostock, Institute for Biosciences, Albert-Einstein-Str. 3, 18059 Rostock, Germany
[6]Current address: Royal Netherlands Institute for Sea Research (NIOZ), Department of Estuarine and Delta Systems, and Utrecht University, Korringaweg 7, 4401 NT Yerseke, The Netherlands
[7]Leibniz Institute for Baltic Sea Research Warnemuende (IOW), Department of Marine Chemistry, Working group on Trace Gas Biogeochemistry, Seestr. 15, 18119 Warnemünde, Germany
[8]Current address: Freie Universität Berlin, Institute for Space Science, Carl-Heinrich-Becker-Weg 6-10, 12165 Berlin, Germany
[9]Leibniz Institute for Baltic Sea Research Warnemuende (IOW), Department of Marine Geology, Microanalysis Group, Seestr. 15, 18119 Warnemünde, Germany

*Correspondence to:* Hagen Radtke (hagen.radtke@io-warnemuende.de)

**Abstract.** Sediments play an important role in organic matter mineralisation and nutrient recycling, especially in shallow marine systems. Marine ecosystem models, however, often only include a coarse representation of processes beneath the sea floor. While these parametrisations may give a reasonable description of the present ecosystem state, they lack predictive capacity for possible future changes, which can only be obtained from mechanistic modelling.

This paper describes an integrated benthic-pelagic ecosystem model developed for the German Exclusive Economic Zone (EEZ) in the Western Baltic Sea. The model is a hybrid of two existing models: the pelagic part of the marine ecosystem model ERGOM and an early diagenetic model by Reed et al. ~~, 2011.~~ (2011). The latter one was extended to include the carbon cycle, a determination of precipitation and dissolution reactions which accounts for salinity differences, an explicit description of adsorption of clay minerals and an alternative pyrite formation pathway. We present a one-dimensional application of the model to seven sites with different sediment types. The model was calibrated with observed pore water profiles and validated with results of sediment composition~~and bioturbation rates collected within the framework of the SECOS project.~~ , bioturbation rates and bentho-pelagic fluxes gathered by in situ incubations of sediments (benthic chambers). The model results generally give a reasonable fit to the observations, even if some deviations are observed, e.g. an overestimation of sulphide concentrations

in the sandy sediments. We therefore consider it a good first step towards a three-dimensional representation of sedimentary processes in coupled pelagic-benthic ecosystem models of the Baltic Sea.

# 1 Introduction

## 1.1 Importance of the bentho-pelagic coupling

Shallow coastal waters are the most dynamic part of the ocean due to the various effects of natural forcing and anthropogenic activities, they are characterised by the processing and accumulation of land-derived discharges (nutrients, pollutants etc.) which influence not only the coastal ecosystem but also the adjacent deeper sea areas. Shallow marine ecosystems often differ significantly from those in the deeper parts of the sea (Levinton, 2013). One important reason for this is the influence of sedimentary processes on the pelagic ecosystem. This influence can take place in a number of different functional ways, including:

- Remineralisation of organic matter produced in the water column fuels the subsequent release of nutrients and enhances the productivity of these regions (Berner, 1980).
- At the same time, nutrients can be buried in the sediment in a particulate form (Sundby et al., 1992) or be removed by denitrification (Seitzinger et al., 1984).
- Sulphate reduction in the sediments may lead to a release of toxic hydrogen sulphide (Hansen et al., 1978).
- Benthic biomass and primary production of benthic microalgae exceeds that of the phytoplankton in the overlying waters (Glud et al., 2009; Pinckney and Zingmark, 1993; Colijn and De Jonge, 1984) and represents a major food source for benthic organisms (Cahoon et al., 1999). In shallow regions, benthic primary production oxygenates the water column and competes with the pelagic one for nutrients (Cadée and Hegeman, 1974).
- Sediments serve as habitats for the zoobenthos, thereby affecting the overlying waters mainly via bioturbation or filtration (Gili and Coma, 1998).
- Other benthic organisms are food for opportunistic benthic/pelagic predator species, whose presence influences the pelagic system as well (Rudstam et al., 1994).
- Organisms typically inhabiting the pelagic may have benthic life stages and therefore rely on sediment properties for reproduction (Marcus, 1998).

This list, which could be continued, illustrates the importance of bentho-pelagic coupling for the functioning of shallow marine ecosystems.

### 1.2 Mechanistic sediment representation

In spite of this importance, the representation of the sediments in marine ecosystem models is often strongly oversimplified. This is understandable, since these models are constructed to answer specific research questions, and if these focus on pelagic processes, it can be desirable to represent sediment functions by the simplest-as-possible parametrisations. The drawback of using simple parametrisations is that they are mostly obtained from the present-day state. An example for such a parametrisation could be a percentage of organic matter which is remineralised in the sediments after its deposition and returned to the water column as nutrients. When ecosystem models are used not only to understand the present, but also to estimate future ecosystem changes in response to external drivers, this causes a problem: the use of such simple parametrisations means an implicit no-change assumption. In other words, the quantitative relationships described by the parametrisation will remain unchanged in future conditions, e.g. after the construction of a fish farm or in a changing climate. It is not straightforward to estimate the error introduced into the model system if this assumption is not valid.

An alternative to empirical parametrisations is the use of mechanistic models which try to derive the functionality of the subsystem from process understanding. For nutrient recycling in the sediments, this could be an early diagenetic model which estimates the final nutrient fluxes from a set of individual diagenetic processes.

Our aim is to construct a three-dimensional fully coupled model of pelagic and sediment biogeochemistry which does not make the no-change assumption. Specifically, we want to understand:

- How changes in early diagenetic processes affect the reaction of a shallow marine ecosystem to climate change?
- If pelagic ecosystem modelling can provide realistic deposition of particulate organic matter to reproduce the local variability in early diagenetic processes?

In this paper, we report about first successful approaches of this goal: the construction of a combined benthic-pelagic biogeochemical model formulated in a one-dimensional, vertically resolved domain. The model is calibrated and applied to a specific area of interest, the south-western Baltic Sea. It provides the basis for the development of a three-dimensional framework.

### 1.3 Combining models of sedimentary and pelagic biogeochemistry

Marine biogeochemical models and process-resolving sediment models are very similar to each other in terms of their approach. They both try to describe a complex biogeochemical system with a limited set of state variables. Transformation processes are formulated as a parallel set of differential equations ~~, e. g. (van Cappellen and Wang, 1996).~~ (e.g., van Cappellen and Wang, 1996). These have to obey the principle of mass conservation for any chemical element whose cycle is part of the model system. But in spite of these similarities, and even though both types of models have been extensively applied at least since the 1990s, there have not been many attempts, at least published ones, to combine them into one single benthic-pelagic model system. The review of Paraska et al. (2014), which compares existing sediment model studies, lists 83 publications of which 10 ~~included~~ include a coupling to the water column.

~~A recent attempt to combine sediment and water column biogeochemistry in one model is the study by Yakushev et al. (2017), who developed one of the~~ In the simplest case, this coupling is only one-way: water column biogeochemistry is calculated first and then used as input for a sediment model. This type of models has e.g. been applied to the North Sea (Luff and Moll, 2004) and Lake Washington (Cerco et al., 2006). In these studies, full three-dimensional models were used for pelagic biogeochemistry investigations. The models aimed to explain regional patterns in sediment biogeochemistry.

To the best of our knowledge, the first fully coupled benthic-pelagic model system with vertically resolved benthic processes was published by Soetaert et al. (2001). They presented a modelling approach where the biogeochemistry of the Goban Spur shelf ecosystem (north-east Atlantic) was described in a horizontally integrated, one-dimensional model. In the present communication we present a similar approach, adapted to understand the role of the sediments for the ecosystem of the south-western Baltic Sea.

A number of fully coupled benthic-pelagic models have been published for different regions, each differing in the way the compartments are vertically resolved. In our study, we use several fixed-depth vertical layers both in the water column and in the sediment (Soetaert et al., 2001; Soetaert and Middelburg, 2009; Meire et al., 2013). Other studies use a two-layer sediment, where the boundary between the layers is defined by the oxic-anoxic transition rather than a fixed depth (Lee et al., 2002; Lancelot et al., 200 The opposite is true in the model of Reed et al. (2011), where the water column is resolved with two layers only, while the sediment processes which are clearly the focus of the study, are resolved on a fine vertical grid. These one-dimensional model studies also differ in the complexity of the biogeochemical reactions involved. One of the most complex early diagenetic models ~~published so far and integrated it~~ was recently published by Yakushev et al. (2017). This is integrated into the Framework for Aquatic Biogeochemical Models (FABM, www.fabm.net). ~~The FABM~~ This generic interface allows coupling to any biogeochemical model within its framework~~. We would like to refer to their study for a good overview of existing models which bring together water column biogeochemistry with a sophisticated sediment modelling approach. They range from~~ , from one-dimensional ~~, sediment-centered approaches with a small pelagic extension, e. g. (Reed et al., 2011), to full three-dimensional pelagic ecosystem modelswhich have a complex representation of sedimentary processes and nutrient pools included, e. g. ERSEM (Butenschön et al., 2016).~~ setups (as we described before) to three-dimensional applications. Our one-dimensional approach presented here can also be seen as an intermediate step towards a fully coupled three-dimensional ecosystem model, with a vertically resolved sediment model coupled under each grid cell. The way to go from the current model to the 3-d version is already pointed out in the model description.

There are a few successful regional applications of three-dimensional setups with coupled water column and sediment biogeochemistry. Sohma et al. (2008) present such a model for Tokyo Bay, where they use it to explain the occurrence of hypoxia and to understand the carbon cycle in the bay (Sohma et al., 2018). Brigolin et al. (2011) developed a fully coupled 3-d model for the Adriatic Sea and use it to estimate the seasonal variability of N and P fluxes. The ERSEM model (Butenschön et al., 2016) is another example of two-way coupling of complex benthic and pelagic biogeochemical models, which treats sediments in a different way: Here, they are vertically resolved into three different layers (oxic, anoxic, sulphidic), and the pore water exchange between them follows a near-steady-state assumption. Another recent example is a Black Sea study by Capet et al. (2016), in which the authors ~~applied~~ apply a hybrid approach with a vertically integrated early diagenetic model. ~~To obtain~~

~~the~~ The partitioning between different oxidation pathways, ~~which is~~ typically determined by the vertical zonation, ~~they ran~~ is obtained by running a one-dimensional, vertically resolved model (OMEXDIA ~~,~~ (Soetaert et al., 1996a)) over a range of different boundary values and ~~fit~~ fitting a statistical meta-model through its output.

~~To our best knowledge, the first fully coupled benthic-pelagic model system with vertically resolved benthic processes was published by Soetaert et al. (2001). They presented a modelling approach where the biogeochemistry of the Goban Spur shelf ecosystem (North-East Atlantic) was described in a horizontally integrated model. In the present communication we present a similar aproach, adapted to understand the role of the sediments for the ecosystem of the~~ Our region of interest is the Baltic Sea, in the first instance, its south-western ~~Baltic Sea. The presented one-dimensonal aproach can be seen as an intermediate step towards a fully coupled three-dimensional ecosystem model , with a vertically resolved sediment model coupled under each grid cell. The way to go from the current model to the 3-d version is already pointed out in the model description~~part where coastal marine sediments play an important role in the transformation and removal of nutrients from the water column. We combine two existing models which have already been successfully applied in the Baltic Sea, namely, the pelagic ecosystem model ERGOM (Neumann et al., 2017) and the early diagenetic model by Reed et al. (2011), to obtain a full benthic-pelagic model of the southwestern Baltic Sea. In the latter, several modifications were implemented as will be described.

### 1.4 The German part of the Baltic Sea and the SECOS project

The Baltic Sea is a marginal sea with only narrow and shallow connections to the adjacent North Sea. The small cross sections of these channels, the Danish Straits, and the correspondingly constrained water exchange have several implications for the Baltic Sea system~~, including the following~~:

- It is ~~an essentially~~ essentially a non-tidal sea.
- It is brackish due to ~~a~~ mixing between episodically inflowing North Sea water with Baltic river waters which ~~cause~~ causes an overall positive freshwater balance.
- It shows a pronounced haline stratification.
- It is prone to eutrophication due to the accumulation of mostly river-derived nutrients.

The German Exclusive Economic Zone (EEZ) in the Baltic Sea is situated to the south of the Danish Straits. It consists of different bights, islands and peninsulas and exhibits a strong zonal gradient and a strong temporal variability in salinity. This varies from 12 to over 20 g kg$^{-1}$ north of the Fehmarn island to 7 to 9 g kg$^{-1}$ in the Arkona Sea (IOW, 2017). ~~In river-influenced near-coastal areas, even~~ Even lower salinities occur ~~.~~

in river-influenced near-coastal areas. Most of the sediment area is characterised by erosion or transport bottoms which only intermittently store deposited material before it is transported further into the central basins of the Baltic Sea (Emeis et al., 2002). Still, during this storage period, organic material is already partly mineralised and inorganic nitrogen is partly removed from the ecosystem by denitrification processes (Deutsch et al., 2010). This transformation of a ~~eutrophic~~ bioavailable sub-

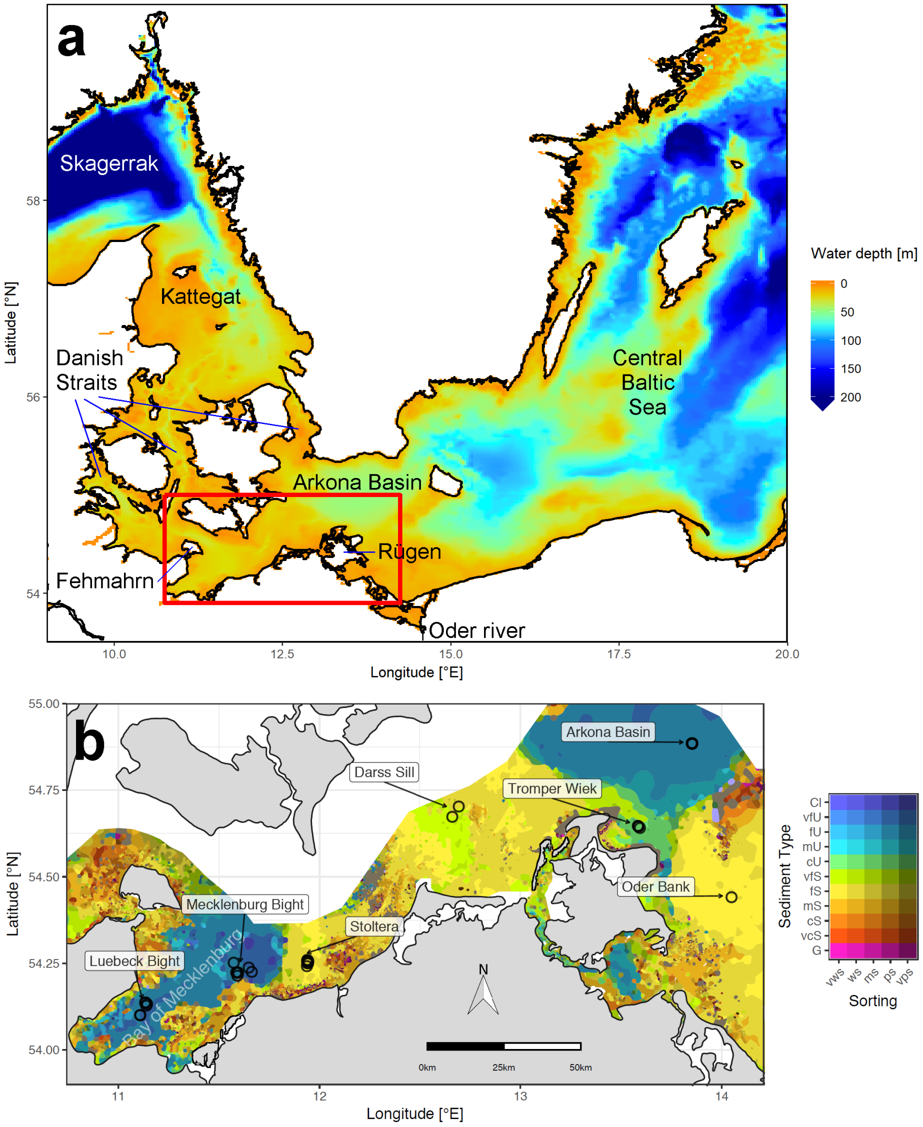

**Figure 1.** (a) Bathymetry of the Western Baltic Sea and location of our area of interest. (b) The investigation area of the SECOS project. The map shows granulometry, redrawn from Tauber (2012) and ~~Lipka et al. (2018a)~~Lipka (2018), and the seven stations considered in this model study. Sediment Type: Cl = clay, vfU = very fine silt, fU = fine silt, mU = medium silt, cU = coarse silt, vfS = very fine sand, fS = fine sand, mS = medium sand, cS = coarse sand, vcS = very coarse sand, G = gravel; Sorting: vws = very well sorted, ws = well sorted, ms = moderately sorted, ps = poorly sorted, vps = very poorly sorted.

stance into a non-reactive form and its subsequent removal is one example of the type of ecosystem services (e.g., Haines-Young and Potsch coastal sediments can perform.

Understanding and quantifying the scope and scale of such sedimentary services in the German Baltic Sea has been the aim of the SECOS project (The Service of Sediments in German Coastal Seas, 2013 - 2019). The project contained a strong empirical part, including several interdisciplinary research cruises focused on ~~the sediments~~ sediments characterisation. Seven study sites were selected, based on different granulometric parameters, each of them representative of a larger area. These were sampled several times in order to capture the effect of seasonality on biogeochemical functioning (see Figure 1). The sampled stations include three sandy sites: Stoltera (ST), Darss Sill (DS) and Oder Bank (OB), ~~a silty site: Tromper Wiek (TW), and~~ three mud sites: Lübeck Bight (LB), Mecklenburg Bight (MB) and Arkona Basin (AB) and a silty site: Tromper Wiek (TW). The TW site has both an intermediate grain size and an intermediate organic matter content, compared to the sandy and muddy sites. In this work, we focus on the development of our coupled one-dimensional benthic-pelagic model system for the German Baltic Sea. We use empirical data obtained from repeated sampling of the SECOS stations to calibrate and validate our early diagenetic model. Further work, discussing the fully coupled three dimensional application of the model to assessing sedimentary services in the German Baltic Sea will be described in a forthcoming paper.

### 1.5 ~~Article structureThe rest of this paper is~~ Differences in biogeochemistry between permeable and impermeable sediments

In the study area, different types of sediments dominated by varying grain size fractions are found ranging from sand to mud. This implies differences in the biogeochemical processes associated with organic matter mineralization and physical processes that are responsible for pore water and elemental transport in the sediment and across the sediment-water interface. Due to their relatively larger grain sizes, sand acts as a permeable substrate, which means that lateral pressure variations may induce advection of interstitial water. These pressure variations may be caused by waves or by the interaction between horizontal near-bottom currents and ripple formation. In muddy sediments, in contrast, molecular diffusion often controls the transport of dissolved species, which may, however, be superimposed by the bioirrigating activity of macrozoobenthos (Boudreau, 1997; Meysman et al., 2006).

These substantial differences cause differences in the biogeochemical properties of the substrate types. Porewater advection in permeable sediments does not only transport solutes but also particulate material. Fresh and labile organic matter (POC and DOC) from the fluff layer can be quickly transported into permeable sediments, the latter in this way acting as a kind of bioreactor. The typically low contents of reactive organics in sand led for a long time to the consideration of sands as “geochemical deserts” (Boudreau et al., 2001). In parallel, the low content of clay minerals and associated organic matter is often accompanied by lower microbial cell numbers when compared to muddy substrates (e.g., Llobet-Brossa, 1998; Böttcher et al., 2000). It has, however, been shown that microbial turnover rates also in sands may be high (Werner et al., 2006; Al-Raei et al., 2009). Actually, the supply of fresh organic material may lead to fast microbial degradation rates comparable to those of the organic-rich muddy sediments where more refractory organic material is accumulating at depth. The high mixing rates of pore water in the sands then bring together reactants for secondary reactions like coupled nitrification-denitrification, which makes these areas an effective biological filter, even if pore water concentrations are low compared to impermeable sediments. In our area of investigation, oxygen fluxes and sulphate reduction rates are comparable between sandy and muddy sites, while the organic content differs by an order of magnitude (Lipka et al., 2018b).

### 1.6 Fluff layer representation

As mentioned earlier, the transport of fluffy layer material from coast to basin areas is an important process in our region of interest. Previous studies with a pelagic ecosystem model (Radtke et al., 2012), which includes fluff layer dynamics, support this experimental finding and highlight the role of this mechanism for the overall nutrient exchange between coasts and basins. For this reason, we explicitly include the fluff layer in our model as a third compartment in addition to water column and sediment. This approach, which is similar to Lee et al. (2002), is in contrast to most other coupled benthopelagic models. We see the explicit representation of the fluff layer dynamics as one of the major advantages of our model.

### 1.7 Article structure

This article is structured as follows. In Section 2 ~~presents~~ we present a description of the model and the processes which are included. In Section 3, we summarise which empirical data were used and give a brief explanation on how they were obtained. In Section 4, we describe how these data were used to fit the model to the different stations, since the seven stations mentioned before serve as the test case for our model. The model results are shown and discussed in Section 5, where we provide a summary of the scope of model application and its limitations. The paper ends ~~in~~ with Section 6~~with~~ , in which conclusions and an outlook ~~which especially points at the future application of the model in~~ toward the model's future application within a three-dimensional ~~ecosystem models .~~ ecosystem model framework are given.

## 2 Model description

In this section, we give a description of the combined benthic-pelagic model. We start in Section 2.1 with a brief introduction to the two ancestor models it descended from. The model is a purely biogeochemical, not a physical model, so section 2.2 describes how the physics affecting the biogeochemical processes are prescribed. We then explain the model compartments and state variables in Section 2.3. Before giving the full model equations in Section 2.5, we first explain the vertical transport processes which occur in these equations in Section 2.4.

The core of model is obviously the biogeochemical processes represented within it. Their description therefore forms the major part of this manuscript. Biogeochemical processes in the water column are described in Section 2.6 and those in the sediment follow in Section 2.7. The carbonate system is the same in both compartments and is described separately in Section 2.8. Since most of the biogeochemical processes included in our model are already contained in preceding models in exactly the same way, we decided to only give a qualitative description of them in the main text. The quantitative details, including the values of the model constants we used, are presented in a separate, complete description in the supplementary material. In contrast, we give a detailed and quantitative description of the "new" processes in the main text, i.e. those that are less common or those that differ from the ancestor models, since we assume that this will be the most interesting part for the majority of readers. The supplementary material also contains a table of the model constants and the sensitivities of the model results to changes in the individual parameter values.

The model description is completed by giving details on numerical aspects in Section 2.9. Finally, in Section 2.10, we give a short note on the procedure by which we automatically generate the model code from a formal description of the model processes.

### 2.1 Ancestor models

~~The~~ The combined benthic-pelagic model is based on two ancestors~~.~~:

- The water column part is based on ERGOM, an ecological model developed originally for the Baltic Sea (Neumann, 2000). It has been continuously developed since its first publication, the latest improvements include introducing refractory dissolved organic nitrogen (Neumann et al., 2015), and transparent exopolymers ~~. It should be mentioned that the light absorption scheme described in Neumann et al. (2015) is not part of the model described here, since they were both developed simultaneously.~~

  ~~Since the beginning,~~ (Neumann et al., 2017). From the start, ERGOM contained three functional groups of phytoplankton, representing large-cell (diatom) and small-cell (flagellate) primary producers as well as diazotroph cyanobacteria, and the ability to simulate hypoxic/anoxic conditions.

  ERGOM is typically used in a three-dimensional context as a part of marine ecosystem models. With some modifications, it has been applied for different ecosystems such as the North Sea (Maar et al., 2011) and the Benguela upwelling system (Schmidt and Eggert, 2016). It is an intermediate-complexity model for the lower trophic levels up to zooplankton and has been applied for a broad range of scientific questions.

- The sediment part is based on a model developed for a study on the effect of seasonal hypoxia on sedimentary phosphorus accumulation in the Arkona Sea (Reed et al., 2011). This model is, as many others of its kind, a descendant of the van Cappellen and Wang (1996) model~~. This paper~~, which focused on the sedimentary iron and manganese cycle, ~~but also contained~~ and the mineralisation pathways of oxic mineralisation, denitrification, and sulphate reduction. An extensive literature survey (combined with model fitting to observations) allowed the estimation of a large quantity of model constants such as solubility products and half-saturation constants. These were later on inherited by several early diagenetic models, including the one presented in this article. These models solve the diagenetic equations, typically applied at a well-defined single site as a one-dimensional setup.

  Like the present one, the model by Reed et al. (2011) is a prognostic model and solves the time-dependent equations rather than making a steady-state assumption.

### 2.2 Physical parameters used in the model simulations

Since our model is a purely biogeochemical model, it requires a physical environment in which it is embedded. In a final, three-dimensional application, this will be a hydrodynamic host model, and the biogeochemical model described in this communication will be coupled into it. Since we do an intermediate step first and run the model in one-dimensional setups, we need to provide physical quantities as model input. The variables which influence the biogeochemical processes in the water column are

- temperature,
- salinity,
- light intensity,
- bottom shear stress and
- vertical turbulent diffusivity.

These are prescribed by forcing files[1] which need to be provided in order to run the one-dimensional model. We obtain these data from a three-dimensional model simulation of the Baltic Sea ecosystem (Neumann et al., 2017). This simulation was performed using the Modular Ocean Model (MOM) version 5.1 (Griffies, 2018). The model had a horizontal resolution of 3 n.m. and a vertical resolution of 2 m and covered the entire Baltic Sea. Open boundary conditions were applied in the Skagerrak at the transition to the North Sea. The model was driven by atmospheric forcing data from the coastDat dataset (Weisse et al., 2009) which were extended in time using data from the German Weather Service (Schulz and Schattler, 2014). The ERGOM ecosystem model, as described in the previous section, was implemented in the physical host model, so it produced a hindcast simulation of both physics and biogeochemistry of the Baltic Sea ecosystem. We extracted model output from the simulated year 2015 at the different locations as input for the 1-d model. Since we run the 1-d model for a longer period, the physical forcing is repeated every year.

### 2.3 Model compartments and state variables

The one-dimensional model consists of four compartments as shown schematically in Figure 2:

1. The water column,
2. a fluff layer deposited on the sediment surface,
3. the sedimented solids, and
4. the pore water between them.

---

[1] `physics/temperature.txt`, `physics/salinity.txt`, `physics/light_at_top.txt`, `physics/bottom_stress.txt`, `physics/diffusivity.txt`, found in the subdirectories `stations/station_??` in the supplementary material

The water column and the sediment are vertically resolved, the former in layers of 2 m depth such that their number depends on the water depth of the specific site, the latter in 22 layers increasing in depth from 1 mm at the sediment surface to 2 cm at the bottom of the modelled sediment in 22 cm depth. These specific numbers are not intrinsic to the model but can be changed in the input files[2]. The current choice of 22 cm for the sediment depth was taken according to the availability of pore water data.

The chosen vertical resolution must be seen as a compromise between speed and accuracy. Especially for the 3-d application, we want to keep the numerical effort of the calculations as small as possible. A comparison to a run with double resolution is shown in Appendix E, it shows minor deviations between the resolutions.

Sediment porosity is prescribed[3] and site-specific. As a simplifying assumption, accumulating organic material does not change the porosity. Similarly, the amount of material accumulated in the fluff layer does not change the remaining volume in the bottom water cell.

The tracers (model state variables) present in each of the compartments are listed in Table 1. All of the tracers have a fixed stoichiometric composition which is shown in Appendix A. Where stoichiometric ratios change, such as during detritus decomposition, more than one tracer is needed. This means we can check mass conservation at design time of the model by formulating it in a process-based way as outlined in Radtke and Burchard (2015). To check this mass conservation, the chemical reaction equations need to be formulated in a complete way, which is why "virtual tracers" such as water may be included in the process formulation, even if they do not occur as state variables in the model.

Total alkalinity is a parameter describing the buffering capacity of a solution against adding acids, it describes the amount of a strong acid that needs to be added to titrate it to a pH of 4.3. In our model, it is represented as a "combined tracer", which means that its rate of change depends on its constituents $(OH^-, H_3O^+, PO_4^{3-})$ which are actively produced or consumed. The ~~tracer value changes by 1 unit if (see Table 1)~~

- ~~`ohminus` is changed by 1 unit or~~
- ~~`h3oplus` is changed by -1 unit or~~
- ~~`t_po4` is changed by 0.5 units.~~

~~The~~ reasoning behind this is explained in Section 2.8.

The state variables will not be discussed one-by-one here, but rather in the section about the biogeochemical processes (Sections 2.6 and 2.7), where their role in the ecosystem will be explained.

~~Virtual tracers do not occur as a state variable in the model, but only as balancing terms in the biogeochemical process equations. They make it easier to check that the mass balance of all chemical elements is maintained.~~

---

[2] `physics/cellheights.txt, physics/sed_cellheights.txt`

[3] `physics/sed_inert_ratio.txt`

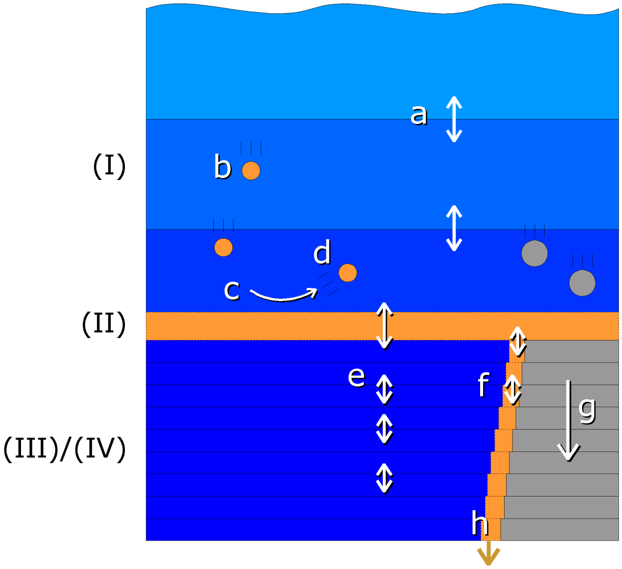

**Figure 2.** Schematic view of the compartments and vertical exchange processes in the model. Compartments: (I) water column, (II) fluff layer, (III) pore water, (IV) solid sediment. Both water column and sediment consist of several vertically stacked grid cells. Vertical transport processes: a = turbulent mixing, b = particle sinking, c = sedimentation, d = resuspension, e = bioirrigation combined with molecular diffusion, f = bioturbation, g = sediment growth, h = burial. Bioactive solid material is shown in orange, bioinert solid material in grey and water in blue.

## 2.4 Transport processes

The processes which transport the tracers vertically are schematically shown in Figure 2. Their detailed implementation is discussed here.

Horizontal exchange (transport) is neglected in our one-dimensional model. This is obviously an inadequate approximation for the water column processes, as we do not consider basins, but rather single stations, some of which are situated in proximity to river mouths, where lateral transport processes have a major impact (Schneider et al., 2010; Emeis et al., 2002; Christiansen et al., 2002). We solve this issue in the future application of the biogeochemical model in a three-dimensional model system (Cahill et al., in prep.).

In this model, we are not specifically interested in the water column as such but rather see it as being responsible for delivering the right amount of sedimenting detritus at the right time. To obtain this, we relax the wintertime nutrients in the surface layer to a realistic value. This may be seen as a ~~parameterisation~~ parametrisation of a lateral exchange process. In addition, transport of fluff layer material away from or towards the modelled location is a lateral process included in the model.

~~The parametrisations of these lateral transport processes are not discussed in this section, but together with the biogeochemical processes to which they closely correspond in Section 2.6. All other physical processes included will be described here, but~~

**Table 1.** Tracers used in the ERGOM SED v1~~.2sed~~.0 model

| name | W | F | S | P | description | unit |
|---|---|---|---|---|---|---|
| `t_lpp` | + | | | | large-cell phytoplankton | mol kg$^{-1}$ (N units) |
| `t_spp` | + | | | | small-cell phytoplankton | mol kg$^{-1}$ (N units) |
| `t_cya` | + | | | | diazotroph cyanobacteria | mol kg$^{-1}$ (N units) |
| `t_zoo` | + | | | | zooplankton | mol kg$^{-1}$ (N units) |
| `t_det_?` | + | | | | detritus, N+C, fast decaying (1) to inert (6) | mol kg$^{-1}$ (N units) |
| `t_detp_?` | + | | | | phosphate in detritus, fractions 1 to 6 | mol kg$^{-1}$ (N units) |
| `t_don` | + | | | | autochthonous dissolved organic nitrogen | mol kg$^{-1}$ |
| `t_poc` | + | | | | particulate organic carbon | mol kg$^{-1}$ |
| `t_ihw` | + | | | | suspended iron hydroxide | mol kg$^{-1}$ |
| `t_ipw` | + | | | | suspended phosphate bound to ~~iron-III~~ Fe-III | mol kg$^{-1}$ |
| `t_mow` | + | | | | suspended manganese oxide | mol kg$^{-1}$ |
| `t_n2` | + | | | + | dissolved molecular nitrogen | mol kg$^{-1}$ |
| `t_o2` | + | | | + | dissolved molecular oxygen | mol kg$^{-1}$ |
| `t_dic` | + | | | + | dissolved inorganic carbon | mol kg$^{-1}$ |
| `t_alk` | + | | | + | total alkalinity | mol kg$^{-1}$ |
| `t_nh4` | + | | | + | ammonium | mol kg$^{-1}$ |
| `t_no3` | + | | | + | nitrate | mol kg$^{-1}$ |
| `t_po4` | + | | | + | phosphate | mol kg$^{-1}$ |
| `t_h2s` | + | | | + | hydrogen sulphide | mol kg$^{-1}$ |
| `t_sul` | + | | | + | elemental sulphur | mol kg$^{-1}$ |
| `t_so4` | + | | | + | sulphate | mol kg$^{-1}$ |
| `t_fe2` | + | | | + | ferrous iron | mol kg$^{-1}$ |
| `t_ca2` | + | | | + | dissolved calcium | mol kg$^{-1}$ |
| `t_mn2` | + | | | + | dissolved manganese-II | mol kg$^{-1}$ |
| `t_sil` | + | | | + | silicate | mol kg$^{-1}$ |
| `t_ohm_quickdiff` | + | | | + | OH- ions with realistically quick diffusion | mol kg$^{-1}$ |
| `t_ohm_slowdiff` | + | | | + | OH- ions which move unrealistically slow with alkalinity | mol kg$^{-1}$ |
| `t_sed_?` | | + | + | | sedimentary detritus N+C, fractions 1 to 6 | mol m$^{-2}$ (N units) |
| `t_sedp_?` | | + | + | | phosphate in sedimentary detritus, fractions 1 to 6 | mol m$^{-2}$ (N units) |
| `t_ihs` | | + | + | | iron hydroxide in the sediment | mol m$^{-2}$ |
| `t_ihc` | | + | + | | iron hydroxide in the sediment - crystalline phase | mol m$^{-2}$ |
| `t_ips` | | + | + | | iron-bound phosphate in the sediment | mol m$^{-2}$ |
| `t_ims` | | + | + | | iron monosulphide | mol m$^{-2}$ |
| `t_pyr` | | + | + | | pyrite | mol m$^{-2}$ |
| `t_mos` | | + | + | | manganese oxide in the sediments | mol m$^{-2}$ |
| `t_rho` | | + | + | | rhodochrosite | mol m$^{-2}$ |
| `t_i3i` | | + | + | | potentially reducible ~~iron-III~~ Fe-III in illite-montmorillonite mixed layer minerals | mol m$^{-2}$ |
| `t_iim` | | + | + | | ~~iron-II~~ Fe-II adsorbed to illite-montmorillonite mixed layer minerals | mol m$^{-2}$ |
| `t_pim` | | + | + | | phosphate adsorbed to illite-montmorillonite mixed layer minerals | mol m$^{-2}$ |
| `t_aim` | | + | + | | ammonium adsorbed to illite-montmorillonite mixed layer minerals | mol m$^{-2}$ |
| `h2o` | | virtual | | | water molecule | |
| `h3oplus` | | virtual | | | hydronium ion | |
| `ohminus` | | virtual | | | hydroxide ion | |
| `i2i` | | virtual | | | structural ~~iron-II~~ Fe-II in illite-montmorillonite mixed-layer minerals | |

W: Water column, F: Fluff layer, S: Solid sediment, P: Pore water, `?`: reactivity classes 1 to 6.

~~only in a qualitative way. For a quantitative description including the model constants we refer to the online supplementary material.~~ The physical processes which are explicitly included in our model are described here.

### 2.4.1 Turbulent mixing

The vertical exchange due to turbulent mixing in the water column is prescribed externally[4] by a turbulent diffusivity. In our case, it is taken from a three-dimensional MOM5 model run ~~(Radtke, unpublished)~~Neumann et al. (2017). In this model setup, turbulent vertical mixing is estimated by the KPP turbulence ~~parameterisation (Large et al., 1994)~~scheme (K profile parametrisation, Large which considers both local mixing and, in case of unstable stratification, (non-local) convection. We only take into account the local part of the mixing and apply it to all tracers in the water column.

### 2.4.2 Particle sinking

In our model, suspended particulate matter sinks at a constant rate through the water column. We choose 4.5 m day$^{-1}$ for detritus, 1 m day$^{-1}$ for manganese and iron oxides, including the phosphate adsorbed by them, and 0.5 m day$^{-1}$ for large-cell phytoplankton and particulate organic carbon. In contrast, cyanobacteria are not sinking but, due to their positive buoyancy, they show an upward movement of 0.1 m day$^{-1}$. In reality, the sinking rate differs between individual particles; the currently chosen average values are a result of fitting the previous ERGOM model with the simplified sediment representation to observations.

### 2.4.3 Sedimentation and resuspension

~~The shear~~ Shear stress at the bottom determines whether erosion or sedimentation takes place. We apply the combined shear stress of currents and waves calculated by the same MOM5 model as the turbulent mixing. If this shear stress $\tau$ is below a critical value of ~~0.016~~$\tau_c = 0.016$ N m$^{-2}$ (Christiansen et al., 2002), the sinking suspended matter accumulates in the fluff layer compartment. If it is exceeded, the fluff layer material is resuspended into the lowest water cell at a constant relative rate $r_{ero} = 6$ day$^{-1}$.

In our model, no material will ever be resuspended from the sediment itself, which starts below the fluff layer. This means that our model is incapable of realistically capturing extreme events like storms or bottom trawling which winnow the upper layers of the sediment, removing ~~the organic material~~organic material, which has a lower sinking velocity, by separating it from the heavier mineral components (Bale and Morris, 1998). It also neglects a washout, that is, the removal of organic matter from the sediment pores by advective transport of pore water by strong bottom currents (Rusch et al., 2001). In our model, sediment reworking by currents and waves is not explicitly represented, but rather parametrised together with the bioturbation process. This process allows a bi-directional exchange of particulate material between ~~sediment and~~ the sediment and the fluff layer, see Section 2.4.5. The upward component of the transport represents winnowing of sediments (Bale and Morris, 1998).

---

[4] `physics/diffusivity.txt`

### 2.4.4 Bioerosion

In environments with oxic bottom waters, we assume that in addition to waves and currents, macrofaunal animals or demersal fish can resuspend organic material from the fluff layer by active movements (Graf and Rosenberg, 1997). Therefore, under oxic conditions, we assume that ~~3~~$r_{biores} = 3$ % day$^{-1}$ of the fluff material is resuspended independently from the shear stress conditions. This number was estimated from calibration of a three-dimensional Baltic Sea ecosystem model (Neumann and Schernewski, 2008) where the process proved to be critical for transporting organic matter to the deep basins below a depth of approx. 60 m. In these depths, a resuspension due to wave-induced shear stress is no longer possible.

### 2.4.5 Bioturbation

Bioturbation describes the movement and mixing of particles inside the sediment caused by ~~animals~~the zoobenthos.[5] In fact, it is ~~hard~~ difficult to discriminate what causes the vertical mixing of particles; also physical effects like bottom shear may have the same effect. We therefore include them in our “bioturbation” process.

We consider bioturbation to act as a vertical diffusivity $D_{B,solids}(z)$ on the concentrations of the different solid species in the sediment. This implies we exclude non-local mixing processes, even if they may be important in nature (Soetaert et al., 1996b), and try to represent them by local mixing.

~~The vertical mixing follows the equation~~

~~$$\frac{\partial}{\partial t}(1-\phi)c \quad = \quad \frac{\partial}{\partial z}\left((1-\phi)D_{B,solids}\frac{\partial c}{\partial z}\right),$$~~

~~(Boudreau, 1997). Here $c(z,t)$ denotes a tracer concentration with respect to the volume of the solids only , $D_{B,solids}(z)$ is the bioturbation intensity and $\phi(z)$ is the porosity. This equation only takes~~ We only take intraphase mixing into account, which means we assume that the porosity $\Phi(z)$ remains constant over time. ~~The factor $(1-\phi)$ relates the concentration to the total (solid + liquid) volume of the sediment.~~

The ~~same equation~~ diffusivity $D_{B,solids}(z)$ is also applied to describe the transport between the uppermost sediment layer and the fluff, which is caused by benthic organisms. In reality, the fluff layer may strongly differ in its compaction (porosity) depending on the turbulence conditions. ~~We, however,~~ However, we assume it to be perfectly compacted ($\phi = 0$) to be able to apply the above equation to describe the exchange process, and therefore assume a thickness of 3 mm. This is not a physical assumption but rather a numerical trick which we use to transport the fluff material into the sediments. In reality, ~~this~~ the fluff layer may be up to a few centimetres thick, and the incorporation of organic matter is done by macrofaunal activities ~~, e. g. (van de Bund et al., 2001)~~(e.g., van de Bund et al., 2001).

The value of 3 mm describes a volume estimate of SPM (suspended particulate matter) taken from this region: typical SPM concentrations in the lowermost 40 cm of the water column are about 8 mg/l higher compared to the value 5 m above the sea floor (Christiansen et al., 2002). As the density of these particles is just slightly higher than that of the surrounding water,

---

[5] While bioturbation in reality causes both a transport of solids and solutes, we use the term “bioturbation” in the model to describe the transport of solids only, while the transport of solutes is done by the “bioirrigation” process.

we can estimate their volume at approximately 3 l m$^{-2}$ which gives 3 mm of height if perfectly compacted. We see this explicit treatment of the fluff layer as a major advantage compared to a deposition of sinking particles directly into the surface sediments. We regard it as essential for the application of the model in a three-dimensional setting.

The vertical structure of bioturbation intensity, $D_{B,solids}(z)$, is parametrised vertically as follows:

$$D_{B,solids}(z) = \begin{cases} D_{B,solids,max} & \text{for } z < z_{full} \\ D_{B,solids,max} \exp\left(-\frac{z - z_{full}}{z_{decay}}\right) & \text{for } z_{full} < z < z_{max} \\ 0 & \text{for } z_{max} < z \end{cases} \tag{1}$$

In the uppermost part of the sediment, we assume a constant bioturbation rate. Below that, it decays exponentially with depth until it reaches a maximum depth, which may be below the bottom of our model. So, we externally prescribe (a) the maximum mixing intensity[6] and (b) three length scales describing the vertical structure of bioturbation[7], which are the depth down to which the maximum mixing rate is applied ($z_{full}$), the length scale of exponential decay of the mixing rate below this depth ($z_{decay}$), and the maximum depth of mixing ($z_{max}$).

The present formulation of the model has no explicit dependence of bioturbation depth on the availability of oxidants, i.e. bioturbation will take place in oxic as well as in sulphidic environments; adding this dependence should be essential if the model was applied to sulphidic areas.

### 2.4.6 Bioirrigation

Bioirrigation describes the mixing of solutes within the pore water and the exchange with the bottom water. ~~To model it , we apply a similar equation,~~

$$\frac{\partial}{\partial t}\phi c = \frac{\partial}{\partial z}\left(\phi D_{B,liquids}\frac{\partial c}{\partial z}\right),$$

~~(Boudreau, 1997). Here $c(z,t)$ denotes a tracer concentration with respect to the volume of the pore water only and $D_{B,liquids}(z)$ is the bioirrigation intensity . Again we assume that the porosity is constant in time. We also use this equation for the solute exchange between the pore water and the overlying bottom water cell.~~ We describe it as a mixing intensity $D_{B,liquids}(z)$. The vertical profile of bioirrigation intensity is assumed identical to that of bioturbation. The maximum bioirrigation rate is assumed constant in time and prescribed externally[8].

---

[6] `physics/sed_diffusivity_solids.txt`

[7] `physics/sed_depth_bioturbation.txt`

[8] `physics/sed_diffusivity_porewater.txt`

### 2.4.7 Molecular diffusion

Molecular diffusion in the sediment ~~is~~ can be described by the equation

$$\underline{\frac{\partial}{\partial t}}\phi(z)\frac{\partial}{\partial t}c(z,t) = D_0(z)\frac{\partial}{\partial z}\left(\underline{\frac{\phi}{\theta^2}\frac{\partial c}{\partial z}}\frac{\phi(z)}{\theta(z)^2}\frac{\partial c(z,t)}{\partial z}\right), \tag{2}$$

(Boudreau, 1997). Here $D_0$ describes the molecular diffusivity in a particle-free solution, which is effectively reduced by the effect of hydrodynamic tortuosity $\theta$. This describes the effect that the solutes need to travel a longer path as the direct way may be obstructed by solid particles. It is estimated from porosity by $\theta^2 = 1 - 2.02\ln(\phi)$ (Boudreau, 1997).

A diffusive exchange between the pore water and the overlying bottom water is controlled by the thickness of a diffusive boundary layer. While in reality this relates to the viscous sublayer thickness and is therefore inversely related to the velocity of the bottom water (Boudreau, 1997), we for simplicity assume a constant diffusive boundary layer thickness of 3 mm.

In reality, the diffusive boundary layer thickness is on the order of 1 mm at low bottom shear situations and becomes even shallower if the bottom shear increases (e.g., Gundersen and Jorgensen, 1990). We choose a larger value because we need to account for the transport through the fluff layer as well. A future model version might include a dependence of this parameter on the bottom shear stress.

Molecular diffusivities for the different solute species are calculated from water viscosity following Boudreau (1997). The water viscosity is determined from salinity and temperature (assumed to be identical to that in the bottom water cell).

A problem occurs with the combined tracers DIC and total alkalinity, as they do not represent a specific ion but rather a set of different species with different molecular diffusivities. For simplicity, we approximate DIC diffusivity to be that of the $HCO_3^-$ ion, the most common one at the pH values we expect. For total alkalinity, we take a two-step approach: ~~In~~ in the first step, we also take the diffusivity of the $HCO_3^-$ ion. But this is an underestimate especially for the $OH^-$ ions which increase in their concentration as the solution becomes alkaline. To take their higher diffusivity into account, we introduce two additional tracers, `t_ohm_slowdiff` and `t_ohm_quickdiff`. Before the molecular diffusion is applied during a model time step, they are both set equal to the $OH^-$ concentrations. During the diffusion time step, the former diffuses with the reduced $HCO_3^-$ diffusion rate, the latter with the $OH^-$ diffusivity. So afterwards, total alkalinity is corrected by adding the difference of the two, `t_ohm_quickdiff-t_ohm_slowdiff`. This results in a smoothed alkalinity profile.

### 2.4.8 Sediment accumulation

In nature, sediments grow upwards as new particulate matter ~~sediments~~ is deposited onto them. In our model, this process is taken into account, but represented as a downward ~~movement~~ advection of material in the sediment. So, our coordinate system moves upward with the sediment surface.

We assume that the sediment growth is supplied by terrigenous, bioinert material, and prescribe[9] a growth rate from literature for the mud stations only ~~,~~ (Table 7). ~~For the sand and silt stations we~~ We do not assume sediment growth for the sand and silt stations.

---

[9] `physics/sed_inert_deposition.txt`

We use a simple Euler-Forward advection to move the material from each grid cell into the cell below. Material leaving the model through the lower boundary is lost. ~~Only~~ Except for organic carbon, we assume that a part of it is mineralised, as will be explained in Section 2.7.1. In the top cell, new organic material from the fluff layer enters by sediment growth.

### 2.4.9 ~~Parameterisation~~ Parametrisation of lateral transport

The Baltic Sea sediments can be classified as accumulation, transport and erosion bottoms (Jonsson et al., 1990). The lateral transport of matter is characterised by ~~movement~~ the advection of fluff layer material from the transport and erosion bottoms in the shallower areas to the accumulation bottoms in the deep basins (Christiansen et al., 2002). As this process is not represented in our 1-d model setups, we need to parametrise it.

For the sandy and silty sediments, we assume a transport away from the site. This is described by a constant removal rate for all material deposited in the fluff layer.

For the mud stations, we assume a transport of organic material towards the site. This is described by a constant input of detritus. Our model contains six detritus classes which degrade at different rates, as will be explained later, in Section 2.6.4. We assume that the quickest-degradable part of the detritus is already mineralised ~~during the lateral migration~~ in the shallow coastal areas, before its lateral migration to the mud stations, and therefore exclude the first two classes from this artificial input.

In the 3-d version of the model, these processes are no longer required, as the material is dynamically removed from the shallow sites ~~is transported to the deeper ones~~ and transported to deeper ones by advection.

## 2.5 Model equations

### 2.5.1 Equations of motion

In this subsection, we will describe the equations of motion solved by the model. The equations in the water column can be derived from the assumption that the vertical (upward) flux of a tracer can be described by an advective and a diffusive flux which follows Fick's law:

$$F_z^{wat}(z,t) = w \cdot c^{wat}(z,t) - D^{wat}(z,t)\frac{\partial}{\partial z}c^{wat}(z,t)\,, \tag{3}$$

where $c^{wat}(z,t)$ denotes the tracer concentration and $D^{wat}$ is the turbulent diffusivity given as external forcing[10]. For particulate matter, the constant $w$ describes its vertical velocity relative to the water, which is negative if the particles are sinking. For dissolved tracers, $w$ is set to zero. We further assume that the water itself does not move vertically. In this case, conservation

---

[10] `physics/diffusivity.txt`

of mass yields an advection-diffusion equation:

$$\begin{aligned}\frac{\partial}{\partial t}c^{wat}(z,t) &= -\frac{\partial}{\partial z}F_z^{wat}(z,t)+q_c^{wat}(z,t)\\ &= -w\frac{\partial}{\partial z}c^{wat}(z,t)+\frac{\partial}{\partial z}\left(D^{wat}(z,t)\frac{\partial}{\partial z}c^{wat}(z,t)\right)+q_c^{wat}(z,t)\,, \end{aligned} \tag{4}$$

where $q_c^{wat}(z,t)$ describes the biogeochemical sources minus sinks of the considered state variable.

The equations in the sediment are different because we need to take porosity into account and treat dissolved tracers (in the pore water) and solid tracers differently. For the pore water tracers, the upward flux is given by

$$F_z^{pw}(z,t) = -\phi(z)\cdot D^{pw}(z,t)\frac{\partial}{\partial z}c^{pw}(z,t)\,, \tag{5}$$

where $\phi(z)$ is the porosity of the sediment (the ratio between pore water volume and total volume) which we assume as constant in time. The concentration $c^{pw}(z,t)$ relates to the pore water volume only. The effective diffusivity $D^{pw}$ is the sum of two contributions, the effective molecular diffusivity $\frac{D_0}{\theta^2}$ and the effective (bio)irrigation diffusivity $D_{B,liquids}(z)$. The advection-diffusion equation is then given by

$$\phi(z)\frac{\partial}{\partial t}c^{pw}(z,t) = \frac{\partial}{\partial z}\left(\phi(z)\cdot D^{pw}(z,t)\frac{\partial}{\partial z}c^{pw}(z,t)\right)+q_c^{pw}(z,t)\,, \tag{6}$$

which is a well-known early diagenetic equation (Boudreau, 1997). For the solid-state tracers, their concentration $c^{sed}(z,t)$ relates to the volume of the solids only, and the flux is given by

$$F_z^{sed}(z,t) = (1-\phi(z))w(z)c^{sed}(z,t)-(1-\phi(z))\cdot D^{sed}(z,t)\frac{\partial}{\partial z}c^{sed}(z,t)\,, \tag{7}$$

where $w(z)$ is a velocity for a virtual vertical downward transport. It results from sediment growth due to deposition of particulate material, but as we keep the sediment-water interface at a constant position in our model, we need to describe the increasing depth in which we find individual sediment particles as a downward advection. Volume conservation of the particulate material requires that we can write $w(z)$ as

$$w(z) = \frac{w_0}{1-\phi(z)}, \tag{8}$$

such that the vertical velocity gets smaller in depths where the sediment is more compacted, and $w_0$ describes a theoretical velocity which would occur at perfect compaction ($\phi=0$)[11]. The advection-diffusion equation then reads

$$(1-\phi(z))\frac{\partial}{\partial t}c^{sed}(z,t) = -w_0\frac{\partial}{\partial z}c^{sed}(z,t)+\frac{\partial}{\partial z}\left((1-\phi(z))\cdot D_{B,solids}(z)\frac{\partial}{\partial z}c^{sed}(z,t)\right)+q_c^{sed}(z,t)\,. \tag{9}$$

---

[11] `physics/sed_inert_deposition.txt`

Practically, we do not store the concentration $c^{sed}(z,t)$ (mol m$^{-3}$) as a state variable but rather the quantity of the tracer per area in a specific layer, $C^{sed}(k,t)$ (mol m$^{-2}$), where $k$ is a vertical index. The transformation is straightforward,

$$C^{sed}(k,t) = \int\limits_{z_{bot,k}}^{z^{top,k}} (1-\phi(z))\, c^{sed}(z,t)\, dz\,. \tag{10}$$

For particulate tracers, we also consider a storage in the fluff layer, $C^{fluff}(t)$, which is measured in mol m$^{-2}$. The equation for $C^{fluff}(t)$ is derived in the following subsection.

### 2.5.2 Boundary conditions

Boundary conditions are required for the partial differential equations given above. We give two boundary conditions for the water column concentrations: one at the sea surface, $z_{surf}$ and one at the sediment-water interface, $z_0$. We also give two boundary conditions for the sediment concentrations: one at the sediment-water interface, $z_0$, and one at the lower model boundary, $z_{bot}$. We start describing the boundary conditions from bottom to top for the dissolved tracers, and then continue describing them from top to bottom for the particulate / solid-phase state variables.

The pore water tracers have a zero-flux boundary condition at the bottom of the model:

$$F_z^{pw}(z_{bot},t) = 0. \tag{11}$$

An exception to the zero-flux boundary is the parametrisation of sulphide production in the deep which will be discussed later.

At the sediment-water interface, we assume that the dissolved tracers are exchanged between pore water and water column via a diffusive boundary layer of a depth $\Delta z_{bbl}$. So, our upper boundary condition for the pore water tracers is given by

$$F_z^{pw}(z_0,t) = -\phi(z_0)\cdot D^{pw}(z_0,t)\,\frac{c^{wat}(z_0,t)-c^{pw}(z_0,t)}{\Delta z_{bbl}}\,. \tag{12}$$

This flux can be directed into or out of the sediment, depending on where the concentration is larger.

To satisfy mass conservation, the vertical flux applied as the lower boundary condition for the dissolved-species concentrations in the water column depends on the upward flux from the sediment:

$$F_z^{wat}(z_0,t) = F_z^{pw}(z_0,t) + \tilde{Q}_c^{fluff}(t). \tag{13}$$

The additional term $\tilde{Q}^{fluff}(t)$ represents the sources minus sinks of the dissolved state variable which are caused by biogeochemical transformations of the fluff layer material. At the sea surface, we apply a zero-flux condition, both for dissolved and for particulate state variables:

$$F_z^{wat}(z_{surf},t) = 0. \tag{14}$$

An exception is only made for tracers which are modified by gas exchange with the atmosphere, e.g. oxygen.

Now the boundary conditions for the particulate state variables are different. The reason is that the water column and the sediment do not directly interact, but we consider the fluff layer as an intermediate layer between the two. Particulate material which sinks to the bottom is deposited in the fluff layer, from where it is incorporated into the sediments.

At the bottom of the water column, there can be two possible situations.

- If the bottom shear stress is lower than the critical shear stress, we assume a deposition of particulate material. This sinking material ($w < 0$) vanishes from the water column because of sedimentation. It appears in the fluff layer.
- If the bottom shear stress exceeds the critical shear stress, particulate material from the fluff layer is eroded and enters the water column.

In both cases, we additionally consider the bioresuspension process which was described above in Section 2.4.4. We can therefore formulate the boundary condition for particulate material as

$$F_z^{wat}(z_0,t) = \begin{cases} \min(w,0) \cdot c^{wat}(z_0,t) + r_{biores}(t) \cdot C^{fluff}(t) & \text{for } \tau(t) \leq \tau_c \\ r_{ero} \cdot C^{fluff}(t) + r_{biores}(t) \cdot C^{fluff}(t) & \text{for } \tau(t) > \tau_c \end{cases} . \qquad (15)$$

The fluff interacts with the surface sediment layer in two ways. Firstly, sediment growth means an incorporation of fluff layer material into the surface sediments. Secondly, bioturbation which is considered as a diffusion-analog mixing leads to an exchange of particulate material between fluff layer and surface sediment. So, the boundary condition for solids at the sediment surface is given by

$$F_z^{sed}(z_0,t) = w_0 \frac{C^{fluff}(t)}{\Delta z_{fluff}} - (1-\phi(z_0)) \cdot D^{sed}(z_0,t) \frac{\frac{C^{fluff}(t)}{\Delta z_{fluff}} - c^{sed}(z_0,t)}{\Delta z_{fluff}} . \qquad (16)$$

Here, $\Delta z_{fluff}$ represents a virtual thickness of the fluff layer assuming it was perfectly compacted, see the discussion in Section 2.4.5. In this way, the benthofaunal processes of incorporating fluff layer material into the surface sediments can be simply described as a diffusion-analog flux of particulates. The opposite processes which cause a removal of fine-grained material from the sediments, winnowing or washout, can in the same way be described as a diffusion process, in this case upward. This occurs in the model especially when the fluff layer material is resuspended during periods of high bottom shear and the concentration $C^{fluff}(t)$ is correspondingly low.

The concentration change in the fluff layer is then defined by mass conservation, and is simply given by

$$\frac{\partial}{\partial t} C^{fluff}(t) = F_z^{sed}(z_0,t) - F_z^{wat}(z_0,t) + Q_c^{fluff}(t) \qquad (17)$$

for all particulate state variables. Here, $Q_c^{pw}(t)$ describes the sources minus sinks term from the biogeochemical transformations of the considered state variable.

Finally, the burial of particulate material at the lower model boundary can be described by the following boundary condition:

$$F_z^{sed}(z_{bot},t) = w_0 c^{sed}(z_{bot},t) . \qquad (18)$$

So, we assume the particulate material to be buried forever when it leaves the model domain. An exception, as mentioned before, is the parametrisation of deep sulphide formation which is described in Section 2.7.

### 2.6 Biogeochemical processes in the water column

In this section, we describe the biogeochemical processes acting in the water column. These are mostly identical to previously published ERGOM versions (e.g., Neumann and Schernewski, 2008; Neumann et al., 2015), which contained a more simple, vertically integrated sediment model. As in the previous section, we provide the quantitative description including the model constants in the online supplement.

A reaction network table giving the reaction equations including their stoichiometric coefficients is given in Table 2.

#### 2.6.1 Primary production and phytoplankton growth

There are three classes of phytoplankton in the model, representing large-cell and small-cell microalgae as well as diazotroph cyanobacteria. Their growth is determined by a class-specific maximum growth rate, but contains two limiting factors ~~,~~ for nutrients and light. The light limitation is a saturation function with optimal growth at a class-specific optimum level or at 50% of the surface radiation. The short wave light flux at the surface is taken from a dynamically down-scaled ERA40 atmospheric forcing (Uppala et al., 2005), using the regional Rossby Centre Atmosphere model (RCA). Nutrient limitation is a quadratic Michaelis-Menten term for DIN (nitrate + ammonium) or phosphate, depending on which one is limiting, based on Redfield stoichiometry. Diazotroph cyanobacteria are only limited by phosphate and not by DIN, but they are only allowed to grow in a specific salinity range. Cyanobacteria and small-cell algae also require a minimum temperature to grow (Wasmund, 1997; Andersson et al., 1994).

~~In case that~~ However, according to Engel (2002) although nutrients are limiting ~~, photosynthesis continues at the same rate and consumes DIC, producing dissolved oxygen. Carbon is then exudated in the form of transparent exopolymers (Engel, 2002), which~~ an enhanced polysaccharide exudation could be the result of a cellular carbon overflow, whenever nutrient acquisition limits biomass production but not photosynthesis. These transparent exopolymers are included in our model, they are assumed to have a constant sinking velocity.

#### 2.6.2 Phytoplankton respiration and mortality

We assume a constant respiration of phytoplankton which is proportional to its biomass. As the model maintains the Redfield ratio, the ~~respiration~~ degradation of biomass (catabolism) goes along with an excretion of ammonium and phosphate. This simplified description of phytoplankton growth does not describe day/night metabolism or temperature dependence. A small fraction of the nitrogen is released as dissolved organic nitrogen (DON). In the model, this represents the DON fraction which is less ~~utilizable~~ utilisable by phytoplankton, while the fraction with high bioavailability is considered to be part of the ammonium state variable.

~~Phytoplankton~~ Due to simplification, in our model phytoplankton experiences a constant background mortality~~.~~, although we know this is far away from reality where it is species-specific and depends on abiotic (e.g. nutrient, light etc.) and biotic conditions. An additional mortality is generated by grazing of zooplankton as described next.

#### 2.6.3 Zooplankton processes

Zooplankton is only represented as one bulk state variable.

It grows by assimilating any type of phytoplankton, however, it has a smaller food preference for the cyanobacteria class compared to the other classes. The uptake becomes limited by a Michaelis-Menten-function if the zooplankton´s food approaches a saturation concentration. Feeding can only take place in oxic waters and is temperature-dependent. It shows a maximum at an optimum temperature and a double-exponential decrease when this temperature is exceeded.

Both zooplankton respiration and mortality represent a closure term for the model. They are meant to include the respiration and mortality of the higher trophic levels (fish) which feed on zooplankton, therefore we use a quadratic closure. Mortality is additionally enhanced under anoxic conditions which, however, do not occur in our study area.

#### 2.6.4 Mineralisation processes

The description of detritus[12] differs from the previous ERGOM versions. We have split the detritus into six classes, depending on its degradability. This degradability is described as a decay rate constant, which ranges from 0.065 $\text{day}^{-1}$ for the first class to $1.6 \cdot 10^{-5}$ $\text{day}^{-1}$ for the fifth class, while the last one is assumed to be completely bioinert. This type of model is known as a “multi-G model” ~~, (Westrich and Berner, 1984).~~ (Westrich and Berner, 1984).

Details on the specific choice of the classes are given in Appendix B.

The mineralisation is, however, temperature dependent by a $Q_{10}$ rule (Thamdrup et al., 1998; Sawicka et al., 2012), as it is realised by microbial processes; the values given above are valid at 0°C. The 0°C choice is somewhat arbitrary. Actually, the model is not very sensitive to this choice, as an enhanced baseline temperature, meaning a lower decomposition rate of each class, would be compensated for by a shift in the class composition, leaving higher concentrations of quickly-degradable detritus classes which means overall a very similar total decomposition rate, see Appendix B.

When organic detritus is created by plankton mortality, it is partitioned into the different classes in a constant ratio. This ratio was determined from a fit of the multi-G model to an empirical relation between detritus age and its relative decay rate which was proposed by Middelburg (1989). The fraction of non-decaying detritus was estimated from empirically determined carbon burial rates in the Baltic Sea (Leipe et al., 2011).

The chemical composition of detritus is, in contrast to phyto- and zooplankton, not determined by the Redfield ratio. It is enriched in carbon and phosphorus by 50 %, such that it has a C:N:P ratio of 159:16:1.5. This resembles detritus compositions as they were determined in sediment traps and by investigating fluffy layer material in the Baltic Sea (Heiskanen and Leppänen, 1995; Emeis et al., 2000, 2002; Struck et al., 2004).

---

[12] Throughout the manuscript, we use the term “detritus” in its biological meaning. Here it describes dead particulate organic material only, as opposed to its use in geology, where the term includes deposited mineral particles.

In the water column, detritus can be mineralised by three different oxidants: oxygen, nitrate and sulphate. They are utilised in this order; if the preferential oxidant's concentration declines, the specific pathway is reduced by a Michaelis-Menten limiter and the next pathway takes over such that the total mineralisation is held constant. In all pathways, DIC, ammonium and phosphate are released. Nitrate reduction also produces molecular nitrogen (heterotrophic denitrification), while sulphate reduction generates hydrogen sulphide.

Mineralisation of particulate organic carbon in transparent exopolymers takes place via the same pathways, but only releases DIC. DON is also mineralised after some time and decays to ammonium (which may represent the transformation to bioavailable DON compounds).

### 2.6.5 Reoxidation of reduced substances

In the presence of oxygen, ammonium is nitrified to nitrate ~~, e. g. (Guisasola et al., 2005).~~ (e.g., Guisasola et al., 2005). The intermediate step, formation of nitrite, is omitted in the model.

Hydrogen sulphide can be reoxidised by oxygen or by nitrate (chemolithoautotrophic denitrification) ~~, e. g. (Bruckner et al., 2013).~~ (e.g., Bruckner et al., 2013). This takes place as a two-step process via the formation of elemental sulphur (Jørgensen, 2006).

All reoxidation processes exponentially increase their rates with temperature.

In the sediments, we additionally assume that $Fe^{2+}$ can be produced as a reduced substance. If it is released from the sediments and enters the water column, it can be reoxidised by oxygen, creating suspended iron oxyhydroxides.

### 2.6.6 Adsorption and desorption reactions

Dissolved phosphate can be adsorbed to iron oxyhydroxide particles suspended in the water column. In the same way, phosphate adsorbed to iron oxyhydroxide particles can be released if the ambient concentration of phosphate is low. The process is identical to the one in the sediments and is discussed in Section 2.7.5 in detail.

## 2.7 Biogeochemical processes in the fluff layer, sediment and pore water

In this section, we qualitatively describe the sedimentary biogeochemical processes contained in the model. For a quantitative description including the model constants, we refer to the online supplementary material. Figure 3 gives a schematic overview of the processes considered in the sediment model. As every model, the chosen set of biogeochemical processes and variables does not aim at completeness in its representation of reality, but rather at the strongest possible simplification which still retains the required complexity to describe the processes we are interested in. For this reason, we do not, for example, consider methane formation explicitly.

The stoichiometry of the processes included in the model is shown in three reaction network tables:

- Primary redox reactions are given in Table 3.
- Secondary redox reactions are given in Table 4.

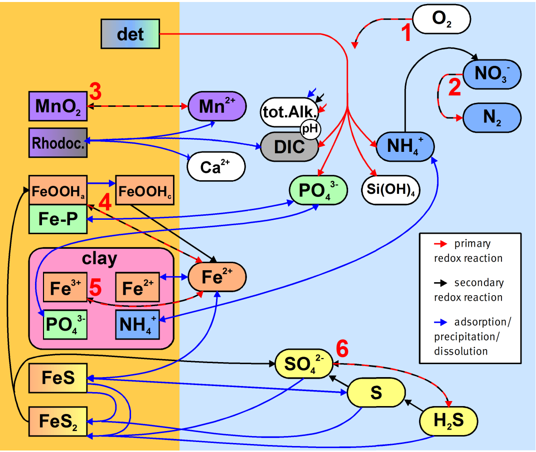

**Figure 3.** Simplified sketch of state variables and processes in the sediment model. Boxes to the left and right indicate sediment and pore water state variables, respectively. pH is not a state variable but calculated from DIC and total alkalinity. Red arrows show primary redox processes, driven by oxidation of organic carbon. The red numbers indicate the order in which the oxidants are utilised. Black arrows show secondary redox reactions, which means reoxidation of reduced substances. Blue arrows show adsorption/desorption or precipitation/dissolution reactions, which may depend on pH. Abbreviations: det = detritus, Rhodoc. = rhodochrosite, tot.Alk. = total alkalinity, DIC = dissolved inorganic carbon

- Adsorption/desorption and precipitation/dissolution reactions are given in Table 5.

### 2.7.1 Mineralisation in general

The mineralisation of detritus is the dominant biogeochemical process in the sediments, as the oxidation of the carbon therein is the major supply of chemical energy for microbes.

As in the water column, oxidants are utilised in a specific order, and a smooth transition to the next mineralisation pathway occurs when the preferred one gets exhausted. However, the number of possible oxidants is increased in the sediment, as here also solid components may act as electron acceptors. The order in which they are utilised is (Boudreau, 1997):

1. oxygen
2. nitrate
3. manganese oxide
4. iron oxyhydroxide
5. ~~iron-III~~ Fe-III contained in clay minerals
6. sulphate

After sulphate is exhausted, typically the formation of methane would start. This process is omitted in the current model, as we designed our model for the top 22 cm of the ~~German~~ south-western part of the Baltic Sea, where we do not expect sulphate to be limiting. This depth restriction is based on the limited length of the sediment cores taken in the empirical part of our research project. We do, however, describe the process implicitly, since we assume that a part of the organic carbon which leaves the model domain through the lower boundary will be transformed to methane, which, as it diffuses upward will be oxidised by sulphate and generate $H_2S$. Therefore, we parametrise this process by a conversion from sulphate to hydrogen sulphide at the lower boundary.

As in the water column, we distinguish between six different classes of detritus with different basic mineralisation rates. Details on the specific choice of the classes are given in Appendix B.

These rates are only controlled by temperature, not by the specific oxidant which is available. There is an ongoing controversy as to what determines the rate of sedimentary carbon decay, whether it is the oxidant (and therefore the accessible energy per mole of carbon) or the degradability of the detrital carbon itself (Kristensen et al., 1995; Arndt et al., 2013). In leaving out the explicit dependence of the oxidant, we do not favour the latter theory; we chose to adopt the decay rates proposed by Middelburg (1989), which may implicitly take the effect of the oxidant into account~~. This can be interpreted as an implicit assumption that this effect will not differ too much between our modelled sites and the ones investigated in their study.~~[13].

Sedimentary organic phosphorus (OP) may degrade faster than the corresponding nitrate and carbon, an effect known as preferential P mineralisation (Ingall and Jahnke, 1997). We include this by introducing additional state variables `t_detp_n` for each class `n` of detritus, describing the OP concentration, as well as a constant factor `pref_remin_p` which describes a ~~constant~~ redox-dependent ratio between the mineralisation speeds of OP and organic carbon and nitrogen. This factor is set equal to 1 under oxic conditions and greater than 1 under anoxic conditions (Jilbert et al., 2011). This approach follows Reed et al. (2011).

### 2.7.2 Specific mineralisation processes

Here we describe the implementation of the primary redox reactions, indicated by the red numbers in Figure 3.

Oxic mineralisation and heterotrophic denitrification are formulated in the same way as in the water column, see Section 2.6.4.

The next pathway is the reduction of Mn-IV to Mn-II which produces dissolved manganese.

The reduction of iron oxyhydroxides should produce dissolved ~~iron-II~~Fe-II. This, however, may precipitate very quickly, especially where hydrogen sulphide is present. So for numerical reasons, we combine these reactions, and the reduced ~~iron-III~~ Fe-III is directly converted into iron monosulphide or considered as adsorbed by clay minerals, as we describe below in 2.7.3.

---

[13] Middelburg's equation states that material which is decomposed later will be decomposed slower. This may be because the material itself is different, or because the oxidant is different. The Middelburg model includes both effects, and splitting them in a mechanistic model would mean preferring one theory or the other. So what we do assume if we just apply the Middelburg model is that the time which a particle spends in the oxic zone, the anoxic zone, and the sulphidic zone is similar in our setting to Middelburg's experiments. In this case, the Middelburg model will include the correct slowing-down of degradation caused by the less efficient oxidant.

Some clay minerals, especially sheet silicates which are abundant in the German part of the Baltic Sea (Belmans et al., 1993), contain structural iron which is available for redox reactions ~~, e. g. (Jaisi et al., 2007).~~ (e.g., Jaisi et al., 2007). We prescribe a station-specific content of these minerals given in Table 7 and assume that they contain a small amount (0.1 mass-%) of reducible iron, because ~~in~~ a particle analysis of sheet silicates from the ~~investigated area~~ area of interest (Leipe, unpublished data), ~~we found~~ showed slightly lower iron contents in the ~~sulfidic~~ sulphidic zone compared to the surface area.

The primary redox reaction follows process 32 in Table 3, we describe it in detail since it is a new process added to our model. Mineralisation of organic carbon under reduction of structural iron in sheet silicates takes place at a rate of

$$\texttt{p\_i3i\_}k\texttt{\_irred\_i2i} = \texttt{t\_sed\_}k \cdot r_k \cdot exp(\tau \cdot T) \cdot (1 - l_{o2}) \cdot (1 - l_{no3}) \cdot (1 - l_{mos}) \cdot (1 - l_{ihs}) \cdot l_{i3i}\,, \tag{19}$$

where `t_sed_`$k$ is the amount of detritus per area in a specific sediment layer, $r_k$ is a basic reactivity for this class (see Appendix B), $\tau = 0.15\ \mathrm{K}^{-1}$ is a temperature sensitivity constant for the mineralisation, and $T$ is the temperature in °C. The limitation functions $l_?$ are of Ivlev type, e.g.

$$l_{o2} = 1 - exp\left(\frac{-[O_2]}{O_{2,min}}\right), \tag{20}$$

they have a value close to one at high concentrations of the corresponding oxidant and become zero if this oxidant is exhausted. Here, $O_{2,min}$ denotes a threshold concentration at which the limitation occurs, but the Ivlev function generates a soft transition between the different oxidation pathways, so they can occur simultaneously. The product of the last five factors in equation (19) means this process will run at a substantial rate only if

- oxygen concentration is low,
- nitrate concentration is low,
- manganese oxides in the sediment are depleted,
- iron oxyhydroxides in the sediment are depleted but
- reducible structural Fe-III in the clay minerals is still abundant.

Sulphate reduction produces hydrogen sulphide. As discussed above, it represents the terminal ~~mineralization~~ mineralisation process in our model. This process, described by processes 33 and 34 in Table 3, follows the formulation by Reed et al. (2011) in our model. Organic material leaving the lower boundary of our model because of sediment growth will also be mineralised by this process. We assume that a fraction of the buried material will be mineralised by either sulphate reduction or methanogenesis, the rest being buried. For the methane produced, we assume that it will not enter the model domain but rather be oxidised by sulphate, producing $H_2S$ below the model domain. We assume for simplicity that all these reactions happen instantaneously, which results in the same net reaction as the sulphate reduction.

### 2.7.3 Precipitation and dissolution reactions

Solids can precipitate from a solution when it becomes ~~oversaturated~~supersaturated. This happens in an aqueous solution when the actual ion activity product exceeds the respective solubility product and a critical degree of supersaturation is reached (e.g., Sunagawa, 1994; Böttcher and Dietzel, 2010).

Diagenetic models often simplify the calculation by multiplying the concentrations rather than the activities ~~, e. g. (van Cappellen and Wa~~ (e.g., van Cappellen and Wang, 1996). The resulting product is then proportional to the actual solubility product as long as the ionic strength of the solution does not change. As the ionic strength of sea water is almost completely defined by its salinity (Millero and Leung, 1976), this assumption is well justified for most marine environments. The Baltic Sea, however, is a brackish sea with strong spatial and temporal changes of bottom salinity, especially in the western part ~~, e. g. (Leppäranta and Myrberg, 2009).~~ (e.g., Leppäranta and Myrberg, 2009). For this reason, we take the activity coefficients, which transform concentrations to activities, into account. This is done by using the Davies equation (Davies, 1938), which determines the individual activity coefficient $a_i$ as (Stumm and Morgan, 2012)

$$\log_{10}(a_i) = -Az_i^2\left(\frac{\sqrt{I}}{1+\sqrt{I}} - 0.3\cdot I\right), \tag{21}$$

where $I$ is the ionic strength expressed in mol $\mathrm{l}^{-1}$, $z_i$ is the ion charge, and $A$ is the Davies parameter, calculated ~~from~~ after Kalka (2018):

$$A = 1.82\cdot 10^6\,\mathrm{l}^{-0.5}\left(\frac{\epsilon(T,S)T_K}{1\,\mathrm{F\,K\,m}^{-1}}\right)^{-1.5}. \tag{22}$$

Here, $\epsilon$ is the dielectric constant of water ~~after Stumm and Morgan (2012), Table 3.3, and~~ calculated after Gadani et al. (2012)[14], and $T_K$ is the temperature in K.

Ca-Rhodochrosite precipitates at elevated concentrations of manganese and carbonate. Its solubility product is composition dependent, as the Ca:Mn ratio varies (Böttcher, 1997; Böttcher and Dietzel, 2010). For Baltic Sea muds where ratios around 0.6 occur, an effective solubility product (including the effect of oversaturation) of $10^{-9.5}$ to $10^{-9}$ $\mathrm{M}^2$ can be deduced from ~~(Jakobsen and Postma, 1989).~~ Jakobsen and Postma (1989). In our model, the reaction follows process 53 in Table 5. 10% of the dissolved manganese will precipitate per day if the solution is undersaturated. Saturation is calculated by the formula (Jakobsen and Postma, 1989)

$$s_{rho} = \frac{a_2\texttt{t\_mn2}\cdot a_2\left[CO_3^{2-}\right]}{10^{-9.5}\,\mathrm{mol}^2\,\mathrm{kg}^{-2}}, \tag{23}$$

where $\left[CO_3^{2-}\right]$ is the concentration of carbonate ions which depends on DIC concentration and pH, see the description of the carbon cycle in Section 2.8. The term $a_2$ is the activity coefficient for ions with a charge of two, see eq. (21). The term in the denominator is the solubility product for rhodochrosite (Jakobsen and Postma, 1989).

---

[14] https://www.mathworks.com/matlabcentral/fileexchange/26294-calculated-dielectric-constant-of-sea-water/content/dielec.m

If the solution becomes undersaturated, rhodochrosite will be dissolved again. Then, process 53 is reversed, and a fixed amount of $10^{-6}$ mol kg$^{-1}$ day$^{-1}$ of manganese-II is released until saturation is reached.

Iron monosulphide precipitates on contact ~~of dissolved iron-II~~ with dissolved Fe-II and sulphide, depending on pH, with a solubility product taken from Morse et al. (1987). But, as stated in Section 2.7.2, we assume for numerical reasons that this process takes place directly after ~~iron-III~~ Fe-III reduction. The solubility product is then used in an inverse way to determine the equilibrium concentration of dissolved ~~iron-II~~ Fe-II at the current pH, sulphide concentration, and salinity~~.~~:

$$a_2 Fe^{2+}_{eq,ims} = 10^{-2.95}\,\frac{a_1\,[H_3O^+]}{a_1[HS^-]}\,, \tag{24}$$

where the $a_i$ are the Davies activity coefficients, see Eq. (21), and $10^{-2.95}$ mol l$^{-1}$ is the solubility product for iron monosulphide (Morse et al., 1987; Theberge and Iii, 1997).

We then assume a precipitation or dissolution of iron monosulphide which relaxes the present concentration of Fe-II against this equilibrium. This is in agreement with a pore water chemistry model for the central Baltic Sea (Kulik et al., 2000), which states that dissolved iron concentrations in the pore water are buffered by iron sulphides (mackinawite and greigite). The dissolution of iron monosulphide also takes place if clay minerals in the same grid cell are capable of adsorbing additional ~~iron-II~~Fe-II. This process is described in Section 2.7.5.

As a simplification, we neglect the change in porosity which would be caused by precipitation (or dissolution) of any solids.

### 2.7.4 Pyrite formation

Pyrite (FeS$_2$) is a crystalline compound formed in early diagenesis (Rickard and Luther, 2007)~~, its~~. Its formation from iron monosulphide is included in most early diagenetic models. This process is not a simple precipitation process, but rather a redox process. While both sulphide and iron monosulphide contain sulphur of oxidation state -2, the redox state of S in pyrite is -1. This implies that an electron acceptor is required to create pyrite. A generally accepted mechanism for pyrite creation is the use of zero-valent sulphur from polysulphides, this may be created by oxidation of sulphate with ~~iron-III~~Fe-III. However, this process alone cannot explain the high degrees of pyritisation in Baltic deep sediments (Boesen and Postma, 1988).

An additional pathway which does not rely on elemental sulphur, but instead reduces hydrogen sulphide to hydrogen gas, has been proposed by Drobner et al. (1990)~~and Rickard and Luther (1997)~~, Rickard and Luther (1997) and Rickard (1997). Similar to how it was done in early diagenetic models ~~, e.g. (Wijsman et al., 2002),~~ (e.g., Wijsman et al., 2002), we include this pathway and therefore assume that whenever iron monosulphide and H$_2$S are present, pyrite is formed from them. The generated H$_2$ will be consumed by sulphate-reducing bacteria (Stephenson and Stickland, 1931), so in the net reaction, sulphate acts as the electron acceptor.

In our model, the reaction therefore follows process 39 in Table 4. The speed of the transformation process is determined by

$$\texttt{p\_ims\_form2\_pyr} = \texttt{t\_ims}\cdot\texttt{t\_h2s}\cdot k_{pyr}\,, \tag{25}$$

where `t_ims` is the concentration of iron monosulfide, `t_h2s` is the concentration of hydrogen sulphide, and $k_{pyr}$ is a kinetic constant for conversion of iron monosulphide to pyrite. Its value of 8.9 kg mol$^{-1}$ day$^{-1}$ was adopted from Wijsman et al. (2002) and Rickard and Luther (1997) which use 8.9 l mol$^{-1}$ day$^{-1}$.

### 2.7.5 Adsorption balances

Adsorption in our model takes place on the surfaces of two particle types: iron oxyhydroxides and clay minerals. Adsorption on silicate particles is not explicitly represented in the model, but parametrised by a reduction of the effective diffusivity of phosphate and ammonium, following Boudreau (1997).

Iron oxyhydroxides adsorb dissolved phosphate. This is a well-known process responsible for the sedimentary retention of phosphate derived from mineralisation processes ~~, e. g. (Sundby et al., 1992).~~ (e.g., Sundby et al., 1992). As both phosphate and hydroxide ions can occupy the adsorption sites at the surface, adsorption is less efficient in alkaline environments.

In our model, we use a formula from Lijklema (1980) which describes the adsorbed P:Fe ratio at a given phosphate concentration and pH.

$$\frac{P_{ads}}{Fe} = 0.298 - 0.0316\,pH + 0.201\sqrt{DIP/1\,\mathrm{mmol\,l}^{-1}} \tag{26}$$

Here, $DIP$ gives the dissolved phosphate concentration. But we use it inversely. We calculate an equilibrium concentration for dissolved phosphate at the current P:Fe ratio and pH.

$$DIP_{eq} = \max\left(\frac{1}{0.201}\frac{P_{ads}}{Fe} - 1.483 + 0.157\,pH, 0\right)^2 \cdot 1\,\mathrm{mmol\,l}^{-1} \tag{27}$$

If the current concentration of dissolved phosphate is above this equilibrium concentration, adsorption takes place and $PO_4$ in the pore water is decreased. If it is below the equilibrium concentration, desorption takes place. The maximum function is added to treat situations when both $pH$ and the amount of adsorbed phoshate get so low that the formula by Lijklema (1980) gives no real solution for $DIP$. In this case, we assume that all currently dissolved phosphate will become adsorbed. The model processes `p_po4_ads_ips` and `p_ips_diss_po4` will change the phosphate concentration in the pore water by

$$\frac{\partial}{\partial t}\texttt{t\_po4} = \texttt{k\_ips\_dissolution}\cdot(DIP_{eq} - \texttt{t\_po4}) + \ldots, \tag{28}$$

where `k_ips_dissolution`= 0.1 day$^{-1}$ is a reaction rate constant we assume. We chose this probably unrealistically low value for reasons of numerical stability.

Following Reed et al. (2011), we define two classes of iron oxyhydroxides. The first one is fresh, amorphous and adsorbs phosphate. The second one is a more crystalline phase, for which we assume no adsorption. The first phase is transformed to the second one with a constant rate in time, implying a continuous phosphate release.

Clay minerals, due to their large surface area, can also adsorb pore water species. We allow an adsorption of phosphate, ammonium and ~~iron-II~~Fe-II. For simplicity, we assume that the ratio of adsorbed species to clay mass is proportional to the pore water concentration, until a saturation threshold is exceeded. For ~~iron-II~~Fe-II, this proportionality constant is derived from Jaisi et al. (2007), for ammonium from Raaphorst and Malschaert (1996), and for phosphate from Edzwald et al. (1976).

In all three cases, we calculate a pore water concentration which is in equilibrium with the current ratio of adsorbed species to clay mineral mass. Then adsorption or release processes take place to relax the present pore water concentration towards the equilibrium value. ~~In the case of iron-II, however, for numerical reasons~~

To calculate $Fe^{2+}_{eq,clay}$, we first determine the mass of clay minerals present in a specific model layer per square meter. This is done by the formula

$$m_{clay} = \rho_{clay} \cdot \Delta z \cdot (1-\phi) \cdot r_{clay} . \tag{29}$$

Here, $\rho_{clay} = 2.7 \cdot 10^3$ kg m$^{-3}$ gives the density of montmorillonite (Osipov, 2012), $\Delta z$ (m) gives the thickness of the layer, $(1-\phi)$ gives the ratio between volume of the solids and total volume of the sediments, and $r_{clay}$ is the volume fraction of clay minerals among the total volume of solids. So, $m_{clay}$ has a unit of kg m$^{-2}$. In the next step, we find out how much iron gets adsorbed to clay depending on the dissolved concentration. For Fe-II concentrations much smaller than 1 mmol l$^{-1}$ as we observe them in our sediments, we can linearise the adsorption isotherms given by Jaisi et al. (2007) and obtain

$$Fe^{2+}_{ads,clay} = \alpha q^{mass}_{max} \left[Fe^{2+}\right] m_{clay} , \tag{30}$$

where $q^{mass}_{max}$ is a mass-specific sorption capacity (mol kg$^{-1}$), $\alpha$ is a binding energy constant (l mol$^{-1}$) and $\left[Fe^{2}+\right]$ is the concentration of iron in the pore water (mol l$^{-1}$). We can rearrange the equation to obtain the equilibrium concentration of dissolved Fe-II:

$$Fe^{2}+_{eq,clay} = \frac{Fe^{2+}_{ads,clay}}{\alpha q^{mass}_{max} m_{clay}} . \tag{31}$$

For the product $\alpha \cdot q^{mass}_{max}$, Jaisi et al. (2007) find values between 500 and 3000 l kg$^{-1}$ for different types of clay, which means 1 kg of clay added to 0.5 to 3 m$^3$ of water would adsorb the same amount of $Fe^{2+}$ as would remain in the solution. We adopt a value of 1000 l kg$^{-1}$ for our model.

For numerical reasons, we allow an immediate precipitation of the desorbed ~~iron-II~~ Fe-II as iron monosulphide in case of ~~its~~ oversaturation, leaving out the intermediate transformation to dissolved Fe-II. The inverse is also true, if iron monosulphide is dissolved, the released ~~iron-II~~ Fe-II may directly be adsorbed by the clay minerals instead of being released to the pore water first.

This is described by process 52 in Table 5.

For the adsorption isotherm of phosphate on clay minerals, we follow the study by Edzwald et al. (1976). They give maximum adsorption capacities $m_{P,ads,max}/m_{clay}$ between of 0.09 mg g$^{-1}$ for $P$ on Kaolinite to 2.58 mg g$^{-1}$ for Illite. These values were obtained at a pH close to 7.5, and pH dependence of adsorption differs between the different clay minerals. Since the composition of the clay minerals is unknown to us, we choose a conservative value of 0.2 mg g$^{-1}$, this could be adapted when such data are available. In contrast to Fe-II adsorption, a half-saturation of P adsorption is already reached at concentrations around 1 mg $l^{-1}$, which corresponds to approx. 0.03 mmol $l^{-1}$. We model this saturation in a very simple way by a linear dependency of dissolved and adsorbed phosphate below a threshold concentration of dissolved phosphate, and a constant amount of adsorbed phosphate if the threshold is exceeded:

$$PO_{4,eq}^{3-,ads} = \frac{1}{M_P} m_{clay} \frac{m_{P,ads,max}}{m_{clay}} \min\left(\frac{\texttt{t\_po4}}{PO_4^{3-,sat}}, 1\right), \tag{32}$$

where $M_P$ = 31 g $mol^{-1}$ is the molar mass of phosphate, $m_{clay}$ is the mass of clay per square meter in the given grid cell, see Eq. (29), $\frac{m_{P,ads,max}}{m_{clay}} = 0.2$ mg $g^{-1}$ is the assumed maximum adsorption capacity, and $PO_4^{3-,sat} = 0.03$ mmol $l^{-1}$ is the concentration of dissolved phosphate at which we assume this saturation is reached. We then define an adsorption and a desorption reaction following process 49 in Table 5. The adsorption process is assumed to happen instantaneously, but for numerical reasons we limit the process rate by demanding that at maximum (a) 10% of the dissolved phosphate is removed per day or (b) 10% of the lack of adsorbed phosphate with reference to the equilibrium concentration is precipitated. This artificial deceleration of the precipitation process had to be included to avoid numerical difficulties. The desorption process works in a similar way. On maximum, 10% of the adsorbed phosphate which exceeds the equilibrium concentration is released per day, or 10% of the saturation concentration $PO_4^{3-,sat}$, whichever is less.

For ammonium adsorption to clay minerals, the processes are in principle identical to those of phosphate. Since the adsorption is weak compared to that of phosphorus (in the range below 1 $\mu$mol $g^{-1}$, Raaphorst and Malschaert, 1996), we, however, neglect the effect by setting the maximum amount of adsorbable ammonium to zero in our present setup. So while the model is able to include the dynamics of ammonium adsorption to clay minerals, we make no use of it in the present application.

### 2.7.6 Reoxidation of reduced substances

Reduced substances can be reoxidised if the appropriate oxidant is present in a sufficient concentration. Table 6 gives a summary of the redox reactions implemented in our model which will be described one by one in this section.

Ammonium is oxidised to nitrate in the presence of oxygen. The rate of this process is proportional to both the ammonium and the oxygen concentration and, as in the water column, increases exponentially with temperature.

Dissolved manganese-II will be oxidised in the presence of oxygen and precipitates as manganese oxide. This is also assumed to be a second-order process proportional to both precursor concentrations.

Dissolved ~~iron-II~~ Fe-II is oxidised by oxygen in a pH-dependent way. The rate of this process is proportional to the ~~iron-II~~ Fe-II and oxygen concentration, as well as to the square of the hydronium ion concentration. It is also influenced by temperature and ionic strength, as described by Millero et al. (1987). For numerical reasons, we also allow a direct oxidation of ~~iron-II~~ Fe-II adsorbed to clay minerals. Alternatively, dissolved ~~iron-II~~ Fe-II can be oxidised by reducing manganese. This process follows Reed et al. (2011). The ~~genereated iron-III~~ generated Fe-III immediately precipitates as iron oxyhydroxide.

Structural iron in clay minerals can be reoxidised as well. We only allow this process in the presence of oxygen, when it transforms back to ~~iron-III~~Fe-III, which is kept bound in the clay minerals.

This reaction follows process 43 in Table 4. The process runs at the speed of

$$\texttt{p\_i2i\_oxo2\_i3i} = \max(\texttt{i3i\_max} - \texttt{t\_i3i}, 0) \cdot \texttt{r\_i2i\_ox} \cdot l_{o2}\,. \tag{33}$$

The oxidation occurs only until the maximum amount of reducible Fe-III in the clay material, `i3i_max`, is reached. It occurs at a rate of `r_i2i_ox`$= 0.1$ day$^{-1}$, a somewhat arbitrary value indicating that the process is typically fast compared to the vertical transport of clay minerals. It is Ivlev-limited by a factor $l_{o2} = 1 - exp\left(\frac{-[O_2]}{O_{2,min}}\right)$ with $O_{2,min} = 2.0 \cdot 10^{-5}$ mol kg$^{-1}$, consistent with the concentration at which carbon oxidation becomes limited.

Hydrogen sulphide can reduce any of the previously mentioned oxidants, being converted to sulphate. The reaction with oxygen or nitrate is carried out as a two-step reaction. The intermediate species formed in these reactions is elemental sulphur, which can be further oxidised to sulphate. These processes follow the same kinetics as in the water column, see Section 2.6.5. Hydrogen sulphide can alternatively react with manganese oxides or iron oxyhydroxides, producing dissolved Mn-II or Fe-II. For the generated ~~iron-II~~Fe-II, we, however, assume either an immediate precipitation to iron monosulphide or an immediate absorption to clay minerals, whichever is more favourable. We assume these reactions to be proportional to both the concentration of sulphide and the metal oxides. Hydrogen sulphide can also reduce structural ~~iron-III~~ Fe-III in the clay minerals, the ~~iron-II~~ Fe-II will in this case remain in the clay.

This reaction follows process 47 in Table 4. The process runs at a speed of

$$\texttt{p\_i3i\_redh2s\_i2i} = \max(\texttt{i3i\_max} - \texttt{t\_i3i}, 0) \cdot \texttt{r\_i2i\_ox} \cdot l_{i3i}\,. \tag{34}$$

The model parameter `r_i2i_ox` describes a relative speed of $0.1$ day$^{-1}$ at which $H_2S$ is reoxidised by this process, a somewhat arbitrary value just expressing our assumption that the process is fast compared to vertical transport of the clay minerals. The model shows low sensitivity to this rate parameter, as shown in the supplementary material. The process is Ivlev-limited by the factor $l_{i3i}$.

Iron monosulphide is typically not directly oxidised but dissolves at low sulphide concentrations. However, if it is exposed to oxygen, we assume a complete oxidation to ~~iron-III~~ Fe-III and sulphate.

Finally, pyrite can be oxidised in the presence of oxygen or manganese-IV, but in marine environments not by ~~iron-III~~ Fe-III (Schippers and Jørgensen, 2002). We assume a complete oxidation to sulphate and iron oxyhydroxides.

## 2.8 Carbon cycle

The carbon cycle in this model is included~~in the typical way~~, following Millero (1995) and Dickson et al. (2007). Four ~~measures~~ parameters describe the state of the dissolved carbonate system in the water:

- pH
- total alkalinity (TA)
- dissolved inorganic carbon concentration (DIC)
- $CO_2$ partial pressure (pCO$_2$)

Knowledge of any two of them allows the determination of the other two parameters. We use TA and DIC as state variables. The reason for this is that both pH and pCO$_2$ can be changed by quick equilibrium reactions with a proton transition which ~~occur~~ occurs faster than our model time step allows, while TA and DIC cannot. For details on these reactions, see Dickson et al. (2007).

~~As we are mainly interested in~~ The DIC concentration can increase by mineralisation of organic carbon and decrease when DIC is assimilated by phytoplankton. Also, it can be modified by CO$_2$ exchange with the atmosphere. Calcification and carbonate dissolution are not considered in our model. Total alkalinity changes if acidic or alkaline substances are added or removed. The substances occurring in our model approach which change alkalinity are $OH^-$, $H_3O^+$ and $PO_4^{3-}$ ions. The effect of dissolved organic matter on total alkalinity (Kuliński et al., 2014; Ulfsbo et al., 2015) is neglected in the present model, it may be included in a future version.

The tracer value changes by 1 unit if (see Table 1)

- `ohminus` is changed by 1 unit or
- `h3oplus` is changed by -1 unit or
- `t_po4` is changed by 0.5 units.

As the pH (for adsorption and precipitation reactions) and ~~pCO$_2$~~ $pCO_2$ (for gas exchange with the atmosphere) are of particular importance, we need to derive these from the state variables. This is done in an iterative procedure. Starting with a guessed pH value (from the last model time step), we aim to correct it until it is consistent with the given values of `t_alk` and `t_dic`. To perform this correction, we calculate the fractionation of DIC into the different species ($CO_2$, $HCO_3^-$, $CO_3^{2-}$). From this, we determine a carbonate alkalinity ~~.~~ as $\left[HCO_3^-\right]+2\left[CO_3^{2-}\right]$, where square brackets denote a concentration. This can be determined by (Dickson et al., 2007)

$$A_{CO2} = \texttt{t\_dic}\frac{k_{1,CO2}\left[H_3O^+\right]+2k_{2,CO2}}{\left[H_3O^+\right]^2+k_{1,CO2}\left[H_3O^+\right]+2k_{2,CO2}}, \tag{35}$$

where $[H3O^+]=10^{-pH}$ and $k_{1,CO2}$ and $k_{2,CO2}$ are the acid dissociation constants for carbonates as taken from Dickson et al. (2007). We do the same for other substances taking part in acid-base dissociation reactions (water, boron, sulphide, phosphate)~~.~~:

$$A_{H2O} = \frac{k_{H2O}}{\left[H_3O^+\right]}-\left[H_3O^+\right], \tag{36}$$

$$A_{boron} = c_{boron}\frac{k_{boron}}{k_{boron}+\left[H_3O^+\right]}, \tag{37}$$

$$A_{H2S} = \texttt{t\_h2s}\frac{k_{1,H2S}}{k_{1,H2S}+\left[H_3O^+\right]}, \tag{38}$$

$$A_{PO4} = \texttt{t\_po4}\frac{-\left[H_3O^+\right]^3+k_{1,PO4}k_{2,PO4}\left[H_3O^+\right]+2k_{1,PO4}k_{2,PO4}k_{3,PO4}}{\left[H_3O^+\right]^3+k_{1,PO4}\left[H_3O^+\right]^2+k_{1,PO4}k_{2,PO4}\left[H_3O^+\right]+k_{1,PO4}k_{2,PO4}k_{3,PO4}}. \tag{39}$$

(40)

The dissociation constants $k$ are taken from Dickson et al. (2007), and the total boron concentration is calculated from salinity as (Moberg and Harding, 1933)

$$c_{boron} = 0.000416\,\mathrm{mol\,kg^{-1}} \cdot \frac{S}{35\,\mathrm{g\,kg^{-1}}}, \tag{41}$$

where $S$ denotes salinity.

The sum of all their alkalinities should then match the known total alkalinity, but a difference occurs because the approximated pH was incorrect. ~~So~~

$$\Delta A = \texttt{t\_alk} - A_{CO2} - A_{H2O} - A_{boron} - A_{H2S} - A_{PO4} \tag{42}$$

So, we do a Newton iteration to find an improved pH estimate~~, using~~.

This is done by calculating the derivative

$$\frac{d\Delta A}{dpH} = \frac{d\Delta A}{d[H_3O^+]} \cdot \frac{d[H_3O^+]}{dpH} = \frac{d\Delta A}{d[H_3O^+]} \cdot (-\ln(10))\,[H_3O^+] \tag{43}$$

and obtaining the new $pH$ estimate as

$$pH^{new} = pH - \frac{\Delta A}{\frac{d\Delta A}{dpH}}. \tag{44}$$

We use a fixed number of ten iteration steps for a better parallel performance of the code.

Finally, we can calculate $pCO2$ as

$$pCO2 = \frac{\texttt{t\_dic}/k_{0,CO2}}{1 + \frac{k_{1,CO2}}{[H_3O^+]} + \frac{k_{1,CO2}k_{2,CO2}}{[H_3O^+]^2}} \tag{45}$$

### 2.9 Numerical aspects

The equations which determine the temporal evolution of the state variables are solved by a mode splitting method~~. Physical~~, i.e. concentration changes due to physical and biogeochemical processes are ~~solved~~ applied alternately in separate ~~time steps.~~ sub-timesteps. For a discussion of this method and alternatives we refer to Butenschön et al. (2012).

#### 2.9.1 Numerics of physical processes

Vertical diffusion is done explicitly by multiplying each vertical tracer vector by a diffusion matrix. This includes turbulent mixing in the water column as well as pore water diffusion, bioturbation (faunal solid transport) and bioirrigation (faunal solute transport). This diffusion matrix is tridiagonal, and for a small time step, which is in our case limited by the thin layers at the top of the sediment, a Euler-Forward method can be applied. Larger time steps could be split into smaller Euler-Forward steps, which means a repeated multiplication by the tridiagonal matrix. We instead use an efficient algorithm to calculate powers of the tridiagonal matrix (Al-Hassan, 2012), and perform the multiplication only once.

### 2.9.2 Numerics of biogeochemical processes

The sources and sinks for the different tracers are calculated from the process rates. These not only include biogeochemistry, but also parametrisations for lateral transport processes as well as sedimentation and resuspension.

To calculate the changes of a tracer concentration with time, we form the sum of the processes consuming or producing it (Radtke and Burchard, 2015).

$$\frac{\partial}{\partial t}T_i = \sum_k p_k \left(q_{ik} - s_{ik}\right) . \tag{46}$$

Here $T_i$ represents the concentration of tracer $i$, $p_k$ is the rate at which process $k$ runs, and $q_{ik}$ (and $s_{ik}$) is the stoichiometric ratio in which process $k$ produces (or consumes) tracer $i$.

In order to ensure both non-negativity of the tracer concentrations and mass conservation, we apply the positive Euler-Forward method from Radtke and Burchard (2015). It is a clipping method which, in ~~case of~~ the case where a tracer concentration becomes negative during one Euler-forward time step, it first executes a partial time step until this tracer is zero. Then the rest of the time step is continued without the processes consuming this tracer, i.e. they are switched off. More than two partial time steps may be needed if more than one tracer is exhausted.

## 2.10 Automatic code generation

The model code is not hand-written. Instead, the model is described in a formal way in terms of its tracers, constants and processes in a set of text files. The model code is then generated by a “code generation tool” (CGT) which fills in this information into a code template file. The advantage is that the same biogeochemical equations can in this way be integrated into different models. While the current version is written in Pascal, the three-dimensional version in MOM5 has been created as a Fortran code. The CGT is open-source software and can be downloaded at www.ergom.net.

# 3 Observed data used for model applications

We use ~~three~~ four different observational datasets for model calibration and validation. The data used are (a) pore water profiles for different dissolved species, (b) sediment elemental composition, ~~and~~ (c) estimates of bioturbation intensity and (d) bentho-pelagic fluxes measured in benthic chamber lander incubations.

## 3.1 Selected stations

All data were collected at seven different stations in the Southern Baltic Sea ~~,~~(see Fig. 1~~. (We~~, we always present the stations from west to east~~.)~~). The mud stations LB and MB are situated in the Mecklenburg Bight, a trough-like bay in the south-western Baltic Sea where salinities are up to ~~20.~~ 20 g kg$^{-1}$. Stations ST and DS are on sandy substrate, the latter one is situated in only 22 m depth near the major sill which impedes the transport of the more saline North Sea water into the inner part of the Baltic Sea. Station AB is situated in the central Arkona Basin in 45 m depth. The Arkona Basin is the most western basin of the inner

Baltic Sea. It accumulates organic matter not only from local primary production, but also laterally imported particles from coastal areas experiencing strong eutrophication, especially from the ~~Oder~~ Odra River (Christiansen et al., 2002). Station TW is a silt station with a median grain size around 40 $\mu$m. The last station, the sandy station OB on the Oder Bank, is not a place of organic matter deposition, but rather of transformation before the detritus is transported to deeper locations. The Oder Bank is a shallow sandy area strongly influenced by the ~~Oder~~ Odra river plume (Voss and Struck, 1997).

All the stations were sampled during twelve cruises which took place between July 2013 and January 2016 so as to cover different seasons (Lipka, 2018). However, not every station was sampled during every cruise. The calibration of the model ~~was already started in parallel to~~ occurred in parallel with the sampling campaign, such that only data from the first seven cruises (until January 2015) ~~could be~~ was used for model fitting.

### 3.2 Pore water analyses

Short sediment cores with intact sediment-water ~~interface~~ interfaces were taken by a multicorer, a device which simultaneously extracts 8 sediment cores from the sea floor. Pore water was extracted at different depths by rhizones. For a detailed description of the analytical methods used, we refer to ~~Lipka et al. (2018a)~~Lipka et al. (2018b). Here we just give a short summary: ammonium concentrations were measured onboard using standard photometric methods ~~, e. g. (Winde et al., 2014).~~ (e.g., Winde et al., 2014). The quantification of major and trace elements was done on land, following the ICP-OES method (Kowalski et al., 2012). Dissolved inorganic carbon was measured by a mass spectrometer in the gas phase after a treatment of the pore water sample with phosphoric acid. Total alkalinity was determined colorometrically after Sarazin et al. (1999). Dissolved sulphide was determined spectrophotometrically by the methylene blue technique (Cline, 1969).

Instead of directly comparing sulphate concentrations between model and reality, which change over time with salinity, we use the sulphate deficit defined as

$$\Delta SO_4 = [SO_4^*]\,\frac{[K]}{[K*]} - [SO_4]\,, \tag{47}$$

where $[SO_4]$ and $[K]$ are the measured concentrations of sulphate and potassium (~~regarded as~~ the latter regarded as a passive tracer) in the pore water and $[SO_4^*]$ and $[K^*]$ are their typical concentrations in sea water of 35 g/kg salinity ~~, Dickson and Goyet (1994)~~(Dic

### 3.3 Sediment composition

Parallel sediment cores from the same multicorer casts as used for the pore water analysis were subsampled in 1 cm steps, freeze-dried under vacuum and homogenised for geochemical analyses. Total carbon (TC) as well as nitrogen (TN) and sulphur (TS) contents were measured by combustion, chromatographical separation of the released gases and their determination with a thermal conductivity detector. The total inorganic carbon (TIC) content was measured by acidic removal of carbonates and analysis of the released CO2 with a nondispersive infrared detector. The total organic carbon (TOC) content was then calculated by the subtraction of TIC from TC values. At the sand stations (ST, DS and OB), the mass fractions were measured in the fine fraction (< 63 $\mu$m) of the sediment only, assuming that the coarse fraction does not contain these elements in a significant amount. ~~So~~Thus, the percentage in the whole sediment was calculated by multiplying with the fine fraction ratio that was determined by laser diffractometry. Analytical details ~~on the used devices~~ related to the devices used, their calibration as well as precision and accuracy can be obtained from Bunke (2018).

### 3.4 Bioturbation intensity estimates

In order to analyse bioturbation intensities ($D_B$), six to 24 cores per station were sliced onboard immediately after retrieval at 0.5 cm intervals to 3 cm depth and at 1 cm intervals to 10 cm for vertical chlorophyll-a (Chl-a) profiles. All samples were deep-frozen (-18°C) and stored until extraction (Sun et al., 1991). In the laboratory, the defrosted sediment samples were homogenised and three parallel subsamples of 1 cm$^3$ volume were taken from each slice. After adding 9 ml of 96% ethanol and an incubation period of 24 h in the dark, the ~~sampled~~ samples were centrifuged at 4000 rpm for 5 minutes, measured photometrically (663 and 750 nm) and chlorophyll was calculated based on HELCOM (1988). The vertical chlorophyll profiles were interpreted using the bio-mixing model developed by Soetaert et al. (1996b). Experimentally derived chlorophyll decay constants of 0.01 d$^{-1}$ for mud and 0.02 d$^{-1}$ for sand (Morys, 2016) and ~~a~~ an artificially small sedimentation rate $\omega$ of 0.00001 cm d$^{-1}$ were used, the latter just reflecting the fact that chlorophyll decay is much faster than sedimentation. The model applied may distinguish between diffusive and non-diffusive mixing. The latter mode of bioturbation was neglected in our study despite the fact that it may be the dominant particle transport process in certain areas (e.g. AB).

### 3.5 Bentho-pelagic fluxes

Total oxygen uptake (TOU) and bentho-pelagic nutrient fluxes ($NO_3^-$, $NH_4^+$, $PO_4^{3-}$) of the sediments were measured in situ with two identical benthic lander systems "Mini Benthic chamber" by courtesy of S. Sommer and P. Linke (GEOMAR Kiel, Germany) during cruises AL434, EMB076, POS475, EMB100 and EMB111 (Lipka, 2018). All systems were equipped respectively with a Plexiglas® chamber (diameter 19 cm), an electronically driven glass syringe water sampler and oxygen optodes (Aanderaa Instruments, Norway, No. 4831) in- and outside of the chamber. Oxygen concentration trend was used as the main parameter for gas fluidity and tightness. Each respective chamber covers a sediment area of 284 cm$^2$ and the chamber water volume was in the range of 5-8 l depending on sediment penetration depth. Incubation times at the seafloor ranged from 9 to 48 h. Discrete chamber water samples were gathered by up to eight glass syringes (volume approx. 45 ml) in intervals of 1-7 h, depending on total deployment time. Photo lights (SolaDive 1200) and a photo camera (GoPro Hero Black Edition 3+) were used for the observation of the chamber deployment, particularly to check for sediment disruption. The start of incubation was defined if initial concentrations inside the chamber at the beginning were close to bottom-water concentrations. Nutrient concentrations were measured with a QuAAtro multianalyser system (Seal Analytical, Southampton, UK) onboard using standard photometric methods (Grasshoff et al., 2009). Nutrient fluxes were calculated from linear increase or decrease of concentration versus time, corrected for the surface area to volume ratio of each chamber. A robust linear regression method which is tolerant to outliers was applied (Huber, 1981; Venables and Ripley, 2002), and the uncertainties of the fluxes were obtained by an ordinary bootstrapping approach (Canty and Ripley, 2017; Davison and Hinkley, 1997). The regression analysis to determine their fluxes was performed in the same way as for the nutrients. TOU was calculated by standard linear regression of $O_2$ concentration versus time (with R$^2$ values above 0.98), within a period while $O_2$ concentration did not sink below 15% of the initial concentration (Glud, 2008). Calibrations of $O_2$ optodes were performed in ambient sea water aerated for 30 min (100% atmospheric saturation) and in saturated seawater - sodium dithionite solution (0% oxygen), regularly cross-checked by Winkler titration (Winkler, 1888).

## 4 Model setup and optimisation

There are three ways in which observations feed into our model~~. There are~~:

1. model constants which were derived in earlier studies and which our model adopted from previous models,
2. initial and boundary conditions, determining tracer concentrations at the beginning and throughout the model run, and
3. calibration data which help to confine uncertain model parameters during a repeated model calibration process.

### 4.1 Use of data as model constants

Most of the observations which help ~~confine~~ constrain our model processes enter our model indirectly, since model constants are inherited from ancestor models. Especially in van Cappellen and Wang (1996), a thorough confinement of model constants based on observations was achieved. We add to that by supplying site-specific observations for porosity for all seven stations, set to a homogeneous value per substrate type estimated from measurements within the SECOS Project (Lipka et al., 2018a). ~~Also, sediment~~ The assumption of a homogenous value is a first approximation which is motivated by the future aim to use the model in a three-dimensional context. While detailed spatial maps of surface porosity exist, vertical profiles are rare. The effect of this simplification is discussed in Appendix D. Sediment growth estimations for the three muddy sites are taken from different sources, as shown in Table 7.

### 4.2 Initial and boundary conditions

The initial conditions for most biogeochemical state variables in the water column are taken from ~~a~~ the previous run of a three-dimensional ERGOM model ~~(Radtke, unpublished),~~ as described in Section 2.2 (Neumann et al., 2017), which contained a simplified sediment model as described e.g. in Radtke et al. (2012). Concentrations of sulphate and calcium were set to salinity-determined values as described by the standard composition of sea salt (Turekian, 1968). Dissolved dinitrogen was initialised at 100% saturation (Hamme and Emerson, 2004).

~~Fluff and sediment, in contrast,~~ In contrast, fluff and sediment were initialised empty. We allowed them to fill up with material derived from the water column during the simulated period of 100 years. While this period of 100 years is not sufficient to fill the considered 22 cm of sediment by accumulation, it is sufficient to almost reach a steady state in the pore water concentrations. While the sixth class of detritus, which is considered non-biodegradable, continues accumulating in the sediments after 100 years, those classes which affect the pore water concentrations decay on smaller time scales.

Since the model conserves nitrogen and phosphorus, the filling of the sediments would have led to a depletion in the water column. To overcome this, we relax the winter concentrations of dissolved inorganic nitrogen and phosphorus (DIN and DIP) against values obtained from the previous 3-d model run. This relaxation is applied every winter, so the nutrients required to fill the model domain are provided from an artificial external source. Their input is large at the beginning of the model run and decreases over time as the sediment reaches a state which is almost in equilibrium with the organic matter supply from the water column above.

### 4.3 Model fit to observed data

Pore water profiles from Lipka (2018) were then used to calibrate the model. The calibration included ~~optimizing~~ optimising model parameters for individual stations, as well as parameters for the whole model domain.

Typically, this type of calibration is done manually by the modeller. But due to the large number of parameters to optimise (115 in total), we decided to do a systematic, algorithm-based optimisation.

Please note that the physical input data and initial conditions used during the model optimisation phase were taken from a preliminary, unpublished 3-d model run. It differs from the cited model version (Neumann et al., 2017) by using a less realistic light model. Furthermore, dissolved organic nitrogen is not included as a state variable. These improvements were made to the ERGOM model during the development phase of the sediment model, and the results of the sediment model show only small differences between the model versions. We use the data from the final, published 3-d model run for the results shown in this article, for reasons of reproducibility. The preliminary forcing data used during the calibration phase are, however, also given in the online supplementary material.

#### 4.3.1 Penalty function

The first step in such an optimisation is to define a metric or a penalty function quantifying the misfit between model and observations. Our aim is then to minimise this function.

We chose to penalise the relative deviation between model and measurement and define the penalty function by

$$P = \sum_{i=1}^{i_{max}} \sum_{j=1}^{j_{max}(i)} r_{i,j}^2 \cdot w_i \,. \tag{48}$$

Here, $i_{max}$ is the number of state variables we compare and $j_{max}(i)$ is the number of observations of this state variable ~~in~~ at all depths and at all stations. The expression $r_{i,j}$ is a measure for the relative deviation between model value $m_{i,j}$ and observation $o_{i,j}$,

$$r_{i,j} = \log_{10}\left(\frac{m_{i,j}+\Delta_i}{o_{i,j}+\Delta_i}\right) . \tag{49}$$

The term $\Delta_i$[15] is included to avoid huge relative errors between values which are close to zero. It denotes the random deviation in this parameter, quantified from duplicate or triplicate measurements of the same parameter in different sediment cores of the same sampling. Obviously $r_{i,j}$ becomes zero if model and observations match. Finally, the weight $w_i$ assigned to each

---

[15] This term differs per variable, but is the same at each station and sampling depth.

comparison in equation (49) is defined as the ratio

$$w_i = \frac{\overline{o}_{i,j}}{\Delta_i} \qquad (50)$$

between the average observed value of the variable and the random deviation. The weight is applied to make sure that fitting the most certain variables ~~has~~ have the highest priority.

The pore water species which are fitted are: ammonium, phosphate, silicate, sulphide, iron, manganese, the total alkalinity, and the relative sulphate deficit[16].

### 4.3.2 Optimisation strategies

After we defined a penalty function, the second step is to choose an algorithm to minimise it. Several such algorithms exist, however, our choice of methods was restricted by the relatively long runtime of a single model iteration. Since it took about 8 minutes to run a single station for 100 years, we had to choose methods which

1. needed a relatively small number of iteration steps and therefore
2. allowed for a high degree of parallelism in the individual optimisation step, in order to effectively search the 115-dimensional parameter space.

Our first choice was the Adaptative Hierarchical Recombination - Evolutionary Strategies (AHR-ES) algorithm, implemented in the R-Package calibraR (Oliveros-Ramos and Shin, 2016). ~~As a genetic algorithm, it considers each vector of model parameters as a genome of an individual. A low value of the penalty function is then considered as a good fitness of the individual. The iteration is then performed in the three steps as follows:~~

1. ~~selection, where only the best currently known vectors are selected,~~
2. ~~recombination, where their genome is combined to produce children, and~~
3. ~~mutation, where their genome is randomly modified, following certain algorithm-specific rules.~~

~~The AHR-ES algorithm is special in the sense that the recombination step produces just one "child", combining the parameter vectors of all surviving individuals in a weighted mean. To calculate these weights, the algorithm takes advantage of not only determining one value of fitness, but rather different "fitnesses" for matching different observations. High weights are then assigned to those genome parameters that influence the output parameters most in which the individual has a high fitness. This optimally breeded child is then cloned several times and, after mutation of the clones, forms the starting population for the next step.~~

~~We used 200 "individuals", each consisting of seven single models for the seven different stations run in parallel, and optimised them over 120 generations. We~~ We were, however, not satisfied with the optimisation result. Possibly we just failed to find out the optimal settings for the algorithm, such as the survival rate.

---

[16] defined as $\Delta SO_4\,[K^*]\,/\,\left(\left[SO_4^*\right]\,[K]\right)$, see eq. 47

~~Our~~ Therefore, our second choice was a simple alternative algorithm: our own extension of the Generalised Pattern Search (GPS) algorithm (Hooke and Jeeves, 1961). Every optimisation step consists of two sub-steps. The first substep is the most simple "grid search" step in which all 115 parameters are varied by a predefined step width. We run 230 sets of 7 models in parallel, such that each parameter can be both increased and decreased. In the second substep, 230 combinations of the most successful changes are formed. Even if no single-parameter change could improve the existing solution, sometimes combinations of them can, which is the basic idea of GPS. The parameter vector with the best score which was obtained in any of the two substeps is then chosen as the starting point for the next step. If none of the two sub-steps lead to an improvement of the overall fit, the step size is reduced by a factor of 2.

The optimisation converged after 30 iteration steps and reduced the error function from 6363 (the value obtained by previous manual tuning) to 4797.

The algorithm obviously does not guarantee that we reach a global optimum, which can be seen as a drawback. The automatic method was started after manual calibration of the model. Since the optimisation method is deterministic, the local optimum is defined by this initial condition. However, in a vector space with a dimension as high as ours, it is anyway ~~hard~~ difficult to find a non-local point with a better score, no matter if it is by manual optimisation or a different search algorithm.

### 4.4 Manual correction of sand and silt stations

For the sand stations and the single silt station, the automatic optimisation resulted in an unrealistic set of parameters. The ~~estimated bioirrigation~~ bioturbation rates were estimated as low as those of the mud stations. However, at these low bioturbation rates, the sediments failed to accumulate realistic amounts of organic matter. The pore water profiles we obtained, however, seemed to match relatively well with the observations. ~~But the~~ This was due to the fact that the realistically low concentrations of solute species were obtained by ~~keeping detritus out of~~ an unrealistically low incorporation of degradable particulate material into the sediments. The model assumed relatively high rates of lateral removal of fluff, such that only a small fraction of the locally produced detritus was actually processed in the sediments.

This illustrates the problem that if the diffusivity is unknown, very different transports can be caused by the same pore water gradient. We therefore decided to manually modify the solution~~by (a ) reducing the fraction of detritus removed from the fluff layer by lateral transport and (b) enhancing bioturbation and bioirrigation rates, both by the same factor.~~ . This modification meant raising bioturbation and bioirrigation intensity by a factor of 10 at each station. Afterwards we reduced the parameter `r_fluffy_moveaway` which describes the rate at which fluff layer material is transported to the deeper areas until realistic concentrations in the pore water profiles were reached.

This led to similar pore water profiles, but higher turnover rates and organic content in the sediments.

## 5 Model results and validation

### 5.1 Comparison to measured pore water profiles

In this section, we compare and discuss observed and simulated pore water profiles of several chemical species relevant for early diagenetic processes. Model results are taken from the last year of the 100-year simulation, which was driven by a repeated forcing every year. After this simulated period, the model almost reached a quasi-steady state, which means the annual cycle of pore water concentrations was nearly repeated year after year at each of the stations. The sixth class of detritus, in contrast, which we defined as non-degradable, did not reach a stable concentration, but continued to accumulate in the sediment during the period of 100 years~~. But~~ , but this continued accumulation did not influence the pore water profiles due to the fact that it was assumed to be bioinert.

#### 5.1.1 Pore water profiles at mud stations

Figure 4 shows a comparison of simulated and measured pore water profiles at the three mud stations. ~~The curvesshow the annual average pore water concentrations simulated by the model, while the shaded areas give the range in which each parameter varies throughout the year. Horizontal lines indicate the range of measurements over all cruises within the project.~~

In the left panels, we see that the rise of alkalinity with depth is captured well by the model, except for the AB site where observations show a higher alkalinity below 10cm depth. The decline in sulphate follows the lower range of the observations.

The panels in the second column show that also the vertical profiles of ammonium and silicate are represented relatively well by the model. However, especially at the Arkona Basin station, the observed range of both ammonium and sulphide shows a strong variation (by an order of magnitude). The model does not capture that but rather sticks to the lower range of the observations. Most probably, the variability in the observations is not due to seasonality, but a consequence of spatial variability between sampling sites, since the samples were taken from two sites 23 km apart.

Surprisingly, the model is able to reflect the differently steep sulphide profiles between the stations LB and MB. While ~~(Lipka et al., 2018a) sees~~ Lipka (2018) see the low sulphide concentrations which occur especially in March 2014 at MB as an indication for a preceding mixing event, our model cannot adopt this interpretation due to its limitation ~~to~~ by a temporally constant vertical mixing. In contrast, our model suggests a higher deposition of iron oxyhydroxides at this site.

The right panels show that the modelled manganese concentrations match the observations quite well. The dissolved iron profiles show their maxima at the correct depths and a relatively large seasonal spread. The measurements show an even larger spread than the model. For the phosphate profiles, the model results mostly resemble the lowest of the measured values, except for station AB where we see a clear underestimation. This can be seen as an artefact of our fitting method, more precisely of the choice of our penalty function. Giving a penalty for the relative error means that the same absolute error is punished heavier if the observation ~~was~~ is smaller, making the model try harder to fit low values compared to high ones.

The model results for the mud stations fit quite well, considering the fact that the real pore water profiles may be shaped by very different temporal variations. These include, for example, mixing events, changing loads of organic matter or temperature and salinity variations. Our model, not knowing the sediments' past, can only try to estimate the average conditions that might produce similar pore water concentrations.

### 5.1.2 Pore water profiles at sand stations

Figure 5 illustrates the model ~~fits~~ fit at the sandy stations.

All of the sandy stations have one major error in common: sulphide concentrations are strongly overestimated at depths below 5 cm. We suppose that the precipitation or reoxidation of sulphide ~~are~~ is underestimated. For all other pore water species, the agreement between measured and modelled ranges is reasonable. Especially the rise of alkalinity with depth is captured well by the model. The sulphate deficit in the empirical data has a large uncertainty, as it is calculated as a small difference of similarly large quantities..

In our model, the sandy sites show a more pronounced seasonal cycle in the pore water profiles compared to the muddy stations. Especially iron and manganese concentrations vary considerably due to the seasonally different supply of quickly degradable organic matter and correspondingly differences in mixing intensity. While the variability in the supply of fresh organic matter is captured by the model, the variation in mixing is not. Still, the simulated ranges are supported by the variability in the observed pore water concentrations.

### 5.1.3 Pore water profiles at the silt station Tromper Wiek

For the station Tromper Wiek, we used data from two different cruises, in April and June 2014. Even if the idea in the SECOS project was to repeatedly sample the same station, the locations were approximately 6 km apart for this station, and the substrate type at the station sampled in April was sand rather than silt. The amount of sulphide in the pore waters showed a large difference between the April and the June cruise, the latter concentrations exceeding the former by a factor of 20. This reflects spatial rather than temporal variations. Some of the depth intervals were only sampled ~~in~~ during the June cruise, which explains the different observed ranges at the different depths.

The good agreement in the profiles of ammonium and phosphate (middle and right panel in Fig. 6) suggests that total mineralisation is captured well. The left panel shows that the model estimates the sulphate deficit at the ~~higher~~ lower range of observations, but the rise of alkalinity with depth at the ~~lower range.~~

higher range. The model overestimates the vertical extent of ~~iron-II~~ Fe-II in the pore waters. However, the model ~~correctly~~ reasonably reproduced the range of iron concentrations, and also the fact that dissolved manganese concentrations were always low compared to those of iron.

## 5.2 Comparison to sediment composition estimates

In Figure 7, we compare the composition of the solid parts of the sediment between model and measurements. ~~The fraction of nitrogen, sulphur and total organic carbon (TOC) in the total mass of the dry sediment is shown for all seven stations.~~

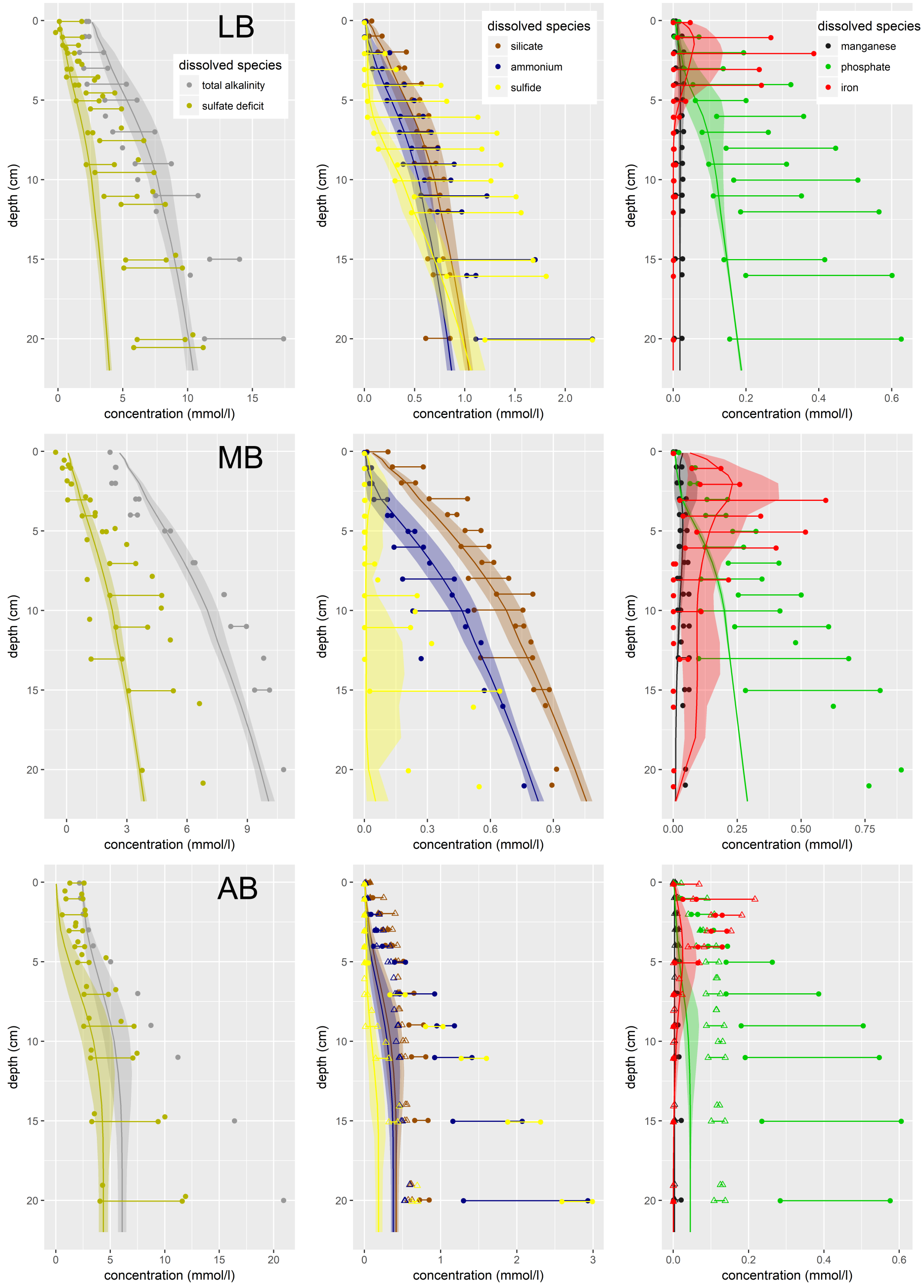

**Figure 4.** Pore water concentrations of several dissolved species at the three mud stations Lübeck Bight (top row), Mecklenburg Bight (middle row) and Arkona Basin (bottom row). Points and horizontal lines indicate the range of measurements. For station AB, empty triangles indicate the range of observations from the January 2015 cruise, which were taken at a different location in the same area, 23 km apart. Curves and shading present the model results and indicate year-average concentrations and the seasonal range. Please note the different horizontal scales.

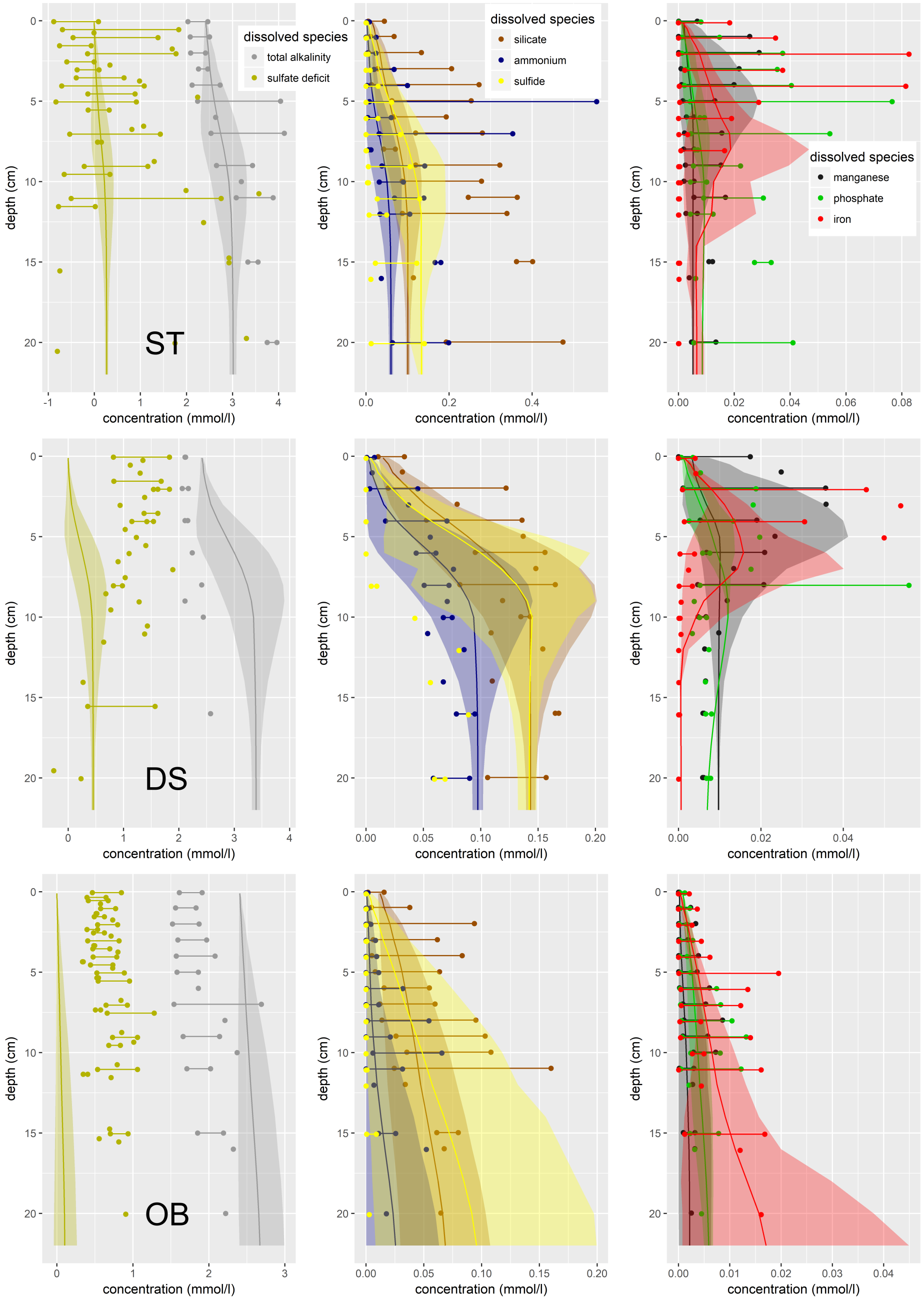

**Figure 5.** Pore water concentrations of several dissolved species at the three sand stations Stoltera (top row), Darss Sill (middle row) and Oder Bank (bottom row). Points and horizontal lines indicate the range of measurements. Curves and shading present the model results and indicate year-average concentrations and the seasonal range. Please note the different horizontal scales.

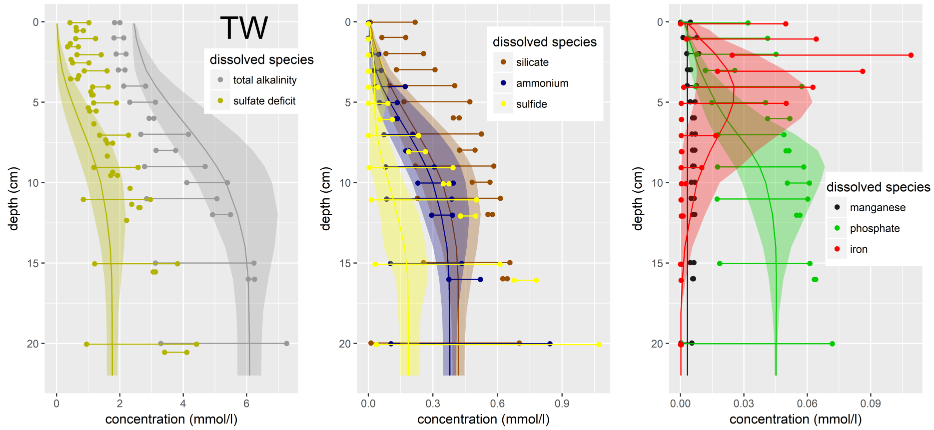

**Figure 6.** Pore water concentrations of several dissolved species at the silt station Tromper Wiek. Points and horizontal lines indicate the range of measurements. Curves and shading present the model results and indicate year-average concentrations and the seasonal range.

~~We see that for~~ For the mud stations LB and MB, the modelled element concentrations show a quantitative agreement with the measurements. The main difference is that the measured values show strong vertical fluctuations, which may be the result of the deposition history. Another difference is that the vertical gradients of sulphur are considerably steeper in the model than in reality. In the mud station AB (Arkona Basin), however, the actual concentrations of all three elements are heavily underestimated. Nonetheless, the depth gradients of the concentrations match quite well, so there is perhaps just a constant offset. This might be caused by the accumulation of bioinert organic material, possibly of terrigenous origin from the ~~Oder~~ Odra river.

In all sand stations (ST, DS, OB), the amount of sulphur in the sediments is underestimated. The observed sulphur in the sediments varies with depth and shows a maximum at around 10 cm depth. The fact that sulphide, in contrast, was overestimated in the pore waters, suggests that the precipitation of ~~sulphide~~ sulphur may be underestimated in the sandy cores.

Particulate N and TOC are present in realistic quantities at the OB station. At the other two sand stations, the N and TOC observations show maxima at the top (station DS) or bottom (station ST) of the profile, which are not captured by the model. These are most likely the traces of past sedimentation or bioturbation events.

Reproducing subsurface TOC maxima, as they occur in permeable sediments, represents a challenge for early diagenetic models. They can be caused by different processes, such as

- non-local, fauna-driven ingestion of fluff material into a specific depth,
- washout of organic material from the surface sediment e.g. during storm events or
- lateral relocation of sediments.

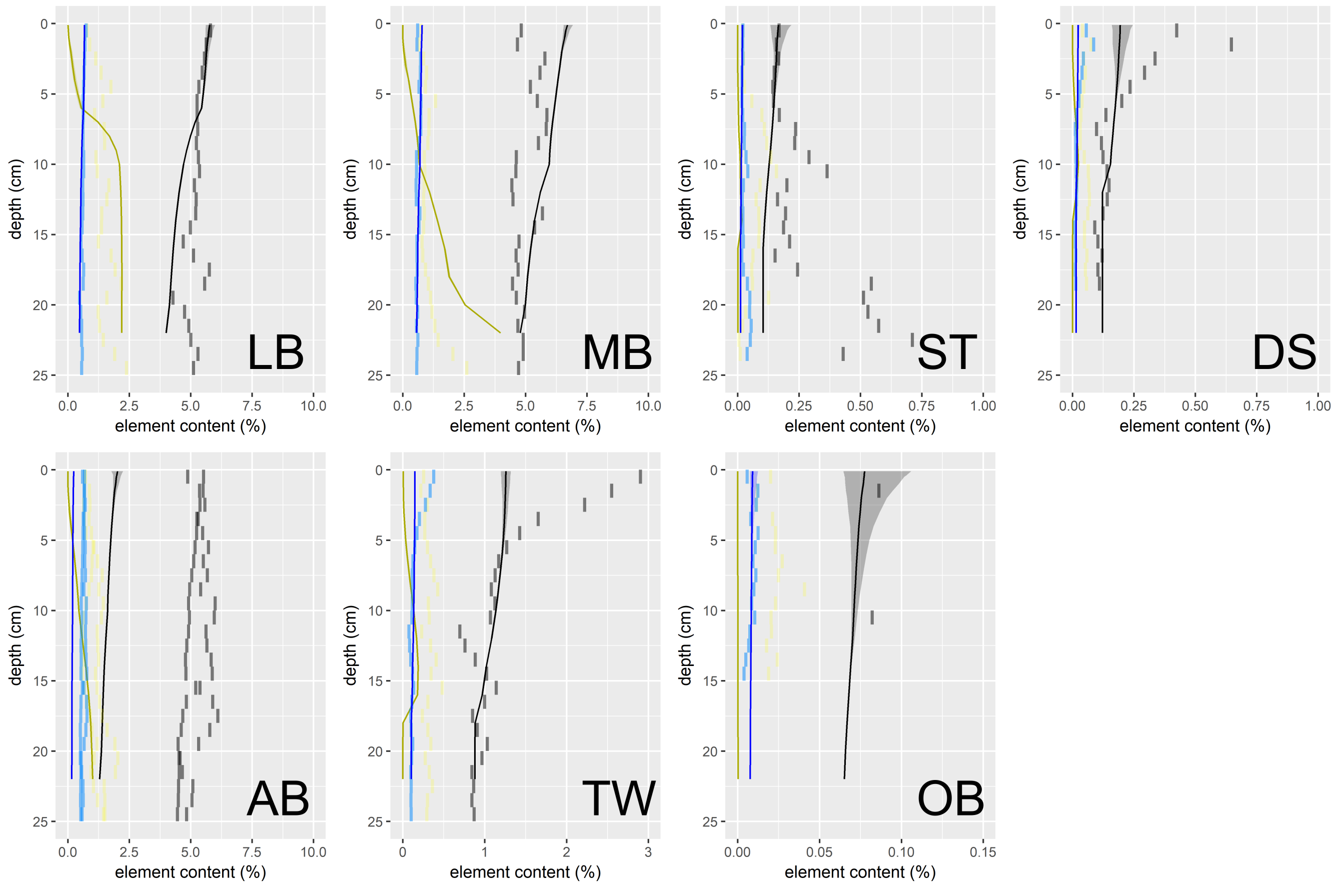

**Figure 7.** Mass fractions of nitrogen (blue), sulphur (yellow) and organic carbon (black) in the dry sediment, model results (curves and shading for seasonal range) versus measurements (vertical segments). Please note that the scales on the horizontal axes differ by a factor of 40.

## 5.3 Comparison to measured bioturbation intensities

The empirically estimated bioturbation intensities span a large range at each station. A reason for this may be that while our model assumes a temporally constant bioturbation, in reality it is highly variable. Mixing events by animals or shear stress alternate with periods without mixing (Meysman et al., 2008). Investigations of individual cores can only give snapshots of this highly variable mixing rate.

In Figure 8a~~shows a comparison of~~, we compare measured bioturbation diffusivities $D_B$ ~~and~~ to those used in the model. Since the observed ranges are very large, they almost always contain the value assumed in the model. An exception is the Tromper Wiek site where exceptionally high $D_B$ values were measured. This may, however, be an artefact based on the method calculating the diffusivities. While ~~in the model,~~ we assume diffusion-analogue mixing ~~, in nature~~ in the model, also non-local mixing occurs in nature. The two processes can be distinguished from the analysis of Chl-a profiles

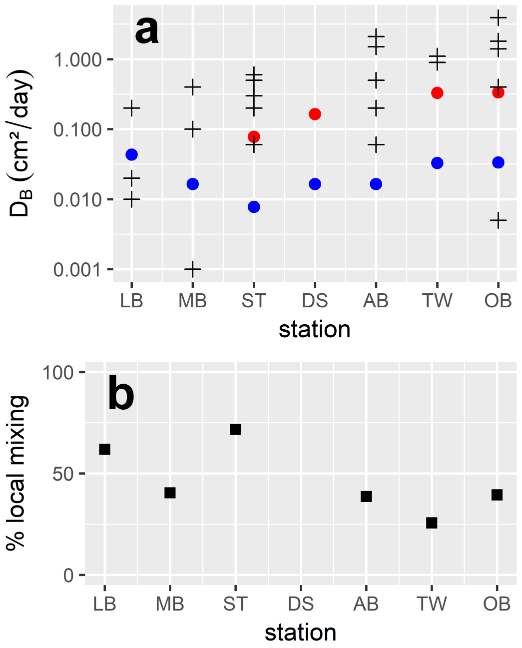

**Figure 8.** (a) Model estimations of bioturbation intensity (blue dots), manually corrected for sand and silt stations (red dots) and Chl-a-based estimates (black crosses)~~for bioturbation intensity~~, data from Morys et al. (2016). Black crosses represent averages over all cores from a single month where the Chl-a profiles in the sediment ~~supported~~ support the assumption of diffusion-analogue mixing. So, variation can be interpreted as temporal variability. (b) The percentage of the cores ~~for which~~ at this station whose Chl-a profiles could be explained by the assumption of a local, diffusion-analogue mixing process~~could explain the observed Chl-a profiles~~.

(Soetaert et al., 1996b; Morys et al., 2016). Figure 8b shows how often the samples from a specific site supported the hypothesis of diffusion-analogue mixing. For the station TW, it was only one fourth of the sediment cores that could be explained assuming local mixing, so non-local mixing was identified as a major process here. $D_B$ values were only calculated for cores where the observed Chl-a profiles could be explained by local mixing alone.

The automatic model calibration yielded diffusivities at the sand and silt stations which were as low as those at the mud stations. Such ~~a~~ weak mixing, however, could not supply enough organic matter to the sediments to reach measured element compositions. Therefore, they were corrected upwards, resulting in higher mixing at the sandy than at the muddy sites. This agrees with recent estimates of the bioturbation potential (Gogina et al., 2017; Morys et al., 2017), an index describing the ability of macrofauna to displace the sediment particles, resulting in a mixing effect. This potential was estimated to be higher in the more shallow sandy areas than in the muds. Also, measured bioturbation rates in the SECOS project were higher in the ~~sands~~ sand than in the ~~muds~~ mud (Morys, in prep.). However, the high variability of bioturbation rates within stations makes it difficult to prove a significant difference in $D_B$ between sandy and muddy areas empirically (Morys et al., 2016).

### 5.4 Comparison to measured bentho-pelagic fluxes

The net fluxes of selected pore water species ($O_2$, $NH_4^+$ and $PO_4^{3-}$) into the sediment or out of it are shown in Figures 9 and 10 for mud and sand/silt stations, respectively. An additional figure showing the fluxes of DIC, $NO_3^-$, $Fe$, $Si$ and $SO_4^{2-}$ is given in the online supplement. The figures compare modelled fluxes to observations from benthic chamber lander incubations. For each of the selected species, we get two contributions in the model: the flux into or out of the sediment itself (by diffusive and by bioirrigation) and a consumption or production by mineralisation of the fluff layer material. We can distinguish between these in the model, but not in the measurements, because (a) the benthic chamber lander measures concentration changes in the bottom water only and (b) at the mud stations, the border between sediment and fluff layer is rather a smooth transition than a discrete boundary.

The comparison of annual-average oxygen fluxes between model and measurements shows a reasonable quantitative agreement. Taking the rather high fluctuations in the measurements into account, we cannot assume a perfect fit. The model correctly reproduces the fact that similar oxygen consumption occurs at sand and mud stations in spite of their order-of-magnitude differences in organic content and pore water concentrations, (Boudreau et al., 2001). The strong seasonality in the model, with $O_2$ consumption being high during summer and low during winter, cannot be confirmed by the measurements, but we need to state that only two valid measurements exist during January and February when the modelled consumption rates are lowest. For the nutrients, we find highly variable fluxes in the observations, some of which show large relative uncertainties. The model results are in reasonable quantitative agreement with these fluxes, but again the clear seasonality in the model cannot be confirmed empirically. Also the peak values of the observed fluxes (more than 4 mmol m$^{-2}$ day$^{-1}$ for $NH_4^+$ and 2 mmol m$^{-2}$ day$^{-1}$ for $PO_4^{3-}$) are much larger than those in the model. Our model also does not show ammonium or phosphate fluxes directed into the sediments, as they do occur in a small fraction of the observations. So, we can state that the modelled fluxes are more smooth than the observed ones. This may either reflect reduced spatiotemporal variability in the model, or artificial variability introduced into the measurements by the sediment disturbance which our incubation method causes.

### 5.5 Scope of model applicability and model limitations

In this paper, we applied our model in a one-dimensional context. The aim was to reproduce early diagenetic processes taking place in the sediments at seven exemplary sites thought to be representative for the south-western Baltic Sea by a mechanistic model. In our fully coupled model, the pelagic biogeochemistry and an assumed lateral transport supplied the organic material which drove the early diagenetic processes in the sediments. A comparison to a variety of different observations showed that the model gives a reasonable reconstruction of sediment biogeochemistry. Still, we found differences in the details. For example, a strong overestimation of sulphide concentrations in sandy sediment pore waters most likely points to the underestimation of sulphide precipitation/reoxidation.

The analysis we show suggests that the processes most relevant for these observations are adequately represented in the model. This does not include all parts of the model. For example, the nitrogen cycle was not compared to observations, which

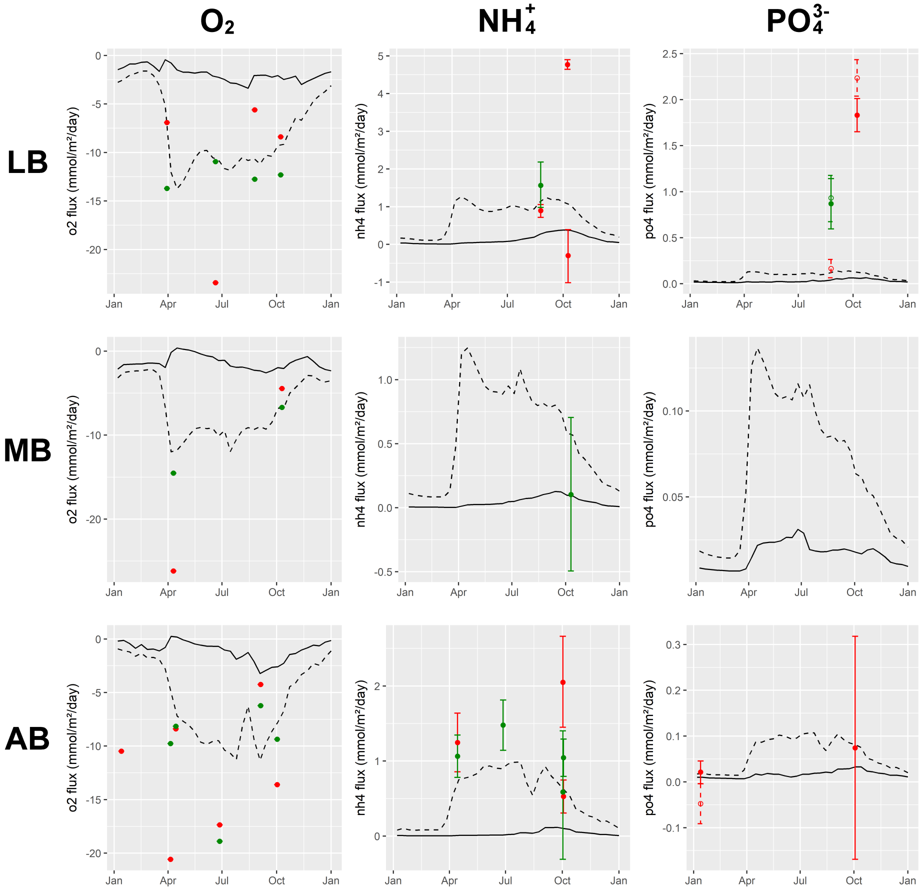

**Figure 9.** Fluxes between sediment and bottom water of selected pore water species at mud stations. Positive values denote fluxes out of the sediment. Solid line: Modelled fluxes between sediment and bottom water only. Dashed line: Fluxes including mineralisation of the fluff layer material. Dots: Measured fluxes by two benthic chambers (BC1 in red and BC2 in green). Vertical ranges: Uncertainties of these fluxes estimated by a bootstrapping method. For phosphate: full circles - estimates based on phosphate determination by photometric methods, empty circles - estimates based on P quantification by the ICP-OES method.

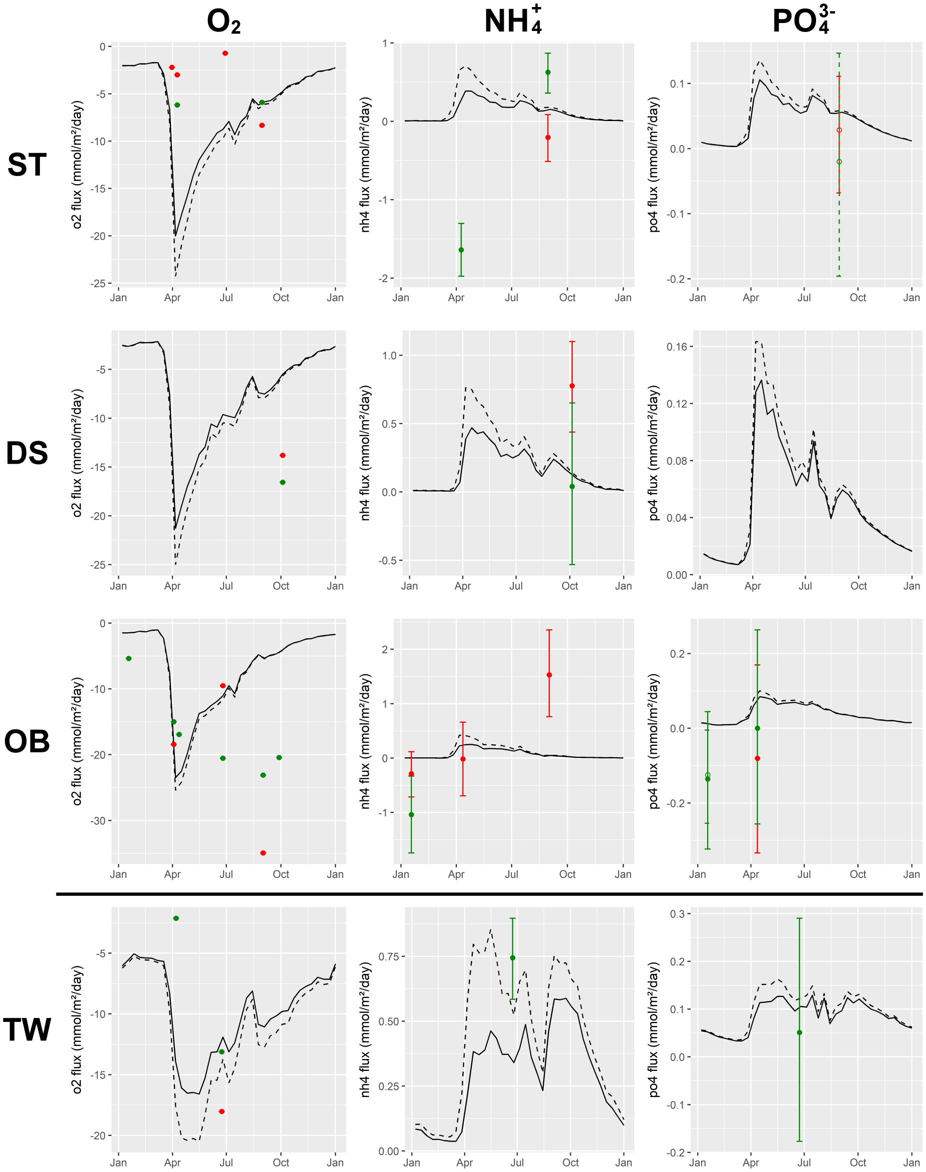

**Figure 10.** Fluxes between sediment and bottom water of selected pore water species at sand stations. Positive values denote fluxes out of the sediment. Solid line: Modelled fluxes between sediment and bottom water only. Dashed line: Fluxes including mineralisation of the fluff layer material. Dots: Measured fluxes by two benthic chambers (BC1 in red and BC2 in green). Vertical ranges: Uncertainties of these fluxes estimated by a bootstrapping method. For phosphate: full circles - estimates based on phosphate determination by photometric methods, empty circles - estimates based on P quantification by the ICP-OES method.

is due to the fact that the project SECOS in which this work was done did not focus on it and so the required observations of nitrification or denitrification rates are missing.

The ultimate aim of the model is its application in a fully coupled three-dimensional framework. A fully coupled pelagic and benthic model could answer a wide range of questions, e.g.

- Are the strongly simplifying sediment parametrisations which we use in marine ecosystem models today consistent with our understanding of sediment biogeochemistry, or is there a mismatch between our assumptions in the pelagic models and the sediment-water fluxes in early diagenetic models, which are directly constrained by observational data?
- How might sedimentary services such as nutrient removal change under different conditions, and what feedbacks into pelagic biogeochemistry can be expected?
- On which time scales can organic material stored in the sediments affect the eutrophication status of the pelagic ecosystem, e.g. for how long will sedimentary nutrient release counteract nutrient abatement measures aimed at reducing the winter nutrient concentrations in the water column?

The applicability of the one-dimensional model is limited. There is little added-value in using this coupled benthic-pelagic model compared to a classical early diagenetic model, since in most cases a one-dimensional description of a pelagic ecosystem will be strongly oversimplified. One could, however, imagine that it can be useful for enclosed marine areas where the horizontal exchange is limited or well-known. An application to a different area than the south-western Baltic Sea will, however, require a new model calibration, since critical parameters like bioturbation intensity might differ. We strongly discourage the use of the model as it is by just applying it to derive estimates on benthic biogeochemical process rates from pelagic biogeochemistry, unless there is a large set of benthic data available against which the model can be validated.

In cases where these data are available, we think that the model system has a high potential to serve as a starting point for detailed studies, because it can be easily modified. Adding, removing or adapting processes is very easy because of the automatic code generation principle. Only a formal mathematical formulation of the process is required, and no coding skills are needed to e.g. add additional state variables to the model system. Also a re-use of parts of the model, e.g. the explicit representation of the fluff layer, is possible.

## 6 Conclusions

In this manuscript, we ~~described~~ describe an integrated model for ocean biogeochemistry. It simulates ocean biogeochemistry both in the water column and in the sediments.

The model was obtained by combining ~~its~~ two ancestor models, the water column model ERGOM ~~(Neumann, 2000)~~(Neumann et al., 201 and the early diagenetic model used in Reed et al. (2011). A few modifications were made to the existing models, partly to include additional processes relevant for the area of interest, the ~~German EEZ in the~~ south-western Baltic Sea. These model extensions include

- closing the carbon cycle in the sediments which allows the determination of pH,
- adding a specific numerical scheme for the diffusion of the tracer “total alkalinity”,
- using ion activities rather than concentrations to determine precipitation and dissolution potentials, allowing us to account for salinity differences,
- the explicit description of adsorption to clay minerals, considering their mineralogy, and
- an alternative pyrite formation pathway via $H_2$ formation.

An automated model calibration approach was used to fit the model to pore water observations at seven sites in the study area. It was successful for the mud stations, but underestimated bioturbation rates and consequently the organic content of the sediment at the sand and silt sites. Therefore, these model parameters were adjusted manually at the sand and silt sites.

This issue illustrates a general problem related to models of this complexity. The large quantity of unknown model parameters results in many degrees of freedom, and different types of observations are needed to constrain them. Even so, a good fit to a constrained set of observations does not guarantee that the model dynamics are captured realistically.

~~We showed a comparison to three different kinds of observations, which in most cases showed good agreement. An exception was the strong overestimation of sulphide concentrations in sandy sediment pore waters. This most likely points to the underestimation of sulphide precipitation/reoxidation.~~

~~The analysis we showed suggests that the processes most relevant for these observations are adequately represented in the model. This does not include all parts of the model. For example, the nitrogen cycle was not compared to observations, which is due to the fact that the project SECOS in which this work was done did not focus on it.~~

Applying the model in a three-dimensional framework (Cahill et al., in prep.) will reduce the degrees of freedom. For example, our model includes parametrisations for (a) lateral removal of fluff material from the sand stations and (b) lateral import of organic material at the mud stations. In a 3-d ocean model, these become intrinsically linked by the constraint of mass conservation. Other degrees of freedom arise from the supply of oxidised iron and manganese to the individual stations. In a 3-d model, the supply and distribution of these substances would be controlled by erosion and deposition and thus determined by the model physics.

Apart from these constraints, the implementation of the model in a 3-d framework is straightforward. Physically, the coupling between different locations would be controlled by the fluff layer, ~~by~~ its erosion and redeposition. Technically, the coupling is simplified due to the use of automatic code generation. Describing the model processes and constants in a formal way, keeping them separate from code for specific models, means it is easy to switch between different “host models”. The major difficulty in going 3-d is the limited amount of validation data, such as pore water profiles and sediment-water fluxes, compared to the strong spatial and temporal variability. A first step is the application of the model to the limited area of the German EEZ for which the model is calibrated.

In the long term, biogeochemical ocean models should aim at a process-resolving description of surface sediments. This is especially true for shallow ocean areas where the efflux of nutrients from the sediment strongly influences water column biogeochemistry, like in our study area. The magnitudes of denitrification and phosphate retention, or the spatial and seasonal patterns in which oxygen consumption occurs, may strongly influence marine ecosystems.

Very often, model studies discussing "what if"-scenarios use a relatively simple sediment representation. This includes studies on nutrient abatement, human-induced stresses on ecosystems (e.g. by fish farming) or climate sensitivity analyses. But the use of a present-day ~~parameterisation~~ parametrisation for future scenarios means a ~~neglect~~ neglection of possible changes. In the context of limited data and process understanding, this implicit "no change"-assumption may be the best we can presently do. But we should be aware of the uncertainty which is introduced by this pragmatic choice. Studying the sensitivity of sediment functions to external drivers in a process-resolving sediment model can be a way to quantify these uncertainties, and possibly derive an ensemble of alternative future parametrisations.

*Code and data availability.* A source code version of the model is provided in the supplement to this article. It includes the initial conditions and physical forcing files required to reproduce the obtained results.

The code is not hand-written, but can be generated automatically from a set of text files describing the model biogeochemistry, and a code template containing the physical and numerical aspects of the model code. All three ingredients required to obtain the model source code (the text files, the code template, and the code generator program) are also included.

These components in their current and previous versions are GPLv3 licensed and can also be downloaded from our website www.ergom.net.

For the calibration and validation data used in this study, we refer to the following publications: the pore water data can be found in Lipka (2018); the sediment composition data are published in Bunke (2018); the bioturbation rate estimates are available in Morys (2016).

## Appendix A: Stoichiometric composition of model state variables

The stoichiometric composition of the model tracers is shown in Table A1.

## Appendix B: ~~Quantitative influence~~ Rates of ~~different model extensions~~organic carbon mineralisation

The study by Middelburg (1989) relates decay rates of organic carbon to the time since the organic material was deposited. They found the following relation to be valid across time scales from days to decades:

$$\ln\left(\frac{k}{1\,\mathrm{year}^{-1}}\right) = -0.95\ln\left(\frac{t}{1\,\mathrm{year}}\right) - 0.81\,, \tag{B1}$$

where $k$ denotes the reactivity of organic carbon and $t$ is the time since detritus was created. In our model, we try to resemble this relation by splitting the detritus into different reactivity classes. The ratios $r_k$ of the different classes $k$ in freshly created detritus and their reactivities at 0°C are listed in Table A2.

We assume a faster detritus mineralisation at higher temperatures. This is controlled by a factor $\exp(T \cdot \tau)$ which we multiply with the decay rates, where $T$ is the temperature measured in °C and $\tau = 0.15\ \mathrm{K}^{-1}$ is a temperature sensitivity constant as it was used in previous versions of the ERGOM model already (Neumann and Schernewski, 2008). The effective decay rate of a quantity of fresh detritus changes over time, since the ratio between the detritus classes $k$ changes as the quickly-decaying fractions are removed faster. In Fig. A1, we illustrate the effective decay rates predicted by our model at different temperatures and compare them to the rates predicted by the Middelburg formula. We can see that (a) the class model gives a good match to the formula and (b) temperature has little influence on the overall decay rate. The latter fact can be understood as already explained in the main text: a higher temperature means a higher decomposition rate of each detritus class. This will in the sum be compensated for by a shift in the class composition. Lower concentrations of quickly-degradable detritus classes will remain, which compensates the faster decay of the less degradable classes. This means an overall very similar total decomposition rate.

## Appendix C: Quantitative influence of different model extensions

Here we use a set of sensitivity experiments to illustrate how the model refinements introduced by us influence the results. In each of these, we switch off one of our model improvements. This means that we use three simplified model versions, in which

1. total alkalinity always diffuses with the bicarbonate diffusivity, no matter how many hydroxide ions contribute to it which, in reality, diffuse faster,
2. the saturation ~~indexes~~ indices for precipitation/dissolution reactions are calculated neglecting the (salinity-dependent) activity coefficients, and
3. the adsorption of ammonium, phosphate and iron onto clay minerals, as well as their reducible ~~iron-III~~ Fe-III content, are neglected.

As an example, we apply these reduced models to the ~~mud station AB.~~ silt station TW. (Please note that the calibration procedure was not repeated after the model modifications, but the model parameters were left unchanged.)

The results are shown in Fig. A2 in dashed lines and compared to the full model. All modifications affect the dissolved concentrations of iron in different directions. This is probably because both pore water pH and the activity coefficients influence the precipitation to iron monosulphide. The ~~third modification (adsorption to clay minerals~~second modification (neglecting activity coefficients) reduces the phosphate concentrations in the pore water. All other pore water species remain virtually unchanged by our model modifications.

## Appendix D: Sensitivity analysis for vertically varying porosity

We used vertically constant porosity in our application of the model. Here we illustrate the effect of this simplification by comparison to a model with a realistic porosity profile, see Fig. A3. A porosity profile was measured at station Tromper Wieck during the April 2014 cruise (Lipka, 2018) and interpolated to the model depths. Below approx. 3 cm depth, where porosity is decreased in the realistic profile, we see enhanced pore water concentrations for the nutrients and for sulphide. This was to be expected because of the higher ratio between solid material and pore water volume. In contrast, iron concentrations are reduced in higher depths while manganese concentrations remain constant. While we do not observe qualitatively different behaviour, the differences between simplified and realistic-porosity model are significant, which means the model might benefit from using realistic porosity profiles.

## Appendix E: Sensitivity analysis for vertical resolution in the sediments

In Fig. A4, we show the pore water profiles at the site Tromper Wiek, simulated with the original and with double resolution in the sediments. For numerical stability reasons, a time step for vertical diffusion of oxygen had to be reduced in the high-resolution run. Apart from that, the runs were identical. It can be seen that most of the vertical profiles look practically identical between the setups. For iron, phosphate and sulphide, we can see deviations which we, however, considered as acceptable if we keep the overall uncertainties in mind.

## Appendix F: Numerical details of applying the Al-Hassan method

For solutes, we assume that the flux (positive upward) between two neighbouring cells takes the form

$$F_{k,k+1}^{solutes} = D\frac{\rho(c_{k+1}-c_k)}{l_{k,k+1}}, \tag{F1}$$

where $D$ is the effective diffusivity calculated as the sum of molecular diffusivity and bioirrigation diffusivity, see Eq. (5), $c_k$ denotes the concentration in the pore water of cell $k$ [mol/kg], and $l_{k,k+1}$ is the distance between the centres of the adjacent cells. This flux means a concentration change in the different grid cells given by

$$\frac{d}{dt}c_k = \frac{F_{k,k+1}^{b,solutes} - F_{k-1,k}^{b,solutes}}{\rho\Phi\Delta z_k} \tag{F2}$$

This allows us to construct a Matrix $M_B$ which transforms the vector of concentrations $(c_0, c_1, ..., c_{kmax})^T$ to its derivative, that is,

$$M_B\boldsymbol{c} = \frac{d}{dt}\boldsymbol{c}. \tag{F3}$$

So, after a time step of $\Delta t$, the concentration vector $\boldsymbol{c}^{new}$ can be determined as

$$\boldsymbol{c}^{new} = \exp(M_B\Delta t)\boldsymbol{c}. \tag{F4}$$

The matrix exponentiation can be defined as

$$\exp(M_B\Delta t) = \lim_{n\to\infty}\left(I + \frac{M_B\Delta t}{n}\right)^n. \tag{F5}$$

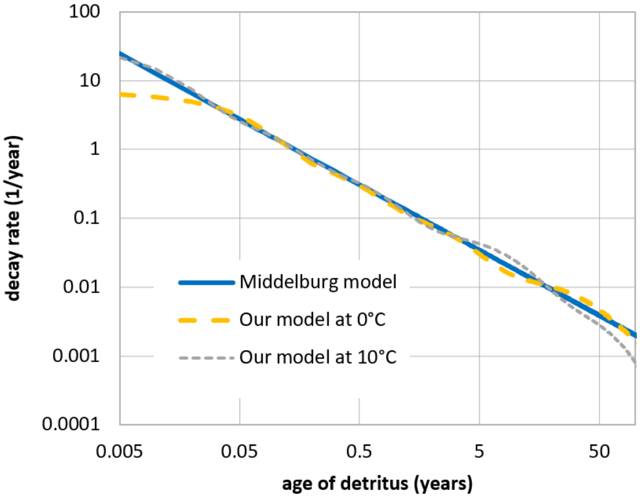

**Figure A1.** Decay rates of organic carbon in detritus depending on its time of creation. Comparison of the reactivity predicted by our model at different temperatures to the Middelburg decay rate prediction, see text.

We approximate the limit by choosing $n = \Delta t / 1$ s and use the method of Al-Hassan (2012) to compute $\boldsymbol{c}^{new}$. This method allows an efficient calculation of powers of tridiagonal matrixes with positive entries, and it is easy to see that $I + \frac{M_B \Delta t}{n}$ is of this shape if $n$ is chosen large enough.

An identical approach is used for the solids.

*Competing interests.* No competing interests are present.

*Acknowledgements.* This study is embedded in the KÜNO Project SECOS (03F0666A) funded by the German Federal Ministry for Education and Research (BMBF). The model optimisation runs were performed on the HLRN supercomputing ~~center~~facilities. Free software which supported this work includes R/RStudio and Freepascal Lazarus. Marko Lipka and Michael E. Böttcher wish to thank I. Schmiedinger, A. Köhler and I. Scherff for their invaluable help in the laboratory. They also wish to express their gratitude to B. Liu for helpful discussions on transport processes. Jana Woelfel and Gregor Rehder thank Peter Linke and Stefan Sommer for the long-lasting loan and technical support (Sergiy Cherednichenko) of the two Mini Benthic chamber landers (GEOMAR, Kiel, Germany).

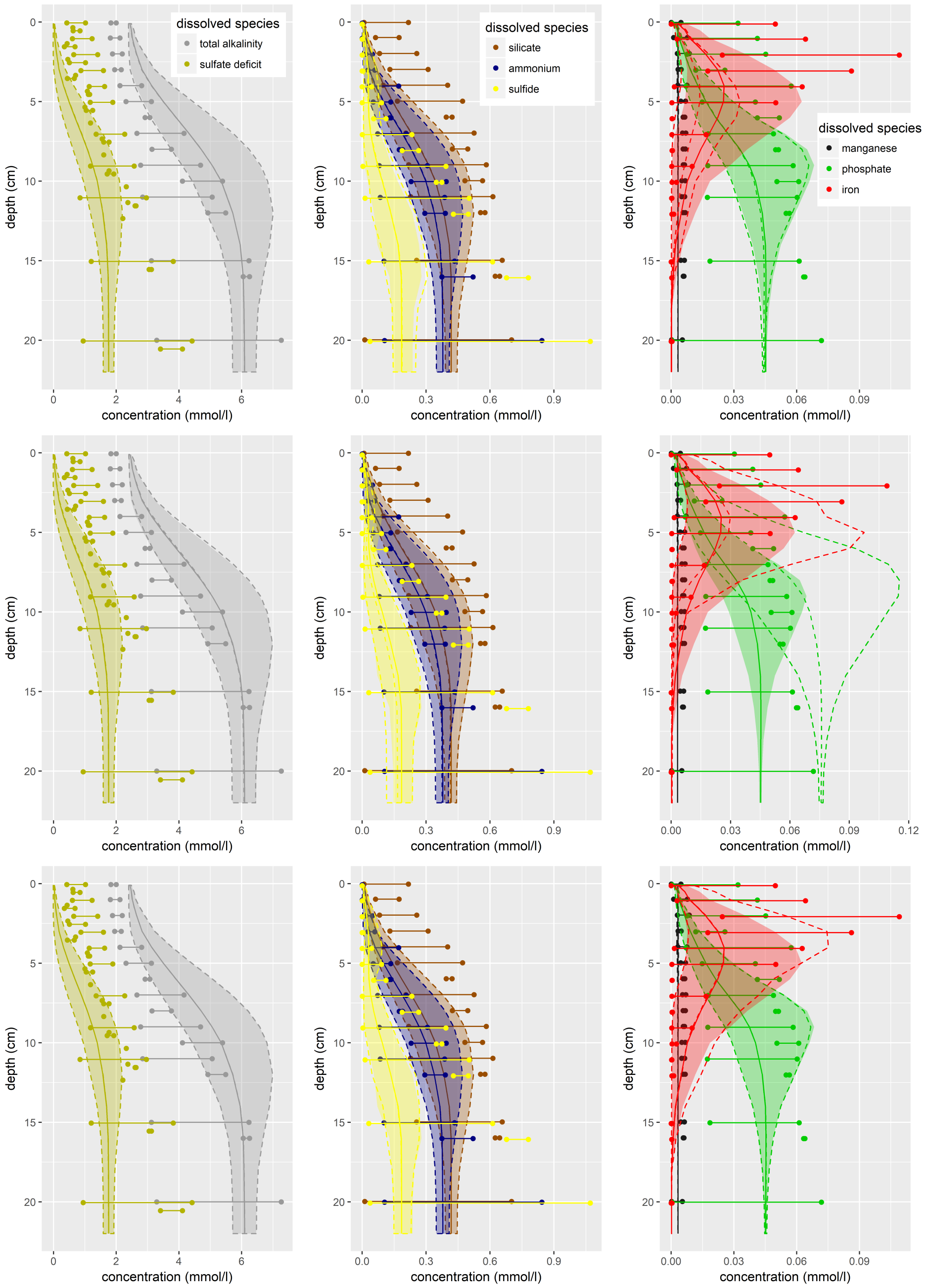

**Figure A2.** Pore water concentrations of several dissolved species at the ~~mud~~ silt station ~~Arkona Basin~~Tromper Wieck. Points and horizontal lines indicate the range of measurements. Solid curves and shading present the model results and indicate year-average concentrations and the seasonal range. Dashed curves show the same, but for a model version which neglects one of our improvements: Top row - without correcting the diffusivity of total alkalinity for hydroxide ions. Middle row - without correcting the solute concentrations by activity coefficients. Bottom row - without assuming adsorption to clay minerals.

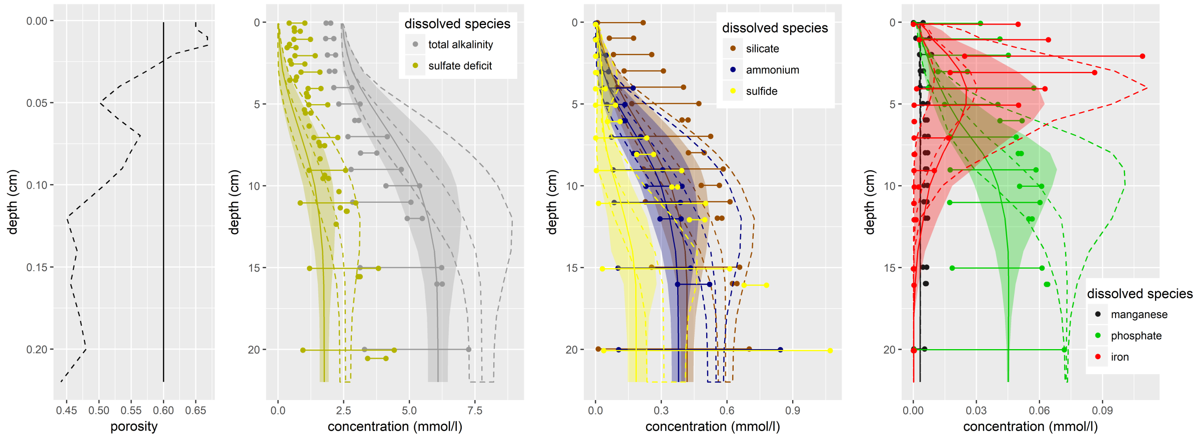

**Figure A3.** Left panel: Porosity at the silt station Tromper Wieck as assumed in the model (solid line) and a porosity profile for a realistic model setup, derived from the April 2014 cruise (dashed line). Three right panels: Pore water concentrations of several dissolved species at the silt station Tromper Wieck. Points and horizontal lines indicate the range of measurements. Solid curves and shading present the original model results and indicate year-average concentrations and the seasonal range. Dashed curves show the same, but for a model version with the realistic porosity profile.

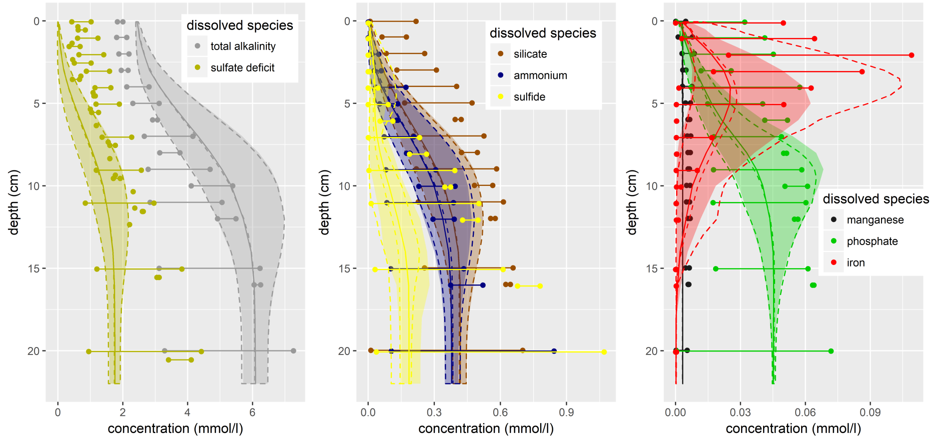

**Figure A4.** Pore water concentrations of several dissolved species at the silt station Tromper Wieck. Points and horizontal lines indicate the range of measurements. Solid curves and shading present the model results and indicate year-average concentrations and the seasonal range. Dashed curves show the same, but for a model version with double vertical resolution.

## References

Al-Hassan, Q.: On Powers of Tridiagonal Matrices with Nonnegative Entries, Journal of Applied Mathematical Sciences, 6, 2357–2368, 2012.

Al-Raei, A. M., Bosselmann, K., Böttcher, M. E., Hespenheide, B., and Tauber, F.: Seasonal dynamics of microbial sulfate reduction in temperate intertidal surface sediments: controls by temperature and organic matter, Ocean Dynamics, 59, 351–370, 2009.

Andersson, A., Haecky, P., and Hagström, Å.: Effect of temperature and light on the growth of micro-nano-and pico-plankton: impact on algal succession, Marine Biology, 120, 511–520, 1994.

Arndt, S., Jørgensen, B. B., LaRowe, D. E., Middelburg, J. J., Pancost, R. D., and Regnier, P.: Quantifying the degradation of organic matter in marine sediments: A review and synthesis, Earth-Science Reviews, 123, 53–86, doi:10.1016/j.earscirev.2013.02.008, 2013.

Bale, A. J. and Morris, A. W.: Organic carbon in suspended particulate material in the North Sea: Effect of mixing resuspended and background particles, Continental Shelf Research, 18, 1333–1345, doi:10.1016/S0278-4343(98)00046-6, 1998.

Belmans, F., van Grieken, R., and Brügmann, L.: Geochemical characterization of recent sediments in the Baltic Sea by bulk and electron microprobe analysis, Marine chemistry, 42, 223–236, 1993.

Berner, R. A.: Early Diagenesis: A Theoretical Approach, Princeton University Press, Princeton, N.J, 1980.

Boesen, C. and Postma, D.: Pyrite formation in anoxic environments of the Baltic, American Journal of Science, 288, 575–603, 1988.

Boudreau, B. P.: Diagenetic models and their implementation, vol. 505, Springer Berlin, 1997.

Boudreau, B. P., Huettel, M., Forster, S., Jahnke, R. A., McLachlan, A., Middelburg, J. J., Nielsen, P., Sansone, F., Taghon, G., and Van Raaphorst, W.: Permeable marine sediments: overturning an old paradigm, EOS, Transactions American Geophysical Union, 82, 133–136, 2001.

Brigolin, D., Lovato, T., Rubino, A., and Pastres, R.: Coupling early-diagenesis and pelagic biogeochemical models for estimating the seasonal variability of N and P fluxes at the sediment–water interface: Application to the northwestern Adriatic coastal zone, Journal of Marine Systems, 87, 239–255, doi:10.1016/j.jmarsys.2011.04.006, http://www.sciencedirect.com/science/article/pii/S0924796311000959, 2011.

Bruckner, C. G., Mammitzsch, K., Jost, G., Wendt, J., Labrenz, M., and Jürgens, K.: Chemolithoautotrophic denitrification of epsilon-proteobacteria in marine pelagic redox gradients., Environmental microbiology, 15, 1505–1513, doi:10.1111/j.1462-2920.2012.02880.x, 2013.

Böttcher, M. E.: Experimental dissolution of $CaCO_3$-$MnCO_3$ solid solutions in $CO_2$-$H_2O$ solutions at 20° C: I. Synthetic low-temperature carbonates, Solid state ionics, 101, 1263–1266, 1997.

Böttcher, M. E. and Dietzel, M.: Metal-ion partitioning during low-temperature precipitation and dissolution of anhydrous carbonates and sulphates, no. 10 in EMU Notes in Mineralogy, pp. 139–187, Mineralogical Society, 2010.

Böttcher, M. E., Hespenheide, B., Llobet-Brossa, E., Beardsley, C., Larsen, O., Schramm, A., Wieland, A., Böttcher, G., Berninger, U.-G., and Amann, R.: The biogeochemistry, stable isotope geochemistry, and microbial community structure of a temperate intertidal mudflat: an integrated study, Continental Shelf Research, 20, 1749–1769, 2000.

Bunke, D.: Sediment mixing processes and accumulation patterns in the south-western Baltic Sea, Ph.D. thesis, University of Greifswald (Germany), Greifswald, https://nbn-resolving.org/urn:nbn:de:gbv:9-opus-20780, 2018.

Butenschön, M., Zavatarelli, M., and Vichi, M.: Sensitivity of a marine coupled physical biogeochemical model to time resolution, integration scheme and time splitting method, Ocean Modelling, 52-53, 36–53, doi:10.1016/j.ocemod.2012.04.008, http://www.sciencedirect.com/science/article/pii/S1463500312000686, 2012.

Butenschön, M., Clark, J., Aldridge, J. N., Allen, J. I., Artioli, Y., Blackford, J., Bruggeman, J., Cazenave, P., Ciavatta, S., Kay, S., and others: ERSEM 15.06: a generic model for marine biogeochemistry and the ecosystem dynamics of the lower trophic levels, Geoscientific Model Development, 9, 1293–1339, 2016.

Cadée, G. C. and Hegeman, J.: Primary production of the benthic microflora living on tidal flats in the Dutch Wadden Sea, Netherlands Journal of Sea Research, 1974.

Cahill, B., Radtke, H., and Neumann, T.: The role of coastal sediments for water column dynamics in the Western Baltic Sea, in prep.

Cahoon, L. B., Nearhoof, J. E., and Tilton, C. L.: Sediment grain size effect on benthic microalgal biomass in shallow aquatic ecosystems, Estuaries, 22, 735–741, 1999.

Canty, A. and Ripley, B.: boot: Bootstrap Functions (Originally by Angelo Canty for S), https://CRAN.R-project.org/package=boot, 2017.

Capet, A., Meysman, F. J. R., Akoumianaki, I., Soetaert, K., and Grégoire, M.: Integrating sediment biogeochemistry into 3D oceanic models: A study of benthic-pelagic coupling in the Black Sea, Ocean Modelling, 101, 83–100, doi:10.1016/j.ocemod.2016.03.006, 2016.

Cerco, C. F., Noel, M. R., and Kim, S.-C.: Three-dimensional management model for Lake Washington, part II: eutrophication modeling and skill assessment, Lake and Reservoir Management, 22, 115–131, 2006.

Christiansen, C., Edelvang, K., Emeis, K., Graf, G., Jähmlich, S., Kozuch, J., Laima, M., Leipe, T., Löffler, A., Lund-Hansen, L. C., Miltner, A., Pazdro, K., Pempkowiak, J., Shimmield, G., Shimmield, T., Smith, J., Voss, M., and Witt, G.: Material transport from the nearshore to the basinal environment in the southern Baltic Sea: I. Processes and mass estimates, Journal of Marine Systems, 35, 133–150, doi:10.1016/S0924-7963(02)00126-4, 2002.

Cline, J. D.: Spectrophotometric determination of hydrogen sulfide in natural waters, Limnology and Oceanography, 14, 454–458, 1969.

Colijn, F. and De Jonge, V. N.: Primary production of microphytobenthos in the Ems-Dollard Estuary., Marine ecology progress series. Oldendorf, 14, 185–196, 1984.

Davies, C. W.: The extent of dissociation of salts in water. Part VIII. An equation for the mean ionic activity coefficient of an electrolyte in water, and a revision of the dissociation constants of some sulphates, Journal of the Chemical Society (Resumed), 0, 2093–2098, doi:10.1039/JR9380002093, 1938.

Davison, A. C. and Hinkley, D. V.: Bootstrap Methods and Their Application, Cambridge University Press, google-Books-ID: 4aCDbm_-t8jUC, 1997.

Deutsch, B., Forster, S., Wilhelm, M., Dippner, J. W., and Voss, M.: Denitrification in sediments as a major nitrogen sink in the Baltic Sea: an extrapolation using sediment characteristics, Biogeosciences, 7, 3259–3271, doi:10.5194/bg-7-3259-2010, 2010.

Dickson, A. G. and Goyet, C.: Handbook of methods for the analysis of the various parameters of the carbon dioxide system in sea water. Version 2, Tech. rep., Oak Ridge National Lab., TN (United States), 1994.

Dickson, A. G., Sabine, C. L., and Christian, J. R.: Guide to best practices for ocean $CO_2$ measurements., Tech. Rep. PICES Special Publication 3, PICES, Victoria, Canada, 2007.

Drobner, E., Huber, H., Wächtershäuser, G., Rose, D., and Stetter, K. O.: Pyrite formation linked with hydrogen evolution under anaerobic conditions, Nature, 346, 742, 1990.

Edzwald, J. K., Toensing, D. C., and Leung, M. C.-Y.: Phosphate adsorption reactions with clay minerals, Environmental Science & Technology, 10, 485–490, 1976.

Emeis, K., Christiansen, C., Edelvang, K., Jähmlich, S., Kozuch, J., Laima, M., Leipe, T., Loeffler, A., Lund-Hansen, L.-C., Miltner, A., and others: Material transport from the near shore to the basinal environment in the southern Baltic Sea: II: synthesis of data on origin and properties of material, Journal of Marine Systems, 35, 151–168, 2002.

Emeis, K.-C., Struck, U., Leipe, T., Pollehne, F., Kunzendorf, H., and Christiansen, C.: Changes in the C, N, P burial rates in some Baltic Sea sediments over the last 150 years—relevance to P regeneration rates and the phosphorus cycle, Marine Geology, 167, 43–59, 2000.

Engel, A.: Direct relationship between $CO_2$ uptake and transparent exopolymer particles production in natural phytoplankton, Journal of Plankton Research, 24, 49–53, doi:10.1093/plankt/24.1.49, 2002.

Gadani, D. H., Rana, V. A., Bhatnagar, S. P., Prajapati, A. N., and Vyas, A. D.: Effect of salinity on the dielectric properties of water, Indian Journal of Pure & Applied Physics, 50, 405–410, 2012.

Gili, J.-M. and Coma, R.: Benthic suspension feeders: their paramount role in littoral marine food webs, Trends in ecology & evolution, 13, 316–321, 1998.

Glud, R. N.: Oxygen dynamics of marine sediments, Marine Biology Research, 4, 243–289, doi:10.1080/17451000801888726, https://doi.org/10.1080/17451000801888726, 2008.

Glud, R. N., Woelfel, J., Karsten, U., Kühl, M., and Rysgaard, S.: Benthic microalgal production in the Arctic: applied methods and status of the current database, Botanica Marina, 52, 559–571, 2009.

Gogina, M., Morys, C., Forster, S., Gräwe, U., Friedland, R., and Zettler, M. L.: Towards benthic ecosystem functioning maps: Quantifying bioturbation potential in the German part of the Baltic Sea, Ecological Indicators, 73, 574–588, doi:10.1016/j.ecolind.2016.10.025, 2017.

Graf, G. and Rosenberg, R.: Bioresuspension and biodeposition: a review, Journal of Marine Systems, 11, 269–278, 1997.

Grasshoff, K., Kremling, K., and Ehrhardt, M.: Methods of seawater analysis, John Wiley & Sons, 2009.

Griffies, S.: Fundamentals of ocean climate models, Princeton university press, 2018.

Guisasola, A., Jubany, I., Baeza, J. A., Carrera, J., and Lafuente, J.: Respirometric estimation of the oxygen affinity constants for biological ammonium and nitrite oxidation, Journal of Chemical Technology & Biotechnology, 80, 388–396, doi:10.1002/jctb.1202, 2005.

Gundersen, J. K. and Jorgensen, B. B.: Microstructure of diffusive boundary layers and the oxygen uptake of the sea floor, Nature, 345, 604, 1990.

Haines-Young, R. and Potschin, M.: Common International Classification of Ecosystem Services (CICES): Consultation on Version 4, August-December 2012, Tech. rep., University of Nottingham, https://cices.eu/content/uploads/sites/8/2012/07/CICES-V43_Revised-Final_Report_29012013.pdf, 2013.

Hamme, R. C. and Emerson, S. R.: The solubility of neon, nitrogen and argon in distilled water and seawater, Deep Sea Research Part I: Oceanographic Research Papers, 51, 1517–1528, 2004.

Hansen, M. H., Ingvorsen, K., and Jøgensen, B. B.: Mechanisms of hydrogen sulfide release from coastal marine sediments to the atmosphere, Limnology and Oceanography, 23, 68–76, doi:10.4319/lo.1978.23.1.0068, https://aslopubs.onlinelibrary.wiley.com/doi/abs/10.4319/lo.1978.23.1.0068, 1978.

Heiskanen, A.-S. and Leppänen, J.-M.: Estimation of export production in the coastal Baltic Sea: effect of resuspension and microbial decomposition on sedimentation measurements, Hydrobiologia, 316, 211–224, 1995.

HELCOM: Part A. Introductory Chapters, in: Guidelines for the Baltic Monitoring Programme for the Third Stage, no. 27A in Baltic Sea Environment Proceedings, Baltic Marine Environment Protection Commission - Helsinki Commission, Helsinki, 1988.

Hooke, R. and Jeeves, T. A.: “Direct Search”Solution of Numerical and Statistical Problems, Journal of the ACM (JACM), 8, 212–229, 1961.

Huber, P. J.: Robust statistics, Wiley series in probability and mathematical statistics, Wiley, New York, 1981.

Ingall, E. and Jahnke, R.: Influence of water-column anoxia on the elemental fractionation of carbon and phosphorus during sediment diagenesis, Marine Geology, 139, 219–229, 1997.

IOW: IOWDB - the oceanographic database of IOW, https://www.io-warnemuende.de/iowdb.html, 2017.

Jaisi, D. P., Dong, H., and Liu, C.: Influence of biogenic Fe (II) on the extent of microbial reduction of Fe (III) in clay minerals nontronite, illite, and chlorite, Geochimica et Cosmochimica Acta, 71, 1145–1158, 2007.

Jakobsen, R. and Postma, D.: Formation and solid solution behavior of Ca-rhodochrosites in marine muds of the Baltic deeps, Geochimica et Cosmochimica Acta, 53, 2639–2648, doi:10.1016/0016-7037(89)90135-X, 1989.

Jilbert, T., Slomp, C. P., Gustafsson, B. G., and Boer, W.: Beyond the Fe-P-redox connection: preferential regeneration of phosphorus from organic matter as a key control on Baltic Sea nutrient cycles, Biogeosciences, 8, 1699–1720, doi:10.5194/bg-8-1699-2011, http://www.biogeosciences.net/8/1699/2011/, 2011.

Jonsson, P., Carman, R., and Wulff, F.: Laminated sediments in the Baltic: a tool for evaluating nutrient mass balances, Ambio, pp. 152–158, 1990.

Jørgensen, B. B.: Bacteria and Marine Biogeochemistry, in: Marine Geochemistry, edited by Schulz, H. D. and Zabel, M., pp. 169–206, Springer-Verlag, Berlin/Heidelberg, dOI: 10.1007/3-540-32144-6_5, 2006.

Kalka, H.: Activity Coefficients (Activity Models), http://www.aqion.de/site/101#fn:lg, 2018.

Kersten, M., Leipe, T., and Tauber, F.: Storm disturbance of sediment contaminants at a Hot-Spot in the Baltic Sea assessed by 234Th radionuclide tracer profiles, Environmental science & technology, 39, 984–990, 2005.

Kowalski, N., Dellwig, O., Beck, M., Grunwald, M., Dürselen, C.-D., Badewien, T. H., Brumsack, H.-J., van Beusekom, J. E., and Böttcher, M. E.: A comparative study of manganese dynamics in the water column and sediments of intertidal systems of the North Sea, Estuarine, Coastal and Shelf Science, 100, 3–17, doi:10.1016/j.ecss.2011.03.011, 2012.

Kristensen, E., Ahmed, S. I., and Devol, A. H.: Aerobic and anaerobic decomposition of organic matter in marine sediment: which is fastest?, Limnology and Oceanography, 40, 1430–1437, 1995.

Kulik, D. A., Kersten, M., Heiser, U., and Neumann, T.: Application of Gibbs Energy Minimization to Model Early-Diagenetic Solid-Solution Aqueous-Solution Equilibria Involving Authigenic Rhodochrosites in Anoxic Baltic Sea Sediments, Aquatic Geochemistry, 6, 147–199, 2000.

Kuliński, K., Schneider, B., Hammer, K., Machulik, U., and Schulz-Bull, D.: The influence of dissolved organic matter on the acid–base system of the Baltic Sea, Journal of Marine Systems, 132, 106–115, 2014.

Lancelot, C., Spitz, Y., Gypens, N., Ruddick, K., Becquevort, S., Rousseau, V., Lacroix, G., and Billen, G.: Modelling diatom and Phaeocystis blooms and nutrient cycles in the Southern Bight of the North Sea: the MIRO model, Marine Ecology Progress Series, 289, 63–78, 2005.

Large, W. G., McWilliams, J. C., and Doney, S. C.: Oceanic vertical mixing: A review and a model with a nonlocal boundary layer parameterization, Reviews of Geophysics, 32, 363–403, 1994.

Lee, J.-Y., Tett, P., Jones, K., Jones, S., Luyten, P., Smith, C., and Wild-Allen, K.: The PROWQM physical–biological model with benthic–pelagic coupling applied to the northern North Sea, Journal of Sea Research, 48, 287–331, doi:10.1016/S1385-1101(02)00182-X, http://linkinghub.elsevier.com/retrieve/pii/S138511010200182X, 2002.

Leipe, T., Tauber, F., Vallius, H., Virtasalo, J., Uścinowicz, S., Kowalski, N., Hille, S., Lindgren, S., and Myllyvirta, T.: Particulate organic carbon (POC) in surface sediments of the Baltic Sea, Geo-Mar Lett, 31, 175–188, 2011.

Leppäranta, M. and Myrberg, K.: Physical oceanography of the Baltic Sea, Springer Science & Business Media, 2009.

Levinton, J. S.: Marine Biology: Function, Biodiversity, Ecology, Oxford University Press, USA, New York, 4 edn., 2013.

Lijklema, L.: Interaction of orthophosphate with iron (III) and aluminum hydroxides, Environmental Science & Technology, 14, 537–541, 1980.

Lipka, M.: Current biogeochemical processes and element fluxes in surface sediments of temperate marginal seas (Baltic Sea and Black Sea), Ph.D. thesis, University of Greifswald (Germany), Greifswald, 2018.

Lipka, M., Wölfel, J., Gogina, M., Liu, B., and Böttcher, M. E.: Spatiotemporal dynamics in solute reservoirs of temperate brackish surface sediments, Annual Report 2017, Leibniz Institute for Baltic Sea Research Warnemuende (IOW), Warnemuende, https://www.io-warnemuende.de/tl_files/forschung/pdf/IOW-Jahresbericht-2017.pdf, 2018a.

Lipka, M., Woelfel, J., Gogina, M., Kallmeyer, J., Liu, B., Morys, C., Forster, S., and Böttcher, M. E.: Solute Reservoirs Reflect Variability of Early Diagenetic Processes in Temperate Brackish Surface Sediments, Frontiers in Marine Science, 5, doi:10.3389/fmars.2018.00413, https://www.frontiersin.org/articles/10.3389/fmars.2018.00413/full, 2018b.

Llobet-Brossa, E.: Microbial Community Composition of Wadden Sea Sediments as Revealed by Fluorescence In Situ Hybridization, Applied and Environmental Microbiology, 64, 6, 1998.

Luff, R. and Moll, A.: Seasonal dynamics of the North Sea sediments using a three-dimensional coupled sediment–water model system, Continental Shelf Research, 24, 1099–1127, 2004.

Maar, M., Møller, E. F., Larsen, J., Madsen, K. S., Wan, Z., She, J., Jonasson, L., and Neumann, T.: Ecosystem modelling across a salinity gradient from the North Sea to the Baltic Sea, Ecological Modelling, 222, 1696–1711, doi:10.1016/j.ecolmodel.2011.03.006, http://www.sciencedirect.com/science/article/pii/S030438001100113X, 2011.

Marcus, N. H.: Minireview: The importance of benthic-pelagic coupling and the forgotten role of life cycles in coastal aquatic systems, Limnology and Oceanography, 43, 763–768, 1998.

Meire, L., Soetaert, K. E. R., and Meysman, F. J. R.: Impact of global change on coastal oxygen dynamics and risk of hypoxia, Biogeosciences, 10, 2633–2653, 2013.

Meysman, F. J., Galaktionov, O. S., Gribsholt, B., and Middelburg, J. J.: Bioirrigation in permeable sediments: Advective pore-water transport induced by burrow ventilation, Limnology and Oceanography, 51, 142–156, 2006.

Meysman, F. J., Malyuga, V. S., Boudreau, B. P., and Middelburg, J. J.: A generalized stochastic approach to particle dispersal in soils and sediments, Geochimica et Cosmochimica Acta, 72, 3460–3478, doi:10.1016/j.gca.2008.04.023, http://linkinghub.elsevier.com/retrieve/pii/S001670370800210X, 2008.

Middelburg, J. J.: A simple rate model for organic matter decomposition in marine sediments, Geochimica et Cosmochimica Acta, 53, 1577–1581, 1989.

Millero, F. J.: Thermodynamics of the carbon dioxide system in the oceans, Geochimica et Cosmochimica Acta, 59, 661–677, doi:10.1016/0016-7037(94)00354-O, 1995.

Millero, F. J. and Leung, W. H.: The thermodynamics of seawater at one atmosphere, American Journal of Science, 276, 1035–1077, doi:10.2475/ajs.276.9.1035, 1976.

Millero, F. J., Sotolongo, S., and Izaguirre, M.: The oxidation kinetics of Fe(II) in seawater, Geochimica et Cosmochimica Acta, 51, 793–801, doi:10.1016/0016-7037(87)90093-7, 1987.

Moberg, E. G. and Harding, M. W.: The Boron Content of Sea Water, Science, 77, 510–510, doi:10.1126/science.77.2004.510, http://science.sciencemag.org/content/77/2004/510.1, 1933.

Morse, J. W., Millero, F. J., Cornwell, J. C., and Rickard, D.: The chemistry of the hydrogen sulfide and iron sulfide systems in natural waters, Earth-Science Reviews, 24, 1–42, doi:10.1016/0012-8252(87)90046-8, 1987.

Morys, C.: Particle dynamics in sediments of the western Baltic Sea, Ph.D. thesis, University of Rostock (Germany), Rostock, http://rosdok.uni-rostock.de/file/rosdok_disshab_0000001661/rosdok_derivate_0000035932/Dissertation_Morys_2017.pdf, 2016.

Morys, C.: Seasonality of bioturbation - what governs the intensity of local and non-local sediment mixing?, in prep.

Morys, C., Forster, S., and Graf, G.: Variability of bioturbation in various sediment types and on different spatial scales in the southwestern Baltic Sea, Marine Ecology Progress Series, 557, 31–49, doi:10.3354/meps11837, 2016.

Morys, C., Powilleit, M., and Forster, S.: Bioturbation in relation to the depth distribution of macrozoobenthos in the southwestern Baltic Sea, Marine Ecology Progress Series, 579, 19–36, doi:10.3354/meps12236, 2017.

Neumann, T.: Towards a 3D-ecosystem model of the Baltic Sea, Journal of Marine Systems, 25, 405–419, doi:10.1016/S0924-7963(00)00030-0, 2000.

Neumann, T. and Schernewski, G.: Eutrophication in the Baltic Sea and shifts in nitrogen fixation analyzed with a 3D ecosystem model, Journal of Marine Systems, 74, 592–602, 2008.

Neumann, T., Siegel, H., and Gerth, M.: A new radiation model for Baltic Sea ecosystem modelling, Journal of Marine Systems, 152, 83–91, doi:10.1016/j.jmarsys.2015.08.001, 2015.

Neumann, T., Radtke, H., and Seifert, T.: On the importance of Major Baltic Inflows for oxygenation of the central Baltic Sea, Journal of Geophysical Research: Oceans, 122, 1090–1101, http://onlinelibrary.wiley.com/doi/10.1002/2016JC012525/full, 2017.

Oliveros-Ramos, R. and Shin, Y.-J.: Calibrar: an R package for fitting complex ecological models, arXiv preprint arXiv:1603.03141, 2016.

Osipov, V. I.: Density of clay minerals, Soil Mechanics and Foundation Engineering, 48, 231–240, 2012.

Paraska, D. W., Hipsey, M. R., and Salmon, S. U.: Sediment diagenesis models: Review of approaches, challenges and opportunities, Environmental Modelling & Software, 61, 297–325, doi:10.1016/j.envsoft.2014.05.011, 2014.

Pinckney, J. and Zingmark, R. G.: Biomass and production of benthic microalgal communities in estuarine habitats, Estuaries, 16, 887–897, 1993.

Raaphorst, W. V. and Malschaert, J. F. P.: Ammonium adsorption in superficial North Sea sediments, Continental Shelf Research, 16, 1415–1435, doi:10.1016/0278-4343(95)00081-X, 1996.

Radtke, H. and Burchard, H.: A positive and multi-element conserving time stepping scheme for biogeochemical processes in marine ecosystem models, Ocean Modelling, 85, 32–41, 2015.

Radtke, H., Neumann, T., Voss, M., and Fennel, W.: Modeling pathways of riverine nitrogen and phosphorus in the Baltic Sea, Journal of Geophysical Research, 117, C09 024, doi:10.1029/2012JC008119, 2012.

Reed, D. C., Slomp, C. P., and Gustafssonb, B. G.: Sedimentary phosphorus dynamics and the evolution of bottom-water hypoxia: A coupled benthic–pelagic model of a coastal system, Limnol. Oceanogr, 56, 1075–1092, 2011.

Rickard, D.: Kinetics of pyrite formation by the H 2 S oxidation of iron (II) monosulfide in aqueous solutions between 25 and 125 C: The rate equation, Geochimica et Cosmochimica Acta, 61, 115–134, http://www.sciencedirect.com/science/article/pii/S0016703796003213, 1997.

Rickard, D. and Luther, G. W.: Kinetics of pyrite formation by the H 2 S oxidation of iron (II) monosulfide in aqueous solutions between 25 and 125 C: The mechanism, Geochimica et Cosmochimica Acta, 61, 135–147, 1997.

Rickard, D. and Luther, G. W.: Chemistry of Iron Sulfides, Chemical Reviews, 107, 514–562, doi:10.1021/cr0503658, 2007.

Rudstam, L. G., Aneer, G., and Hildén, M.: Top-down control in the pelagic Baltic ecosystem, Dana, 10, 105–129, 1994.

Rusch, A., Forster, S., and Huettel, M.: Bacteria, diatoms and detritus in an intertidal sandflat subject to advective transport across the water-sediment interface, Biogeochemistry, 55, 1–27, 2001.

Sarazin, G., Michard, G., and Prevot, F.: A rapid and accurate spectroscopic method for alkalinity measurements in sea water samples, Water Research, 33, 290–294, 1999.

Sawicka, J. E., Jørgensen, B. B., and Brüchert, V.: Temperature characteristics of bacterial sulfate reduction in continental shelf and slope sediments, Biogeosciences, 9, 3425–3435, doi:10.5194/bg-9-3425-2012, https://www.biogeosciences.net/9/3425/2012/, 2012.

Schippers, A. and Jørgensen, B. B.: Biogeochemistry of pyrite and iron sulfide oxidation in marine sediments, Geochimica et Cosmochimica Acta, 66, 85–92, 2002.

Schmidt, M. and Eggert, A.: Oxygen cycling in the northern Benguela Upwelling System: Modelling oxygen sources and sinks, Progress in Oceanography, 149, 145–173, 2016.

Schneider, B., Nausch, G., and Pohl, C.: Mineralization of organic matter and nitrogen transformations in the Gotland Sea deep water, Marine Chemistry, 119, doi:10.1016/j.marchem.2010.02.004, http://www.sciencedirect.com/science/article/pii/S0304420310000228, 2010.

Schulz, J.-P. and Schattler, U.: Kurze Beschreibung des Lokal-Modells Europa COSMO-EU (LME) und seiner Datenbanken auf dem Datenserver des DWD, Tech. rep., German Weather Service, https://www.dwd.de/SharedDocs/downloads/DE/modelldokumentationen/nwv/cosmo_eu/cosmo_eu_dbbeschr_201406.pdf, 2014.

Seitzinger, S. P., Nixon, S. W., and Pilson, M. E.: Denitrification and nitrous oxide production in a coastal marine ecosystem, Limnology and Oceanography, 29, 73–83, 1984.

Soetaert, K. and Middelburg, J. J.: Modeling eutrophication and oligotrophication of shallow-water marine systems: the importance of sediments under stratified and well-mixed conditions, in: Eutrophication in Coastal Ecosystems, pp. 239–254, Springer, 2009.

Soetaert, K., Herman, P. M., and Middelburg, J. J.: A model of early diagenetic processes from the shelf to abyssal depths, Geochimica et Cosmochimica Acta, 60, 1019–1040, 1996a.

Soetaert, K., Herman, P. M., Middelburg, J. J., Heip, C., deStigter, H. S., van Weering, T. C., Epping, E., and Helder, W.: Modeling 210Pb-derived mixing activity in ocean margin sediments: diffusive versus nonlocal mixing, Journal of Marine Research, 54, 1207–1227, 1996b.

Soetaert, K., Herman, P. M., Middelburg, J. J., Heip, C., Smith, C. L., Tett, P., and Wild-Allen, K.: Numerical modelling of the shelf break ecosystem: reproducing benthic and pelagic measurements, Deep Sea Research Part II: Topical Studies in Oceanography, 48, 3141–3177, 2001.

Sohma, A., Sekiguchi, Y., Kuwae, T., and Nakamura, Y.: A benthic–pelagic coupled ecosystem model to estimate the hypoxic estuary including tidal flat—Model description and validation of seasonal/daily dynamics, Ecological Modelling, 215, 10–39, doi:10.1016/j.ecolmodel.2008.02.027, http://linkinghub.elsevier.com/retrieve/pii/S0304380008000963, 2008.

Sohma, A., Shibuki, H., Nakajima, F., Kubo, A., and Kuwae, T.: Modeling a coastal ecosystem to estimate climate change mitigation and a model demonstration in Tokyo Bay, Ecological Modelling, 384, 261–289, 2018.

Stephenson, M. and Stickland, L. H.: Hydrogenase: The reduction of sulphate to sulphide by molecular hydrogen, Biochemical Journal, 25, 215, 1931.

Struck, U., Pollehne, F., Bauerfeind, E., and v. Bodungen, B.: Sources of nitrogen for the vertical particle flux in the Gotland Sea (Baltic Proper)—results from sediment trap studies, Journal of Marine Systems, 45, 91–101, doi:10.1016/j.jmarsys.2003.11.012, 2004.

Stumm, W. and Morgan, J. J.: Aquatic chemistry: chemical equilibria and rates in natural waters, vol. 126, John Wiley & Sons, 2012.

Sun, M., Aller, R. C., and Lee, C.: Early diagenesis of chlorophyll-a in Long Island Sound sediments: A measure of carbon flux and particle reworking, Journal of Marine Research, 49, 379–401, 1991.

Sunagawa, I.: Chapter 2 Nucleation, Growth And Dissolution Of Crystals During Sedimentogenesis and Diagenesis, in: Developments in Sedimentology, edited by Wolf, K. H. and Chilingarian, G. V., vol. 51 of *Diagenesis, IV*, pp. 19–47, Elsevier, doi:10.1016/S0070-4571(08)70435-7, http://www.sciencedirect.com/science/article/pii/S0070457108704357, 1994.

Sundby, B., Gobeil, C., Silverberg, N., and Mucci, A.: The phosphorus cycle in coastal marine sediments, Limnol. Oceanogr, 37, 1992.

Tauber, F.: Online-Karte: Sedimentverteilung auf dem Meeresboden, https://www.geoseaportal.de/mapapps/resources/apps/sedimentverteilung_auf_dem_meeresboden/index.html?lang=de, 2012.

Thamdrup, B., Hansen, J. W., and Jørgensen, B. B.: Temperature dependence of aerobic respiration in a coastal sediment, FEMS Microbiology Ecology, 25, 189–200, doi:10.1111/j.1574-6941.1998.tb00472.x, https://academic.oup.com/femsec/article/25/2/189/587922, 1998.

Theberge, S. M. and Iii, G. W. L.: Determination of the Electrochemical Properties of a Soluble Aqueous FeS Species Present in Sulfidic Solutions, Aquatic Geochemistry, 3, 191–211, doi:10.1023/A:1009648026806, http://link.springer.com/article/10.1023/A%3A1009648026806, 1997.

Turekian, K. K.: Oceans, Prentice-Hall, 1968.

Ulfsbo, A., Kuliński, K., Anderson, L. G., and Turner, D. R.: Modelling organic alkalinity in the Baltic Sea using a Humic-Pitzer approach, Marine Chemistry, 168, 18–26, 2015.

Uppala, S. M., Kållberg, P. W., Simmons, A. J., Andrae, U., Bechtold, V. d., Fiorino, M., Gibson, J. K., Haseler, J., Hernandez, A., and Kelly, G. A.: The ERA-40 re-analysis, Quarterly Journal of the royal meteorological society, 131, 2961–3012, 2005.

van Cappellen, P. and Wang, Y.: Cycling of iron and manganese in surface sediments; a general theory for the coupled transport and reaction of carbon, oxygen, nitrogen, sulfur, iron, and manganese, American Journal of Science, 296, 197–243, doi:10.2475/ajs.296.3.197, 1996.

van de Bund, W. J., Ólafsson, E., Modig, H., and Elmgren, R.: Effects of the coexisting Baltic amphipods Monoporeia affinis and Pontoporeia femorata on the fate of a simulated spring diatom bloom, Marine Ecology Progress Series, 212, 107–115, 2001.

Venables, W. N. and Ripley, B. D.: Modern Applied Statistics with S, Springer, 2002.

Voss, M. and Struck, U.: Stable nitrogen and carbon isotopes as indicator of eutrophication of the Oder river (Baltic Sea), Marine Chemistry, 59, 35–49, 1997.

Wasmund, N.: Occurrence of cyanobacterial blooms in the Baltic Sea in relation to environmental conditions, International Review of Hydrobiology, 82, 169–184, 1997.

Weisse, R., von Storch, H., Callies, U., Chrastansky, A., Feser, F., Grabemann, I., Guenther, H., Plü\s s, A., Stoye, T., and Tellkamp, J.: Regional meteorological–marine Reanalyses and climate change projections: Results for Northern Europe and potential for coastal and offshore applications, Bulletin of the American Meteorological Society, 90, 849–860, 2009.

Werner, U., Billerbeck, M., Polerecky, L., Franke, U., Huettel, M., Van Beusekom, J. E., and De Beer, D.: Spatial and temporal patterns of mineralization rates and oxygen distribution in a permeable intertidal sand flat (Sylt, Germany), Limnology and Oceanography, 51, 2549–2563, 2006.

Westrich, J. T. and Berner, R. A.: The role of sedimentary organic matter in bacterial sulfate reduction: the G model tested, Limnology and oceanography, 29, 236–249, 1984.

Wijsman, J. W. M., Herman, P. M. J., Middelburg, J. J., and Soetaert, K.: A Model for Early Diagenetic Processes in Sediments of the Continental Shelf of the Black Sea, Estuarine, Coastal and Shelf Science, 54, 403–421, doi:10.1006/ecss.2000.0655, 2002.

Winde, V., Böttcher, M., Escher, P., Böning, P., Beck, M., Liebezeit, G., and Schneider, B.: Tidal and spatial variations of DI13C and aquatic chemistry in a temperate tidal basin during winter time, Journal of Marine Systems, 129, 396–404, doi:10.1016/j.jmarsys.2013.08.005, 2014.

Winkler, L. W.: Die Bestimmung des im Wasser gelösten Sauerstoffes, Berichte der deutschen chemischen Gesellschaft, 21, 2843–2854, doi:10.1002/cber.188802102122, 1888.

Yakushev, E. V., Protsenko, E. A., Bruggeman, J., Wallhead, P., Pakhomova, S. V., Yakubov, S. K., Bellerby, R. G. J., and Couture, R.-M.: Bottom RedOx Model (BROM v.1.1): a coupled benthic–pelagic model for simulation of water and sediment biogeochemistry, Geosci. Model Dev., 10, 453–482, doi:10.5194/gmd-10-453-2017, 2017.

**Table 2.** Reaction network table for the processes in the water column. See Table A1 for the composition of state variables. Processes marked with a * also take place in the pore water.

| number | forward (backward) reaction | equation |
|---|---|---|
| 1 | p_no3_assim_lpp | $1.1875\,H_3O^+ + 6.4375\,H_2O + 6.625\,CO_2 + 0.0625\,PO_4^{3-} + NO_3^- \rightarrow 8.625\,O_2 + \mathtt{t\_lpp}$ |
| 2 | p_nh4_assim_lpp | $NH_4^+ + 0.0625\,PO_4^{3-} + 6.625\,CO_2 + 7.4375\,H_2O \rightarrow \mathtt{t\_lpp} + 6.625\,O_2 + 0.8125\,H_3O^+$ |
| 3 | p_no3_assim_spp | $1.1875\,H_3O^+ + 6.4375\,H_2O + 6.625\,CO_2 + 0.0625\,PO_4^{3-} + NO_3^- \rightarrow 8.625\,O_2 + \mathtt{t\_spp}$ |
| 4 | p_nh4_assim_spp | $NH_4^+ + 0.0625\,PO_4^{3-} + 6.625\,CO_2 + 7.4375\,H_2O \rightarrow \mathtt{t\_spp} + 6.625\,O_2 + 0.8125\,H_3O^+$ |
| 5 | p_n2_assim_cya | $7.9375\,H_2O + 6.625\,CO_2 + 0.0625\,PO_4^{3-} + 0.5\,N_2 + 0.1875\,H_3O^+ \rightarrow 7.375\,O_2 + \mathtt{t\_cya}$ |
| 6 | p_lpp_resp_nh4 | $\mathtt{t\_lpp} + 6.625\,O_2 + 0.8125\,H_3O^+$<br>$\rightarrow 0.1\,\mathtt{t\_don} + 0.9\,NH_4^+ + 0.0625\,PO_4^{3-} + 6.625\,CO_2 + 7.4375\,H_2O$ |
| 7 | p_spp_resp_nh4 | $0.8125\,H_3O^+ + 6.625\,O_2 + \mathtt{t\_spp}$<br>$\rightarrow 7.4375\,H_2O + 6.625\,CO_2 + 0.0625\,PO_4^{3-} + 0.9\,NH_4^+ + 0.1\,\mathtt{t\_don}$ |
| 8 | p_cya_resp_nh4 | $0.8125\,H_3O^+ + 6.625\,O_2 + \mathtt{t\_cya}$<br>$\rightarrow 7.4375\,H_2O + 6.625\,CO_2 + 0.0625\,PO_4^{3-} + 0.1\,\mathtt{t\_don} + 0.9\,NH_4^+$ |
| 9 | p_lpp_graz_zoo | $\mathtt{t\_lpp} \rightarrow \mathtt{t\_zoo}$ |
| 10 | p_spp_graz_zoo | $\mathtt{t\_spp} \rightarrow \mathtt{t\_zoo}$ |
| 11 | p_cya_graz_zoo | $\mathtt{t\_cya} \rightarrow \mathtt{t\_zoo}$ |
| 12 | p_zoo_resp_nh4 | $0.8125\,H_3O^+ + 6.625\,O_2 + \mathtt{t\_zoo}$<br>$\rightarrow 7.4375\,H_2O + 6.625\,CO_2 + 0.0625\,PO_4^{3-} + 0.9\,NH_4^+ + 0.1\,\mathtt{t\_don}$ |
| 13 | p_don_rec_nh4 | $\mathtt{t\_don} \rightarrow NH_4^+$ |
| 14 | p_lpp_mort_det_? | $\frac{1}{3}\,H_3O^+ + \mathtt{t\_lpp} \rightarrow \frac{1}{3}\,H_2O + \frac{1}{3}\,NH_4^+ + \frac{2}{3}\,\mathtt{t\_det\_?} + \frac{2}{3}\,\mathtt{t\_detp\_?}$ |
| 15 | p_spp_mort_det_? | $\frac{1}{3}\,H_3O^+ + \mathtt{t\_spp} \rightarrow \frac{1}{3}\,H_2O + \frac{1}{3}\,NH_4^+ + \frac{2}{3}\,\mathtt{t\_det\_?} + \frac{2}{3}\,\mathtt{t\_detp\_?}$ |
| 16 | p_cya_mort_det_? | $\mathtt{t\_cya} + \frac{1}{3}\,H_3O^+ \rightarrow \frac{2}{3}\,\mathtt{t\_detp\_?} + \frac{2}{3}\,\mathtt{t\_det\_?} + \frac{1}{3}\,NH_4^+ + \frac{1}{3}\,H_2O$ |
| 17 | p_zoo_mort_det_? | $\frac{1}{3}\,H_3O^+ + \mathtt{t\_zoo} \rightarrow \frac{1}{3}\,H_2O + \frac{1}{3}\,NH_4^+ + \frac{2}{3}\,\mathtt{t\_det\_?} + \frac{2}{3}\,\mathtt{t\_detp\_?}$ |

**Table 3.** Reaction network table for the primary redox reactions in the sediment and the fluff layer. See Table A1 for the composition of state variables.

| number | forward (backward) reaction | equation |
|---|---|---|
| 25 | `p_sed_?_resp_nh4` | $H_3O^+ + 9.9375\,O_2 + \texttt{t\_sed\_?}$<br>$\rightarrow 0.9375\,Si(OH)_4 + 10.9375\,H_2O + 9.9375\,CO_2 + NH_4^+$ |
| 26 | `p_sed_?_denit_nh4` | $\texttt{t\_sed\_?} + 8.95 H_3O^+ + 7.95\,NO_3^-$<br>$\rightarrow 9.9375\,CO_2 + NH_4^+ + 3.975\,N_2 + 22.8625\,H_2O + 0.9375\,Si(OH)_4$ |
| 27 | `p_sed_?_mnred_mn2` | $\texttt{t\_sed\_?} + 40.75\,H_3O^+ + 19.875\,MnO_2$<br>$\rightarrow 0.9375\,Si(OH)_4 + 70.5625\,H_2O + 19.875\,Mn^{2+} + NH_4^+ + 9.9375\,CO_2$ |
| 28 | `p_sed_?_irred_ims` | $39.75\,H_2S + 39.75\,Fe(OH)_3 + H_3O^+ + \texttt{t\_sed\_?}$<br>$\rightarrow 9.9375\,CO_2 + NH_4^+ + 39.75\,FeS + 110.3125\,H_2O + 0.9375\,Si(OH)_4$ |
| 29 | `p_sed_?_irredips_ims` | $39.75\,FePO_4 + 239.78125\,H_3O^+ + 129.1875\,H_2O + \texttt{t\_sed\_?} + 39.75\,H_2S$<br>$\rightarrow 0.9375\,Si(OH)_4 + 9.9375\,CO_2 + NH_4^+ + 39.75\,FeS + H_2O$<br>$+39.75\,PO_4^{3-} + 358.03125\,H_3O^+$ |
| 30 | `p_sed_?_irred_iim` | $79.5\,H_3O^+ + \texttt{t\_sed\_?} + H_3O^+ + 39.75\,Fe(OH)_3 + 79.5\,OH^-$<br>$\rightarrow 0.9375\,Si(OH)_4 + 188.8125\,H_2O + H_2O + 39.75\,\left(Fe^{2+} + 2OH^-\right)^{ads-clay}$<br>$+NH_4^+ + 9.9375\,CO_2$ |
| 31 | `p_sed_?_irredips_iim` | $39.75\,FePO_4 + \texttt{t\_sed\_?} + 80.5\,H_3O^+ + 49.6875\,H_2O + 79.5\,OH^-$<br>$\rightarrow 0.9375\,Si(OH)_4 + 9.9375\,CO_2 + 39.75\,PO_4^{3-} + NH_4^+ + 39.75\,\left(Fe^{2+} + 2OH^-\right)^{ads-cla}$<br>$+H_2O + 119.25\,H_3O^+$ |
| 32 | `p_i3i_?_irred_i2i` | $\texttt{t\_sed\_?} + H_3O^+ + 39.75\,\left(Fe^{3+} + 3OH^-\right)^{in-clay}$<br>$\rightarrow 0.9375\,Si(OH)_4 + 30.8125\,H_2O + 39.75\,\left(Fe^{2+} + 2OH^-\right)^{in-clay} + NH_4^+$<br>$+9.9375\,CO_2$ |
| 33 | `p_sed_?_sulf_nh4,` | $10.9375\,H_3O^+ + 4.96875\,SO_4^{2-} + \texttt{t\_sed\_?}$ |

**Table 4.** Reaction network table for the secondary redox reactions in the sediment and in the fluff layer.

| number | forward (backward) reaction | equation |
|---|---|---|
| 35 | p_fe2_ox_ihs | $Fe^{2+} + 4.5\,H_2O + 0.25\,O_2 \rightarrow 2\,H_3O^+ + Fe(OH)_3$ |
| 36 | p_ihs_red_iim,<br>p_ihc_red_iim | $H_2S + 8\,Fe(OH)_3 \rightarrow 8\left(Fe^{2+} + 2OH^-\right)^{ads-clay} + 2\,H_2O + SO_4^{2-} + 2\,H_3O^+$ |
| 37 | p_ihs_red_ims,<br>p_ihc_red_ims | $9\,H_2S + 8\,Fe(OH)_3 \rightarrow 8\,FeS + 18\,H_2O + SO_4^{2-} + 2\,H_3O^+$ |
| 38 | p_mn2_ox_mos | $Mn^{2+} + 0.5\,O_2 + 3\,H_2O \rightarrow 2\,H_3O^+ + MnO_2$ |
| 39 | p_ims_form2_pyr | $0.5\,H_3O^+ + 0.25\,SO_4^{2-} + 0.75\,H_2S + FeS \rightarrow FeS_2 + 1.5\,H_2O$ |
| 40 | p_pyr_oxmos_ihs | $1.25\,H_2O + 1.25\,H_3O^+ + FeS_2 + MnO_2 \rightarrow Mn^{2+} + Fe(OH)_3 + 1.625\,H_2S + 0.375\,SO_4^{2-}$ |
| 41 | p_pyr_oxo2_ihs | $4\,H_2O + FeS_2 + 0.25\,O_2 \rightarrow Fe(OH)_3 + 0.5\,H_3O^+ + 0.25\,SO_4^{2-} + 1.75\,H_2S$ |
| 42 | p_imm_oxo2_ihs | $0.25\,O_2 + \left(Fe^{2+} + 2OH^-\right)^{ads-clay} + 0.5\,H_2O \rightarrow Fe(OH)_3$ |
| 43 | p_i2i_oxo2_i3i | $0.5\,H_2O + 0.25\,O_2 + \left(Fe^{2+} + 2OH^-\right)^{in-clay} \rightarrow \left(Fe^{3+} + 3OH^-\right)^{in-clay}$ |
| 44 | p_aim_nit_no3_sed | $2\,O_2 + (NH_3)^{ads-clay} \rightarrow H_3O^+ + NO_3^-$ |
| 45 | p_fe2_mnox_ihs | $MnO_2 + 2\,Fe^{2+} + 6\,H_2O \rightarrow 2\,H_3O^+ + Mn^{2+} + 2\,Fe(OH)_3$ |
| 46 | p_h2s_mnox_so4 | $0.25\,H_2S + 1.5\,H_3O^+ + MnO_2 \rightarrow Mn^{2+} + 2.5\,H_2O + 0.25\,SO_4^{2-}$ |
| 47 | p_i3i_redh2s_i2i | $H_2S + 8\left(Fe^{3+} + 3OH^-\right)^{in-clay} - > 8\left(Fe^{2+} + 2OH^-\right)^{in-clay} + 2\,H_2O + 2\,H_3O^+ + SO_4^{2-}$ |
| 48 | p_ims_oxo2_ihs | $FeS + 2.25\,O_2 + 4.5\,H_2O \rightarrow SO_4^{2-} + Fe(OH)_3 + 2\,H_3O^+$ |

**Table 5.** Reaction network table for adsorption/desorption and precipitation/dissolution processes in the sediment and in the fluff layer.

| number | forward (backward) reaction | equation |
|---|---|---|
| 49 | p_po4_ads_ips<br>(p_ips_diss_po4) | $PO_4^{3-} + Fe(OH)_3 \leftrightarrow 3OH^- + FePO_4$ |
| 50 | p_fe2_prec_ims<br>(p_ims_diss_fe2) | $2OH^- + H_2S + Fe^{2+} \leftrightarrow 2H_2O + FeS$ |
| 51 | p_fe2_prec_iim<br>(p_iim_diss_fe2) | $2OH^- + Fe^{2+} \leftrightarrow (Fe^{2+} + 2OH^-)^{ads-clay}$ |
| 52 | p_ims_trans_iim<br>(p_iim_trans_ims) | $2H_2O + FeS \leftrightarrow H_2S + (Fe^{2+} + 2OH^-)^{ads-clay}$ |
| 53 | p_mn2_prec_rho<br>(p_rho_diss_mn2) | $1.6CO_2 + Mn^{2+} + 0.6Ca^{2+} + 4.8H_2O \leftrightarrow 3.2H_3O^+ + MnCO_3(CaCO_3)_{0.6}$ |
| 54 | p_po4_ads_pim<br>(p_pim_lib_po4) | $PO_4^{3-} + 3H_3O^+ \leftrightarrow (PO_4^{3-} + 3H^+)^{ads-clay} + 3H_2O$ |
| 55 | p_nh4_ads_aim<br>(p_aim_lib_nh4) | $OH^- + NH_4^+ \leftrightarrow H_2O + (NH_3)^{ads-clay}$ |

**Table 6.** Reaction network of secondary redox reactions in the sediment, giving the possible reoxidation processes in the presence of the oxidants listed in the first row.

| reoxidation by | $O_2$ | $NO_3^-$ | $MnO_2$ | $Fe(OH)_3$ |
|---|---|---|---|---|
| $NH_4^+ \rightarrow NO_3^-$ | + | | | |
| $NH_4^{+(ads-clay)} \rightarrow NO_3^-$ | + | | | |
| $Mn^{2+} \rightarrow MnO_2$ | + | | | |
| $Fe^{2+} \rightarrow Fe(OH)_3$ | + | | + | |
| $Fe^{2+(ads-clay)} \rightarrow Fe(OH)_3$ | + | | | |
| $Fe^{2+(in-clay)} \rightarrow Fe^{3+(in-clay)}$ | + | | | |
| $H_2S \rightarrow SO_4^{2-}$ | + | + | + | + |
| $FeS \rightarrow Fe(OH)_3 + SO_4^{2-}$ | (+) | | | |
| $FeS_2 \rightarrow Fe(OH)_3 + 2SO_4^{2-}$ | + | | + | |

**Table 7.** ~~Site-specific~~ Porosity and sediment accumulation rate data used as model input and clay volume content estimated by the model based on an initial guess.

| station | porosity (rel. units) | sed. acc. rate (kg $m^{-2}$ $year^{-1}$) | source of sed. acc. rate | clay minerals content (% of volume) |
|---|---|---|---|---|
| LB | 0.91 | 0.6 | (Kersten et al., 2005) | 0.5 |
| MB | 0.91 | 0.3 | (Leipe et al., 2011) | 0.5 |
| ST | 0.40 | - | - | 0.04 |
| DS | 0.40 | - | - | 0.1 |
| AB | 0.91 | 1.1 | (Emeis et al., 2002) | 0.5 |
| TW | 0.60 | - | - | 0.1 |
| OB | 0.40 | - | - | 0.05 |

**Table A1.** stoichiometric composition of tracers

| tracer | C | Ca | Fe | H | Mn | N | O | P | S | Si | electric charge |
|---|---|---|---|---|---|---|---|---|---|---|---|
| `t_no3` | | | | | | 1 | 3 | | | | -1 |
| `t_lpp` | 6.625 | | | 16.4375 | | 1 | 6.875 | 0.0625 | | | |
| `t_spp` | 6.625 | | | 16.4375 | | 1 | 6.875 | 0.0625 | | | |
| `t_cya` | 6.625 | | | 16.4375 | | 1 | 6.875 | 0.0625 | | | |
| `t_zoo` | 6.625 | | | 16.4375 | | 1 | 6.875 | 0.0625 | | | |
| `t_det_?` | 9.9375 | | | ~~23.0625~~ 22.875 | | 1 | 9.9375 | | | | |
| `t_detp_?` | | | | 0.28125 | | | 0.375 | 0.09375 | | | |
| `t_don` | | | | 4 | | 1 | | | | | +1 |
| `t_poc` | 1 | | | 2 | | | 1 | | | | |
| `t_ihw` | | | 1 | 3 | | | 3 | | | | |
| `t_ipw` | | | 1 | | | | 4 | 1 | | | |
| `t_mow` | | | | | 1 | | 2 | | | | |
| `t_n2` | | | | | | 2 | | | | | |
| `t_o2` | | | | | | | 2 | | | | |
| `t_dic` | 1 | | | | | | 2 | | | | |
| `t_nh4` | | | | 4 | | 1 | | | | | +1 |
| `t_no3` | | | | | | 1 | 3 | | | | -1 |
| `t_po4` | | | | | | | 4 | 1 | | | -3 |
| `t_h2s` | | | | ~~1~~ 2 | | | | | ~~2~~ 1 | | |
| `t_sul` | | | | | | | | | 1 | | |
| `t_so4` | | | | | | | 4 | | 1 | | -2 |
| `t_fe2` | | | 1 | | | | | | | | +2 |
| `t_ca2` | | 1 | | | | | | | | | +2 |
| `t_mn2` | | | | | 1 | | | | | | +2 |
| `t_sil` | | | | 4 | | | 4 | | | 1 | |
| `t_ohm_quickdiff` | | | | 1 | | | 1 | | | | -1 |
| `t_ohm_slowdiff` | | | | 1 | | | 1 | | | | -1 |
| `t_sed_?` | 9.9375 | | | 23.0625 | | 1 | 9.9375 | | | | |
| `t_sedp_?` | | | | 0.28125 | | | 0.375 | 0.09375 | | | |
| `t_ihs` | | | 1 | | | | 3 | | | | |
| `t_ihc` | | | 1 | | | | 3 | | | | |
| `t_ips` | | | 1 | | | | 4 | 1 | | | |
| `t_ims` | | | 1 | | | | | | 1 | | |
| `t_pyr` | | | 1 | | | | | | 2 | | |
| `t_mos` | | | | | 1 | | 2 | | | | |
| `t_rho` | 1.6 | 0.6 | | | 1 | | 4.8 | | | | |
| `t_i3i` | | | 1 | 3 | | | 3 | | | | |
| `t_iim` | | | 1 | 2 | | | 2 | | | | |
| `t_pim` | | | | 3 | | | 4 | 1 | | | |
| `t_aim` | | | | 3 | | 1 | | | | | |
| `h2o` | | | | 2 | | | 1 | | | | |
| `h3oplus` | | | | 3 | | | 1 | | | | +1 |
| `ohminus` | | | | 1 | | | 1 | | | | -1 |
| `i2i` | | | 1 | 2 | | | 2 | | | | |

Tracer `t_alk` has been omitted since it just accumulates the changes to other tracers.

**Table A2.** decay rates of different classes of detritus

| detritus class | 1 | 2 | 3 | 4 | 5 | 6 |
|---|---|---|---|---|---|---|
| mass fraction | 26% | 16% | 16% | 16% | 8% | 18% |
| relative decay rate at 0°C (day$^{-1}$) | 0.0647 | 0.00924 | 0.00136 | 0.000108 | 0.0000162 | inert |